NASA CR 120871
SRD-72-028

ALUMINIDE COATINGS FOR NICKEL-BASE ALLOYS

by

H. C. Fiedler and R. J. Sieraski

METALLURGY AND CERAMICS LABORATORY
RESEARCH AND DEVELOPMENT CENTER
GENERAL ELECTRIC COMPANY
SCHENECTADY, NEW YORK 12301

prepared for

NATIONAL AERONAUTICS AND SPACE ADMINISTRATION

NASA Lewis Research Center
Contract NAS 3-14300
John P. Merutka, Project Manager

November 12, 1971

NOTICE

This report was prepared as an account of Government-sponsored work. Neither the United States, nor the National Aeronautics and Space Administration (NASA), nor any person acting on behalf of NASA:

A.) Makes any warranty or representation, expressed or implied, with respect to the accuracy, completeness, or usefulness of the information contained in this report, or that the use of any information, apparatus, method, or process disclosed in this report may not infringe privately-owned rights; or

B.) Assumes any liabilities with respect to the use of, or for damages resulting from the use of, any information, apparatus, method or process disclosed in this report.

As used above, "person acting on behalf of NASA" includes any employee or contractor of NASA, or employee of such contractor, to the extent that such employee or contractor of NASA or employee of such contractor prepares, disseminates, or provides access to any information pursuant to his employment or contract with NASA, or his employment with such contractor.

Requests for copies of this report should be referred to

National Aeronautics and Space Administration
Scientific and Technical Information Facility
P.O. Box 33
College Park, Md. 20740

1. Report No.	2. Government Accession No.	3. Recipient's Catalog No.
NASACR 120871		

4. Title and Subtitle	5. Report Date
ALUMINIDE COATINGS FOR NICKEL BASE ALLOYS	Nov. 12, 1971
	6. Performing Organization Code
7. Author(s) H. C. Fiedler and R. J. Sieraski	8. Performing Organization Report No. SRD-72-028
	10. Work Unit No.
9. Performing Organization Name and Address General Electric Research & Development Center P.O. Box 8 Schenectady, New York 12301	11. Contract or Grant No. NAS 3-14300
	13. Type of Report and Period Covered Contractor Report
12. Sponsoring Agency Name and Address National Aeronautics and Space Administration Washington, D.C. 20546	14. Sponsoring Agency Code

15. Supplementary Notes

Project Manager, John P. Merutka, NASA Lewis Research Center, Cleveland, Ohio

16. Abstract

The General Electric metalliding process was used to aluminide IN-100 and TD NiCr. Aluminum was deposited over a broad range of deposition rates, with two types of coating structures resulting. Chromium, silicon, titanium and yttrium were also individually deposited simutaneously with aluminum on IN-100. None of these had a marked effect on the oxidation resistance of the aluminide coating. Porosity-free aluminide coatings with good oxidation resistance were formed on TD NiCr providing the aluminum concentration did not exceed 8%, the limit of solubility in the gamma phase.

17. Key Words (Suggested by Author(s))	18. Distribution Statement
Aluminide Coatings IN-100 TD NiCr Superalloys	Unclassified - unlimited.

19. Security Classif. (of this report)	20. Security Classif. (of this page)	21. No. of Pages	22. Price*
Unclassified	Unclassified	70	$3.00

* For sale by the National Technical Information Service, Springfield, Virginia 22151

FOREWORD

The authors are indebted to Dr. N. C. Cook for his willing and extremely helpful discussions and suggestions relating to metalliding cell operation and day to day cell operating problems.

ABSTRACT

The General Electric metalliding process was used to aluminide IN-100 and TD NiCr. Aluminum was deposited over a broad range of deposition rates, with two types of coating structures resulting. Chromium, silicon, titanium and yttrium were also individually deposited simultaneously with aluminum on IN-100. None of these had a marked effect on the oxidation resistance of the aluminide coating. Porosity-free aluminide coatings with good oxidation resistance were formed on TD NiCr providing the aluminum concentration did not exceed 8%, the limit of solubility in the gamma phase.

TABLE OF CONTENTS

ALUMINIDE COATINGS FOR NICKEL-BASE ALLOYS

SUMMARY

The General Electric metalliding process was used to produce aluminide coatings on IN-100 and to form an aluminum enriched solid solution at the surface of TD NiCr. The process consists of the electrodeposition of metals from high purity fluoride salts. These salts flux the cathode surface, assuring maximum diffusion rates.

A unique feature of metalliding as compared to pack aluminiding processes is the ability to continuously control the aluminum deposition rate, and it was primarily this variable that was examined in forming simple aluminide coatings. Two distinctly different types of coating were formed; one primarily by the diffusion outward of nickel at low deposition rates and the other by the diffusion inward of aluminum at high deposition rates. All of these samples showed good oxidation resistance, surviving 200 hours at 1095°C (2000°F), but all showed poor hot corrosion resistance at 900°C (1650°F), with the samples made at low deposition rates being poorest. Many of the latter failed in less than 50 hours.

The feasibility of simultaneously depositing either titanium, silicon, chromium or yttrium along with aluminum on IN-100 was evaluated. This was successful with the first three elements, but only insignificant amounts of yttrium were deposited. Neither oxidation nor hot corrosion testing revealed any advantages of adding silicon or chromium to the coating at the levels examined, and titanium additions were found deleterious. On the basis of these screening tests, high velocity tests of these coatings were judged to be unwarranted.

Aluminum-enriched surfaces were formed on TD NiCr at 1100° to 1200°C (2012° - 2190°F) using low deposition rates. The uniform contraction of the substrate found in IN-100 due to the outward diffusion of nickel when forming NiAl does not occur in TD NiCr. Instead, the vacancies formed by the diffusion of nickel appear to coalesce on large thoria particles, forming voids. Porosity-free coatings were obtained by not exceeding 8% aluminum, the solubility limit of the gamma phase at 1100°C (2012°F). An aluminum content of 5% provided substantial oxidation resistance during the 300 hour test at 1250°C (2200°F).

INTRODUCTION

The two major requirements for alloys used in the high temperature section of aircraft gas turbines are strength and resistance to surface degradation. Ever increasing temperatures have led to the use of coatings for surface protection. The coatings on nickel-base alloys are high in aluminum and their effectiveness depends upon the formation of an adherent layer of Al_2O_3. Goward[1] has reviewed coatings for nickel-base superalloys.

The objective of the program to be reported was to develop aluminide coatings for IN-100 and TD NiCr that would provide long term protection against high temperature oxidation and hot corrosion during their use in aircraft gas

turbines. These coatings were formed using the General Electric metalliding process, in which metals are electrolytically deposited upon the cathode in a molten salt bath.[2] As compared to the conventional pack aluminiding process, metalliding permits precise control of the aluminum deposition rate during the run.

The program was divided into five tasks, all aimed at producing 3-mil-thick coatings. Task I was directed toward optimizing aluminide coatings on IN-100, Task II was exploratory and was to determine the feasibility of simultaneously depositing with aluminum the elements chromium, silicon, titanium or yttrium on IN-100. Sought was a yttrium concentration of 0.5% and concentrations of 1.0 and 5.0% of the other elements. Samples from these tasks were exposed at 1205°C (2000°F) in air and at 900°C (1650°F) in the combustion products of JP-5 jet engine fuel to which sea salt had been added.

Task III involved the formation of a coating on TD NiCr containing about 5% aluminum. The effectiveness of the coatings on TD NiCr was evaluated by exposing at 1205°C (2200°F) in an atmosphere of combusted natural gas.

In Task IV the most promising coatings on IN-100 from the first two tasks were to be subjected to high velocity oxidation and hot corrosion tests. Finally, Task V involved the coating of IN-100 and TD NiCr Erosion Test Bars for NASA evaluation.

Recently, Sanders et al.,[3] have reported on the behavior of IN-100 samples that had been aluminided using the metalliding process. They carefully described the structure both before and after oxidation testing, and were not concerned with the effect of metalliding variables on the coating structure.

MATERIALS

IN-100 was obtained from Howmet Corporation as cast bars, 1 in. in diameter and 4 in. long, for Task I and as cast erosion test specimens (NASA specification CB-301680) for Task V. All were from Heat No. UA032, the chemical analysis of which is given in Table I.

TD Nickel-Chromium was obtained from Fansteel, Inc. as 0.075 in. thick sheet (Lot No. 3185) for Task III and as 0.275 in. thick plate (Lot No. 3013) for Task V. The chemical analyses are given in Table II. The quantity of plate obtained was sufficient for only six Erosion Test Bars and four additional bars were provided by the Lewis Research Center, NASA.

TABLE I

Composition (wt %) of IN-100 Heat UA 032

Chromium	9.4
Cobalt	15.5
Molybdenum	2.9
Titanium	4.3
Aluminum	5.5
Vanadium	0.98
Zirconium	0.07
Boron	0.013
Carbon	0.162
Iron	0.19
Manganese	< 0.10
Sulfur	0.003
Nickel	Balance

TABLE II

Composition (wt %) of TD NiCr

Lot No.	S	C	Cu	Co	Cr	ThO_2	Ni
3013	0.0056	0.027	0.001	0.020	19.70	2.11	Bal.
3185	0.0025	0.025	0.003	0.050	18.99	1.97	Bal.

EXPERIMENTAL PROCEDURE

Preparing Samples for Metalliding

The cast 1 in. diameter IN-100 bars were centerless ground to produce a relatively smooth, contaminant-free surface. After a 0.18 inch hole was drilled along the center axis of the bar, discs approximately 0.06 inch thick were cut using a parting tool. They were then lapped in an attempt to produce parallel sides. All edges were rounded with an approximate 1 mil radius.

A numbering system was utilized wherein each disc set was designated by a letter or letters, with an additional number indicating the disc in the set. They were used both to identify individual discs and as a reference point during processing.

The disc sides were not parallel and had numerous tool marks and scratches. Metallographic polishing with 120, 400, and 600 grit paper removed most of the scratches and provided approximately parallel surfaces for the thickness measurement. The discs received a scouring powder and water scrub with a brush, were rinsed sequentially with water and acetone and air jet dried.

The Td NiCr test coupons were prepared by grinding all surfaces of sheared pieces to produce 2 in. x 0.5 in. x 0.06 in. specimens. The majority of the coupons had edges that were rounded to an approximate 1 mil radius. The coupons received the same treatment as did the IN-100 discs, starting with the scouring-paste scrub.

The cast IN-100 Erosion Test Bars (NASA specification CB301680) freest from surface defects were selected for metalliding. Except for the bars used in the first two runs, number 1 emery paper was used to remove a thin surface layer and the mold flash. Each of the IN-100 and TD NiCr bars was numbered using a Burgess Vibro-Engraver on the end that is held in the test rig. All surfaces were given a scouring powder and water scrub, rinsed sequentially with water and acetone, and dried in an air blast.

Each sample was weighed to the nearest 0.1 mg on an analytical balance. The thickness of the samples was measured to the nearest 0.00001 inch using a Hi-Precision Micrometer, whose calibration is ± 0.00005 inch. The thickness of each disc was measured at a point that was located approximately 90° counter-clockwise from the disc designation stamped on the bottom face of the disc. All measuring instruments used in this program have a calibration traceable to the U.S. Bureau of Standards.

Metalliding

Metalliding Cell

A typical metalliding cell is shown in Fig. 1, with several cells shown in Fig. 2. The essential parts include a furnace and temperature controller, a salt container, an enclosure to maintain atmosphere purity, entrance and exit ports, an inert gas supply, and a system for monitoring and controlling the electrolysis. The orientation shown in Fig. 1 is that seen from the front of the cell, with the cathode to the left of the anode. The Monel 400 doors of both the anode and cathode ports are electrically isolated from the salt container to prevent shorting.

The temperature was monitored and controlled by a meter relay (an on-off controller) and a chromel-alumel thermocouple located one-half inch from the bottom and sidewall of the container. A platinum-platinum, 10% rhodium thermocouple and a portable potentiometer with pointerlight were calibrated by the General Electric Standards Laboratory (± 0.6°C at 1100°C). This unit was used to recalibrate the indicator-controller system. A nitrogen gas sparge tube with approximately 1 standard cubic foot per hour flow was inserted approximately one-third of the way into the 27 inch thermowell. Aluminum foil was used to seal the top of the thermowell. These precautions were used to protect the interior of the thermowell and to prevent thermowell failure due to internal air oxidation.

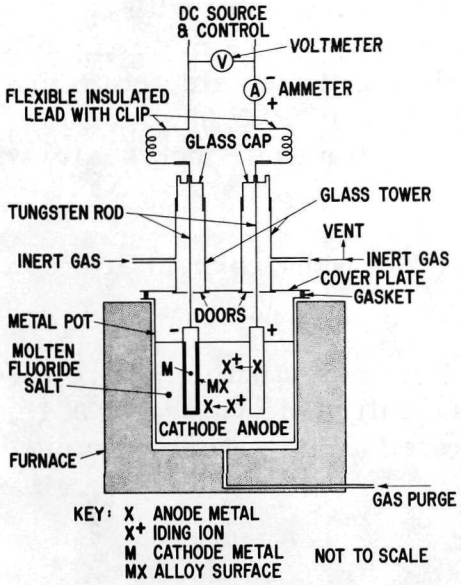

Fig. 1 Essential features of a metalliding cell.

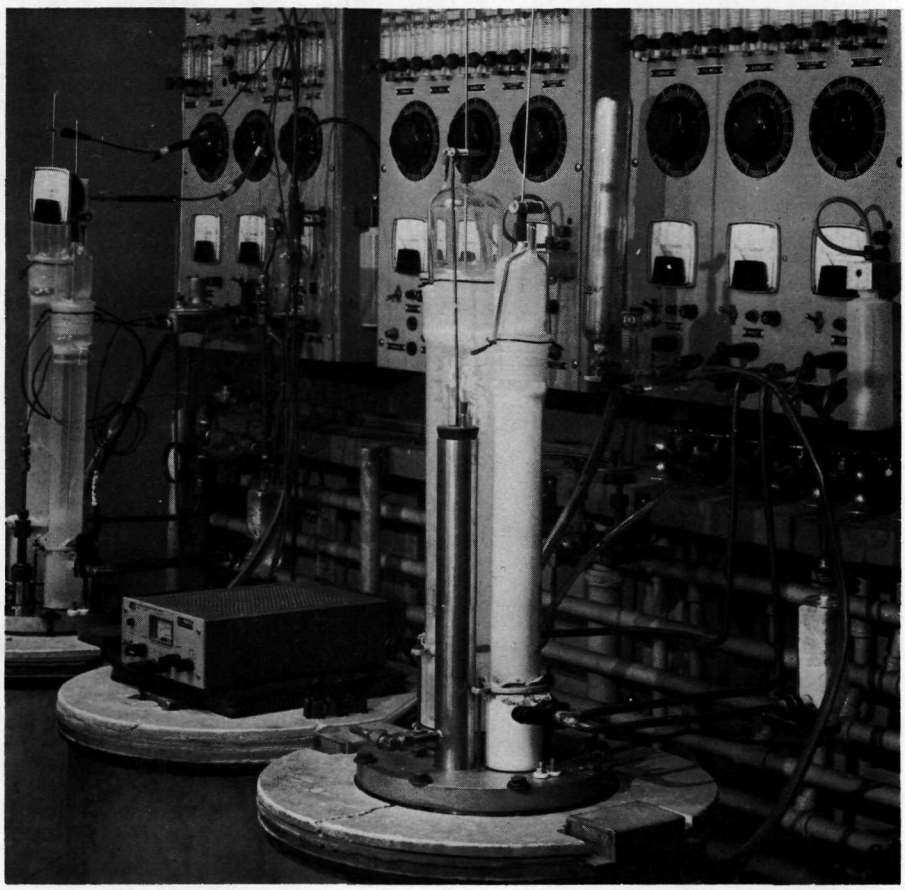

Fig. 2 Metalliding cells with control equipment.

Amperage was measured using DC Ammeters (3 inch scale) with a nominal accuracy of ± 2%, but which were calibrated using a large scale meter, yielding a reproducibility and accuracy of about ± 0.5%. Meters were selected to provide the maximum scale reading, with full scale values of 0.020, 0.050, 0.100, 0.250, 0.500, 1.00, and 2.00 amp. In addition, a meter (four inch scale) with a five amp maximum was used.

Regulated DC power supplies were used to maintain the current at a constant value.

Voltage was measured using a Volt-Ohm Milliammeter with eight voltage scales (six inch scale). The three scales used had full scale values of 0.15, 0.75, and 3.0 volts. The meters were not calibrated as they were only used to monitor coating progress.

Electrode Preparation

All five discs of a set were held on one tungsten holder as shown in Fig. 3. The disc numbers were oriented to face the front of the cell and to be toward the bottom of the cell for the first portion of the run. The holder, in turn, was wired to the hook on the end of the tungsten electrode rod to complete the cathode. The discs and rods received a final acetone degreasing, followed by air jet drying, before being inserted into the cell. The effective cathode surface area was 0.523 dm^2.

Figure 4 shows the method used to hold the Erosion Test bars during metalliding. Small areas of the bar surfaces under the 60 mil tungsten rod were not coated, since these areas are not exposed in subsequent testing.

Since low deposition rates were required to form pore-free coatings on TD NiCr, it was necessary to include additional cathode surface area in order to increase the operating current. The materials used for this purpose were TD NiCr, NiCr, and Nickel 270, with the latter being preferred. Three TD NiCr coupons and two coupons of the other material were included in each run. The holder was essentially the same as that used for the coating of IN-100 discs.

The aluminum anode consisted of pieces of Ni_2Al_3, about one-half inch in diameter, held in a basket made of 12 mesh tungsten screen. The basket, 6 inches long and 1 inch in diameter, was fastened to a tungsten electrode. An anode could be used for about 100 amp-hours.

Forming the Coating

Aluminiding of samples was begun after the cell was judged to be sufficiently free of metal ion impurities. Proper techniques were utilized to minimize the introduction of air into the cell during sample insertion and removal. The cathode surfaces were always degassed for five minutes in the space between the cover plate and the molten salt. The cathode was inserted into the salt with all electrical connections completed but without current flow. The voltage reading

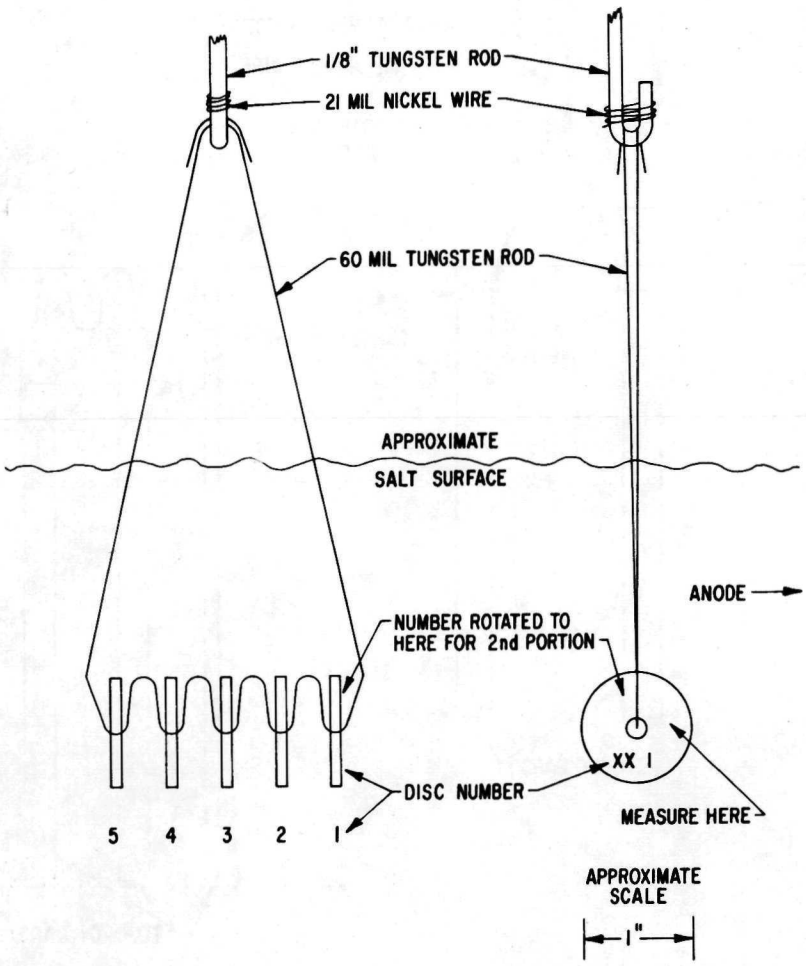

Fig. 3 Fixture used for metalliding IN-100 discs.

indicated the compositional difference between the two electrode surfaces. This provided a check for shorting or poor electrical connections. The pre-set current flow was then started. Voltage, time, current, and temperature readings were taken. Periodically, the temperature controller-indicator unit was recalibrated using the noble metal calibrated thermocouple system. When metalliding discs, the current was shut off at midrun and the same four readings taken. Voltage was monitored for 60 seconds after current flow ceased. The voltage values indicated the type of surface on the cathode, and for high current density runs with an alloy anode, the compositional change in the anode surface. The discs were removed from the cell and rotated 180° on the holder. The disc number was then up-side-down on the top face of the disc as viewed from the front of the cell. After proper flushing and degassing, the run was continued using the same procedure as at the start. The midrun procedure was repeated at the end of the run. For each run the cathode coulombic efficiency was calculated (actual weight gain divided by theoretical weight gain based upon ampere-hours of electrolysis).

Straight aluminiding was primarily done in LiF-0.003 AlF_3, with some samples being prepared in BaF_2-0.016 AlF_3. Simultaneous deposition involved the same method of coating, with the important difference that an additional metalliding agent was added to the salt, and possibly a different anode was used. The cases will be presented individually.

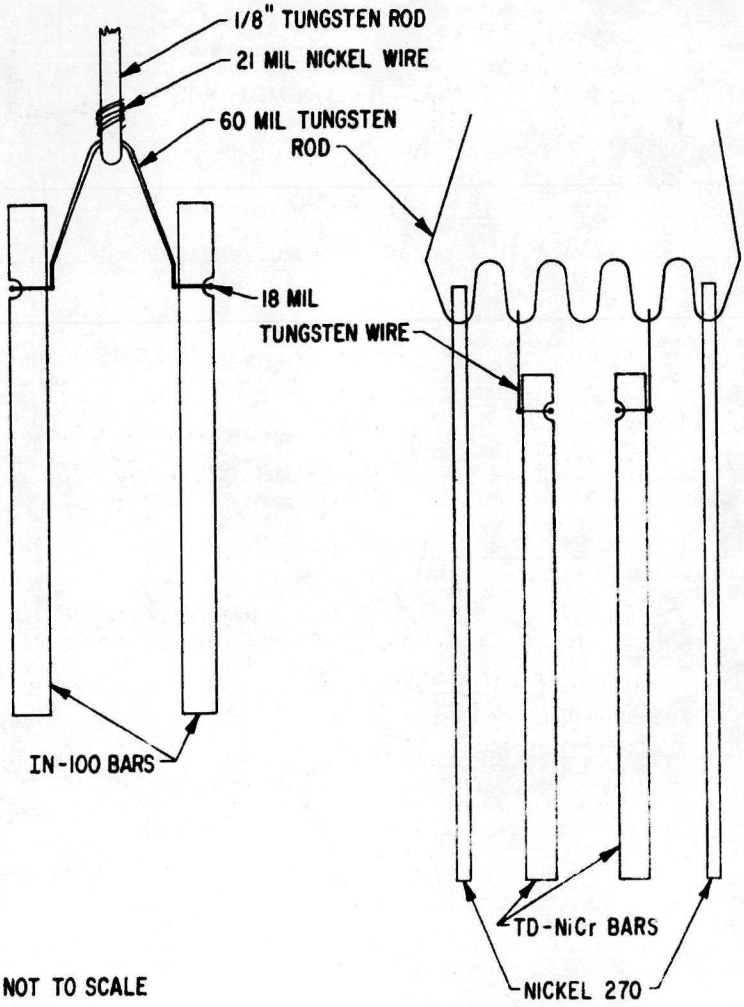

Fig. 4 Fixture used for aluminiding NASA Erosion Test Bars.

Al-Cr

A chromium anode was used to add chromous fluoride. A second attempt to obtain 10% or greater Cr required the addition of chromous fluoride powder at the start of the work. The initial bath was LiF plus 0.003 AlF_3.

Al-Si

SiF_4 was added to the argon sparge gas which was used to gently stir the LiF plus 0.003 AlF_3. Approximately 2 to 10 gram amounts were added before selected runs. A calibrated rotometer was used to measure the SiF_4. A pyrolytic graphite anode was used.

Al-Ti

A-55 titanium was used as the anode for the first half of two runs, which resulted in the desired coatings. The bath was LiF with 0.003 AlF_3. Work starting with a titaniding cell (LiF plus 0.002 TiF_3) and using an aluminum alloy anode did not produce a coating with less

than 15 w/o Ti. A titanium chip getter basket aided in the removal of air from the atmosphere above the molten salt.

Al-Y

Lithium fluoride was unsatisfactory as a solvent due to displacement of lithium metal from the bath. A bath of 50 mole percent BaF_2-CaF_2 with 1.6% added AlF_3 was then utilized. The yttriding work was started by adding 1 gram increments of YF_3 and then coating a disc set. The amount of YF_3 added was greatly increased between runs when a low yttrium concentration was found in the coating. The total amount of YF_3 added was almost six pounds into 35 lbs. of original salt, the final salt composition being approximately 13 mole percent YF_3.

Post Metalliding Cleaning Procedure

Loose salt was removed from the samples before they were placed in the chloride bath at 500°C (932°F) to dissolve the water-insoluble fluoride salt. After the chloride treatment, the remaining salt was washed off with water. Care was used to insure that the samples were not quenched in water, but were allowed to air cool. Finally, the samples were scouring-paste scrubbed with a brush, rinsed, degreased, and air jet dried. The samples were then individually weighed and measured to obtain weight gain and volumetric expansion due to metalliding. The surface was examined under low power magnification for defects. To insure the removal of all the fluoride salt, the samples were then given one or two additional chloride cell treatments.

Oxidation Testing

Discs of IN-100 were exposed in air at 1095°C (2000°F) for up to 200 hours, with cooling to below 66°C (150°F) once every hour. Twelve discs, divided between 4 pins, were tested simultaneously. The position in the disc holder was systematically changed daily, each disc thereby occupying every position during the test. The temperature difference along the length of the sample holder was no more than 6°C (10°F). The cycle consisted of 60 minutes at 1095°C ± 11° (2000°F ± 20°), with 15 minutes being required to attain 1087°C (1990°F) after loading, and 7 minutes being allowed for a fan to cool the discs to below 66°C (150°F). Therefore, 60 minutes at temperature required an 82 minute cycle. The discs were weighed daily on a balance.

Samples of Td NiCr were oxidation tested by being exposed for 300 hours at 1205°C (2200°F) in a low velocity (0.05 Mach) flame tunnel at the Materials and Process Technology Laboratories of the General Electric Company Aircraft Engine Group, Evendale, Ohio. The atmosphere was combusted natural gas, the air to fuel ratio being 10 to 1. The samples were cooled to about 480°C (900°F) six times each hour. Weight measurements were recorded daily.

Hot Corrosion Testing

Hot corrosion tests were conducted by the General Electric Co. Gas Turbine Dept. in a low velocity burner rig with an atmosphere of JP-5 jet engine fuel combustion products. The air-fuel ratio was about 64/1 with approximately 476 ppm sea salt added to the fuel. The temperature was maintained at 900°C± 11° (1650°F ± 20°). The samples were cooled to below 93°C (200°F) in an air blast four times during each 24 hour period and examined. The samples were at temperature for a minimum of 1 hour between cooling cycles. The maximum exposure time was intended to be 400 hours, but all of the coatings failed well before that time had elapsed. The length of time that a disc was allowed to remain in test depended upon the judgment of a technician who was experienced in conducting the hot corrosion test, and who was unaware of the history of the individual discs. At the time that a disc was removed, it was either corroded in more than one area, or was corroded over a substantial fraction of the disc surface.

Sample Evaluation

Unless noted otherwise, samples were etched for metallographic examination in a solution comprised of 33% lactic acid, 33% acetic acid, 22% hydrochloric acid and 12% nitric acid. Metallographic samples prepared in the latter part of the investigation were mounted in Plastimet, a product of Metallurgical Testing and Engineering Laboratory, which bonded to the sample and led to excellent edge retention.

X-ray fluorescence analysis, in which an area of the disc was exposed to chromium radiation, was used to monitor the simultaneous deposition on IN-100 and the aluminiding of TD NiCr. Calibration curves were constructed for the radiation obtained from NiAl samples containing various amounts of either silicon, aluminum, titanium or yttrium, and on alloys of 80Ni-20Cr containing 3.5%, 5%, and 8% aluminum. From the calibration curve and the measured radiation, a good approximation of the concentration of the element of interest was obtained.

Diffusion profiles across the coatings were obtained using an electron microprobe. The electron beam traversed the coating in 2 micron steps. At each step, x-ray intensities of selected elements were measured using 10 second counting intervals. A ratio, corrected for background radiation, was made between the x-ray intensity for each element and its standard. This ratio was then corrected for x-ray fluorescence, absorption and atomic number in order to convert to composition. Diffusion profiles were obtained by plotting weight percent versus distance.

RESULTS AND DISCUSSION

Task I: Aluminiding IN-100

Coating Characteristics

Samples were aluminided with aluminum deposition rate (current density) held constant in the range from 0.21 to 27 mg Al/cm^2/hour (0.062 to 8.0 amp/dm^2). The metalliding parameters and observations on the coatings are summarized in Table III.

TABLE III

Metalliding Parameters and Observations on Coatings: Task I

Disc Set	Current Density (amp/dm^2)	Time (hrs)	Mg/cm^2	Efficiency (%)	Growth (mils)	Coating (mils)	Color
A	0.062	64	13.1	96.9	1.8	5.7	Silver Gray
D	0.50	8	7.5	54.6	1.0	3.1	Blue-Blk.
E	0.50	8	8.2	60.6	1.1	2.7	Black
F	3.83	1	11.0	81.5	1.5	2.9	Pur. Gray
G	0.75	5.5	6.7	48.4	1.0	2.0	Pur. Gray
H	0.125	32	9.6	70.8	1.3	4.0	Silver
I	0.25	16	7.2	53.5	1.0	3.0	Silver
J	1.0	4.1	10.1	73.8	1.4	3.0	Dk. Purp.
K	2.0	2	9.7	71.7	1.4	2.9	Lt. Purp.
L	0.062	63.8	12.5	92.7	1.7	5.2	Lt. Gold
M	1.0	4	7.8	58.9	1.1	2.4	Pur. Gray
N	0.5	8	6.2	45.7	0.9	2.2	Gray
O	1.0	4	10.0	75.1	1.4	3.0	Gray
P	0.75	5.3	9.0	67.3	1.3	2.8	Gray
Q	0.50	6.3	6.9	64.6	1.0	2.2	Blue Gray
R	0.25	12	6.0	59.4	0.8	2.5	Blue Gray
T	0.5	5.5	9.4	67.6	1.3	2.5	Pur. Gray
	4.0	0.3					
U	0.125	24.1	7.6	74.5	1.1	3.2	Silver
V	8.0	0.5	9.4	76.2	1.4	2.3	Dull Gray
X	0.062	45	11.4	118.6	1.6	4.8	Blue-Silver
Y	4.0	1	6.3	50.8	1.0	1.8	Gray

The microstructures of samples aluminided at four current densities are shown in Fig. 5. Microprobe traces across the coatings of these four samples are shown in Figs. 6 and 7. The terms "outer layer" and "inner layer" are used to distinguish the two zones of the coating, and are without any connotation as to how the coatings were formed. The coating thickness measurement reported in Table III is a minimum value and is the sum of the thickness of these two layers.

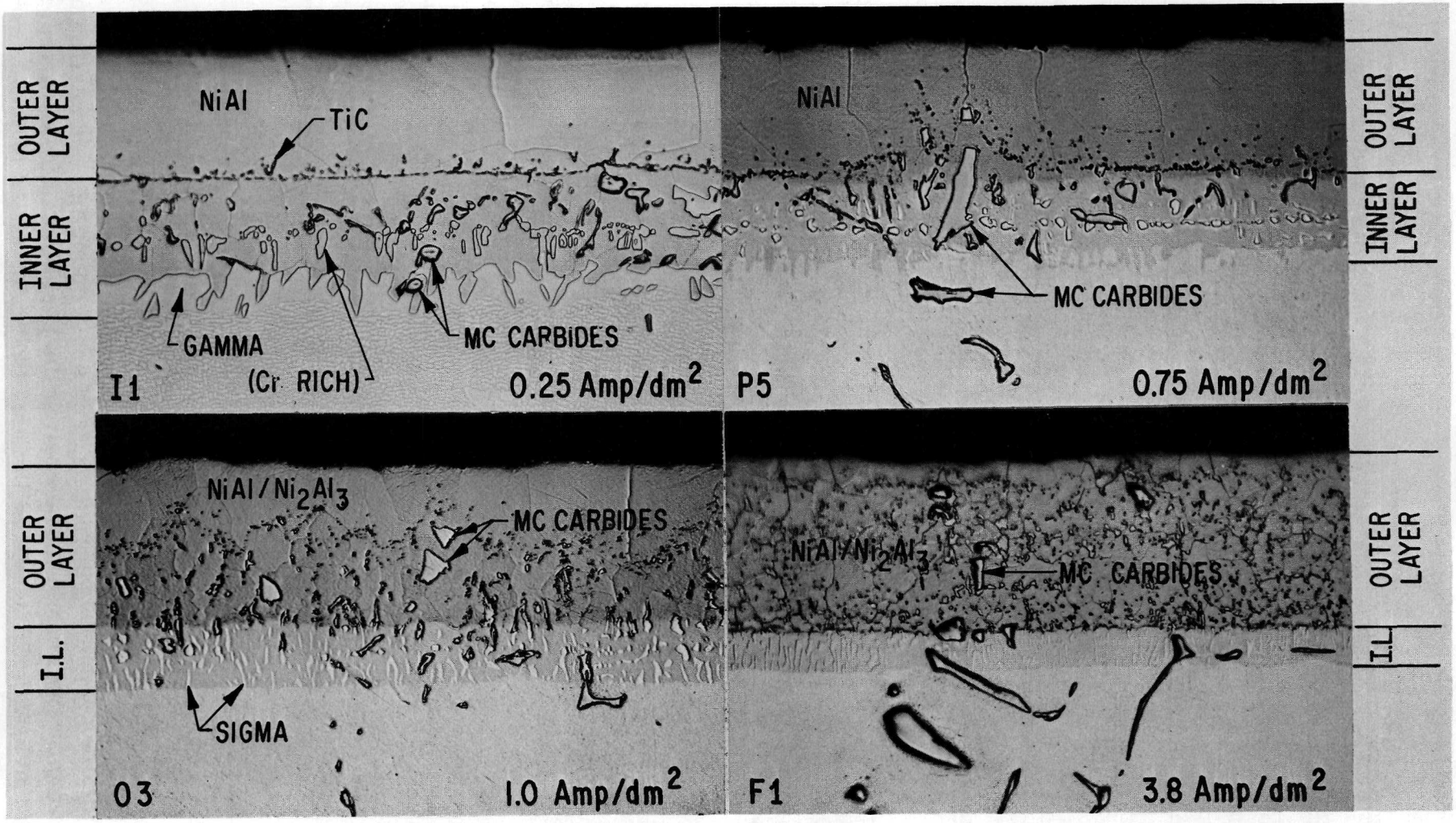

Fig. 5 Photomicrographs of as-aluminided coatings on IN-100 discs made at the current densities indicated. 485X

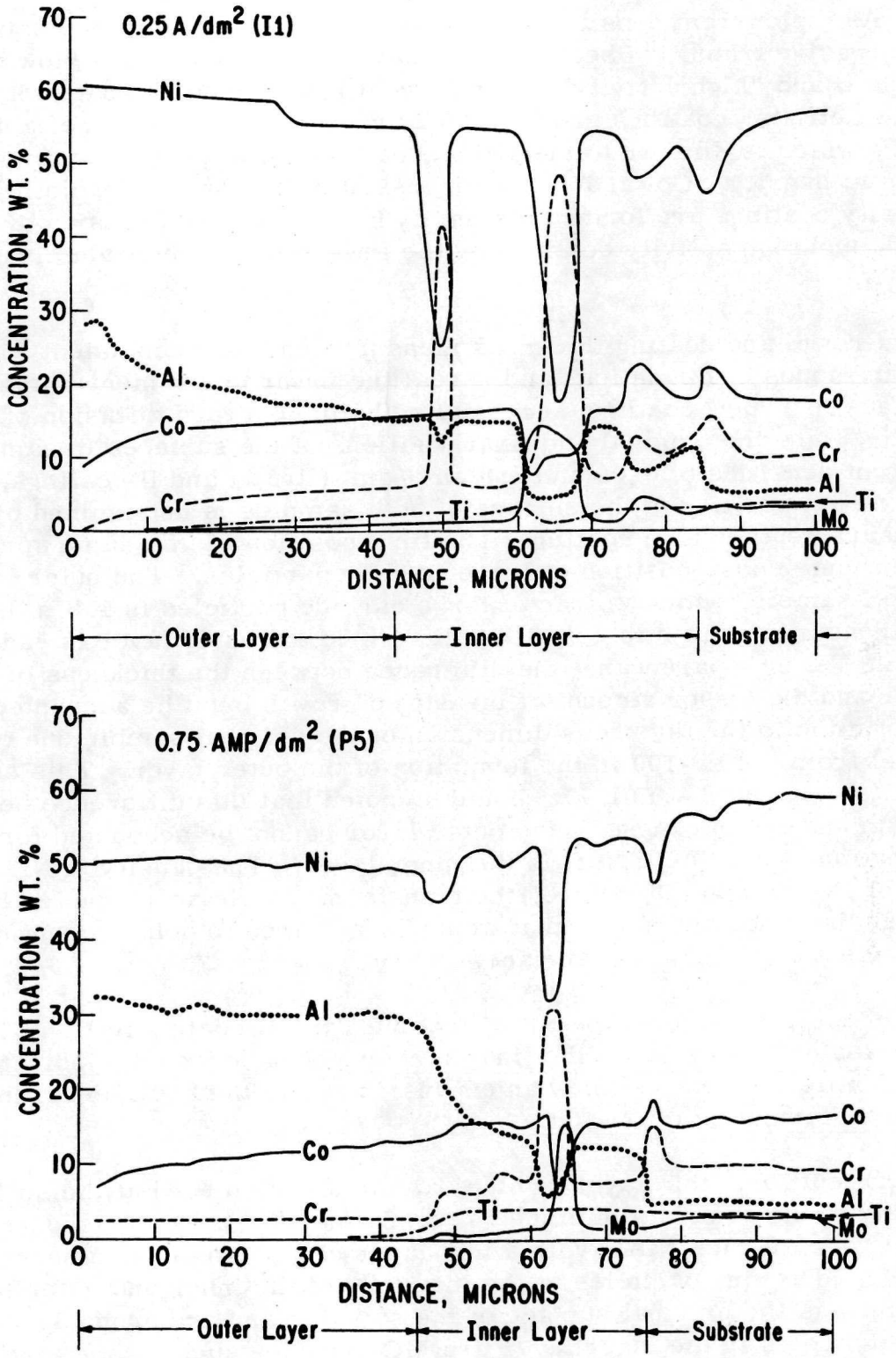

Fig. 6 Electron microprobe traces across the coating and into the substrate of discs of IN-100 aluminided at the current densities indicated.

As the current density is increased, the structure of the coating shows a progressive transition between what have been described as "low activity" (Type I) and "high activity" (Type II) coatings as made by pack aluminiding. "Low activity" coatings are produced by a low concentration of aluminum in the pack, which is similar to metalliding at a low aluminum deposition rate or current density. Goward[1] has discussed these coatings, pointing out that low activity coatings are formed primarily by the outward diffusion of nickel through NiAl, and high activity coatings by the inward diffusion of aluminum through Ni_2Al_3.

Growth and coating thickness measurements are consistent with these different modes of formation, and reveal the inward movement of the original surface in Type I coatings necessitated by the outward diffusion of nickel. Shown in Fig. 8 are the original and final positions of the surfaces in samples made at current densities of 0.06 and 3.8 amp/dm^2 (Type I and II coatings, respectively.) The initial position of the surface of both samples is determined by thickness measurements before coating. The final position of this same surface is revealed by the outermost position of large carbide particles. The outer layer of the Type I sample, which is free of large carbide particles is 1.8 mils thick whereas the measured growth is only 1.0 mil. Since the outer layer is "added-on" coating, it is apparent that the difference between the thickness of the outer layer and the lesser amount of measured growth must be accounted for by a contraction in the thickness dimension of the original sample due to the loss of nickel from the IN-100 in the formation of the outer layer. This contraction is seen to be about 0.8 mil. It should be noted that this difference between the growth and the thickness of the outer layer cannot be accounted for by the transformation of IN-100 to NiAl in the inner layer. The density of NiAl is less than that of IN-100 and, therefore, the transformation is accompanied by an expansion rather than the contraction that would be required to help account for inward movement of the original surface.

In contrast to the Type I coating, the Type II coating in Fig. 8 has carbide particles extending out to the final surface. Measurements indicated a growth of 1.5 mils, which is simply an expansion due to the addition of aluminum and the transformation of IN-100.

Except for a thin layer of blue, aluminum-rich NiAl at the surface, the coating of the sample aluminided at 0.25 amp/dm^2 is comprised primarily of brown, nickel-rich NiAl, with a thin layer of gamma phase adjacent to the matrix. The fine particles at the interface of the inner and outer layer are near to what was the original surface of the sample, and are probably TiC. The large, gray particles in the inner layer are MC carbides such as are found in the matrix, and are rich in molybdenum and chromium. The white particles in the inner layer are seen in the microprobe trace to be rich in chromium which suggests that, following the phase diagram of Taylor and Floyd[4] in Fig. 9, they are comprised of alpha phase (high chromium, high aluminum) and/or gamma phase (high chromium, low aluminum). Similar appearing particles in a sample of metallided IN-100 were labeled chromium carbide by Sanders et al.[3]

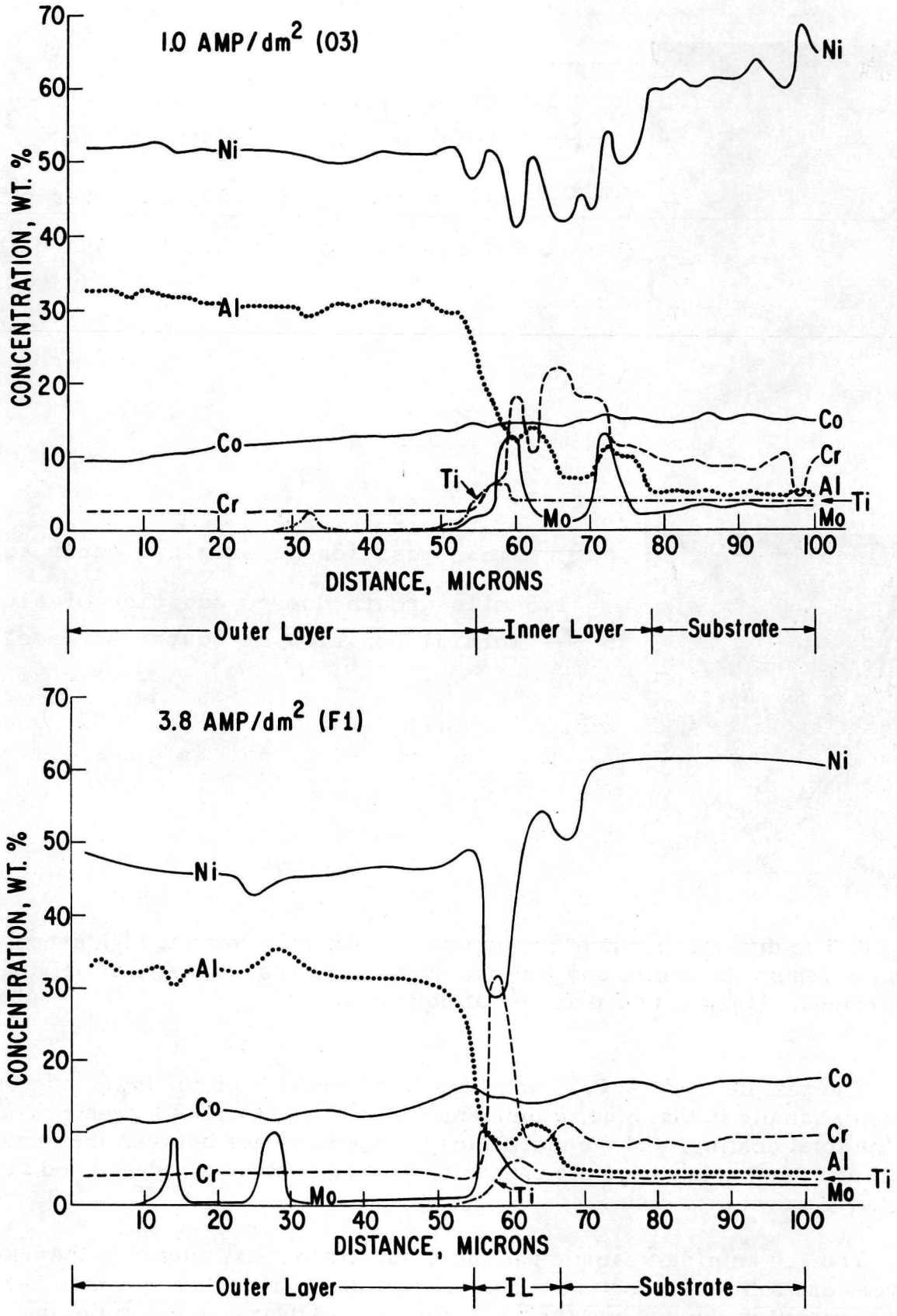

Fig. 7 Electron microprobe traces across the coating and into the substrate of discs of IN-100 aluminided at the current densities indicated.

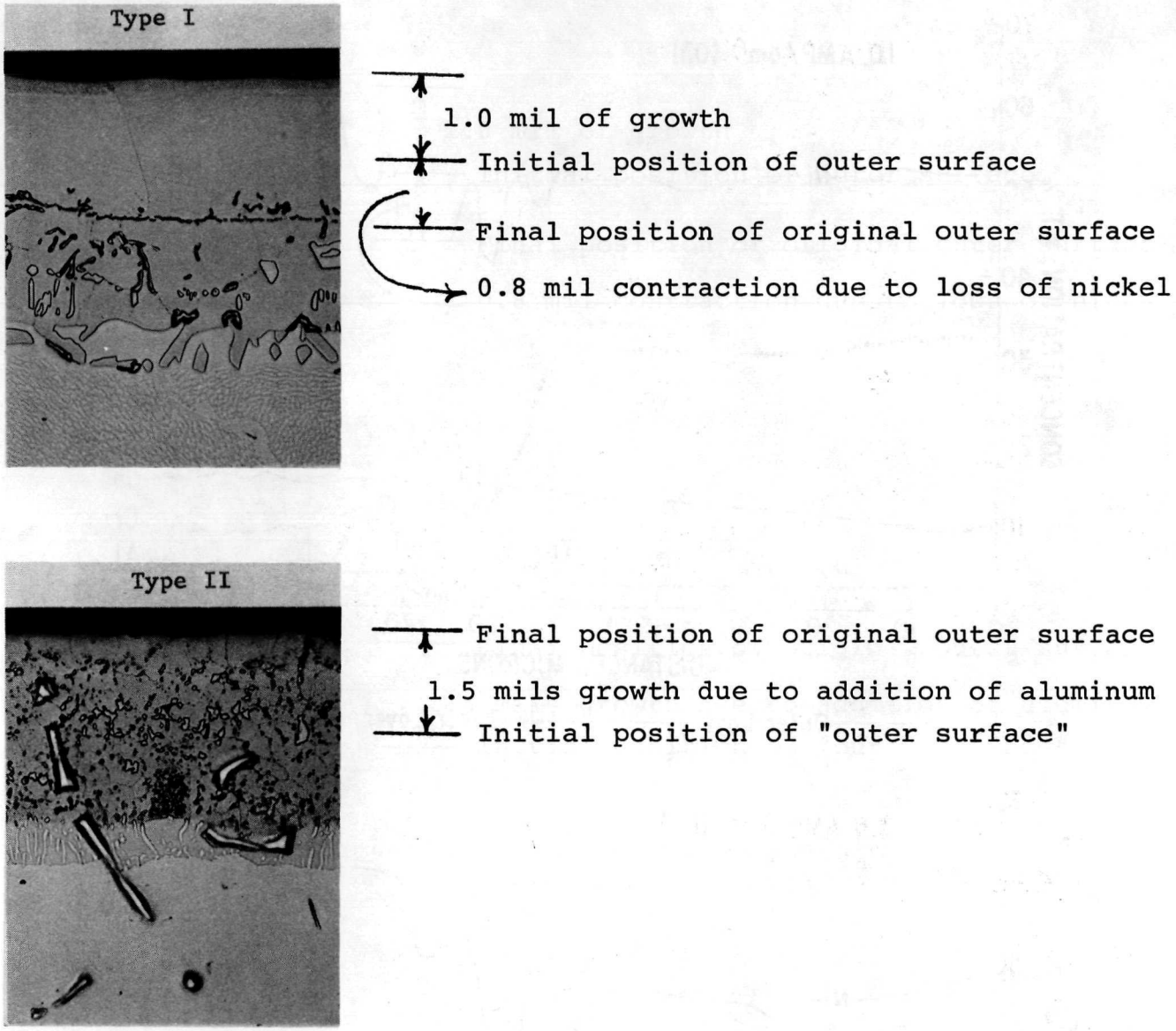

Fig. 8 The different mode of formation of coatings at low and high deposition rates results in inward and outward movement, respectively, of original surfaces. (Disk I1 at top and F1 at bottom.) 500X

The sample made at 0.75 amp/dm^2 is different from the lower current density sample in that blue, aluminum-rich NiAl comprises a greater fraction of the total coating, and the morphology of the interface between the nickel-rich NiAl and gamma has begun to change to the finger structure developed at the higher current densities.

The 1.0 amp/dm^2 sample has more substrate constitutents in the outer layer, and a finger structure has developed in the inner layer, which becomes predominant in the 3.8 amp/dm^2 sample. All of the particles in the inner layer are rich in chromium. Redden[5] identified the finger structure as sigma phase on the basis of etching characteristics and microprobe analysis. Furthermore,

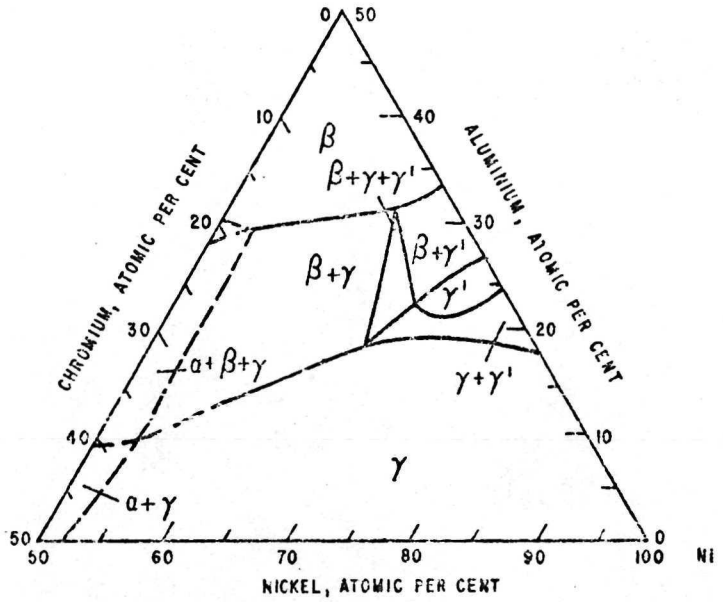

Fig. 9 The nickel-aluminum-chromium phase diagram: isothermal section for 1150°C. (4)

particles extracted by him from the inner layer were identified by x-ray diffraction as sigma. However, Sanders et al., (3) reported the fingers to be gamma phase in a Ni_3Al matrix, and Moore et al., (6) claim the fingers to be Ni_3Al in which some of the nickel is replaced by chromium and cobalt.

In Fig. 10 the 1.0 amp/dm^2 sample has been etched with a solution (100 ml H_2O, 100 ml 5% NaOH, and 5g $KMnO_4$) which is reputed by Redden(5) to stain sigma blue. The fingers are stained blue, indicating they are sigma, but there are also white, unstained particles in the inner layer which are the same alpha and/or gamma phase seen in the 0.75 amp/dm^2 sample.

The outer layer of the higher current density samples, and particularly the 3.8 amp/dm^2 sample, contains many small particles rich in either molybdenum or titanium, and these are probably MC carbide.

Debye-Scherrer patterns were obtained from samples aluminided at 0.75, 1.0, 3.8, and 8.0 amp/dm^2 by mechanically chipping off the coatings. The major phase present in the chippings from all of these samples was NiAl. Trace amounts of secondary phases were also detected, the amounts of which increased with increasing current density. One of these secondary phases is Ni_2Al_3, but since most of its strong reflections coincide with those for NiAl, the relative amount is difficult to estimate. The coating from the sample aluminided at 8.0 amp/dm^2 showed many other extra weak reflections which were not accounted for.

In Fig. 11 the specific coating thickness (Mils/Mg Al/cm^2) is plotted as a function of aluminum deposition rate (current density, amp/dm^2). The coatings formed at high current densities are richer in aluminum, and as a consequence the specific coating thickness decreases with current density. The curve can be used to approximate the amount of aluminum to add at a particular deposition rate in order to obtain a desired coating thickness. The specific volumetric

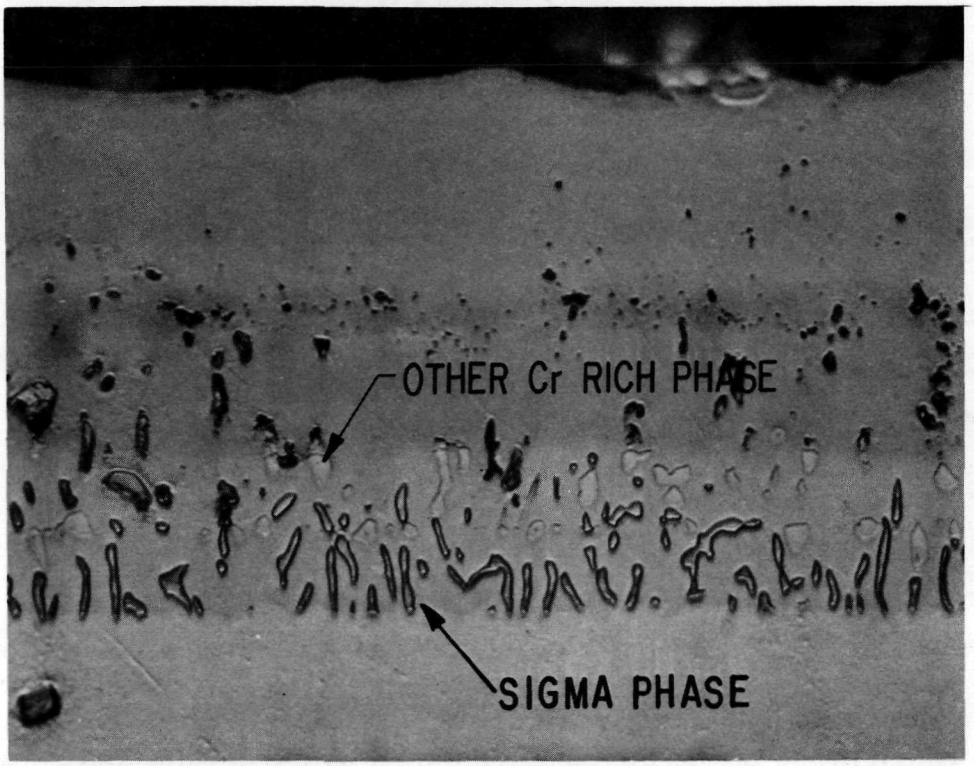

Fig. 10 Coating on disc 03 (1 amp/dm^2) etched with solution containing 5g $KMnO_4$, 100 ml 5% NaOh, and 100 ml H_2O. Sigma phase is stained blue.[5] 1000X

expansion does not greatly change with aluminum deposition rate as seen in Fig. 12. The addition of 1 mg of aluminum/cm^2 causes a net expansion of about 0.14 mils ± 0.01. The more useful function, the growth/penetration (or expansion/coating thickness) ratio is Fig. 13. It can be used to predict surface growth when an aluminide coating of a specified thickness is formed on IN-100.

Since metallided surfaces are free of the powders that adhere to pack cementation coatings, they provide an opportunity to examine the character of the coated surface. Figures 14 and 15 are scanning electron micrographs of the surfaces of samples aluminided at the current densities indicated. The sample aluminided at 0.25 amp/dm^2 is relatively smooth, with the grain boundaries being heavily delineated. The samples aluminided at 0.75 and 1.0 amp/dm^2 are rough, and the sample aluminided at 3.8 amp/dm^2 is smoother, but is rough compared to the low current density sample.

Oxidation Behavior

In Fig. 16 typical weight changes measured during the oxidation test are shown. The coated samples showed a small but continuous increase in weight throughout the test, whereas uncoated IN-100 steadily lost weight, losing over 4 mg/cm^2 during 100 hours of testing.

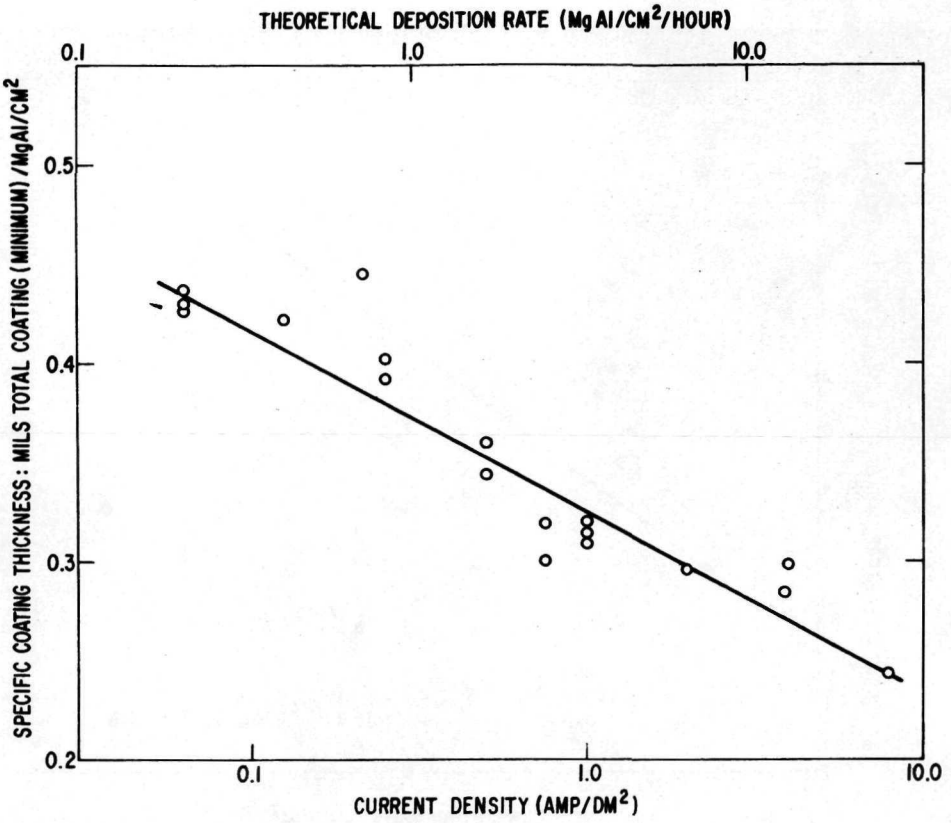

Fig. 11 Specific coating thickness vs aluminum deposition rate on IN-100.

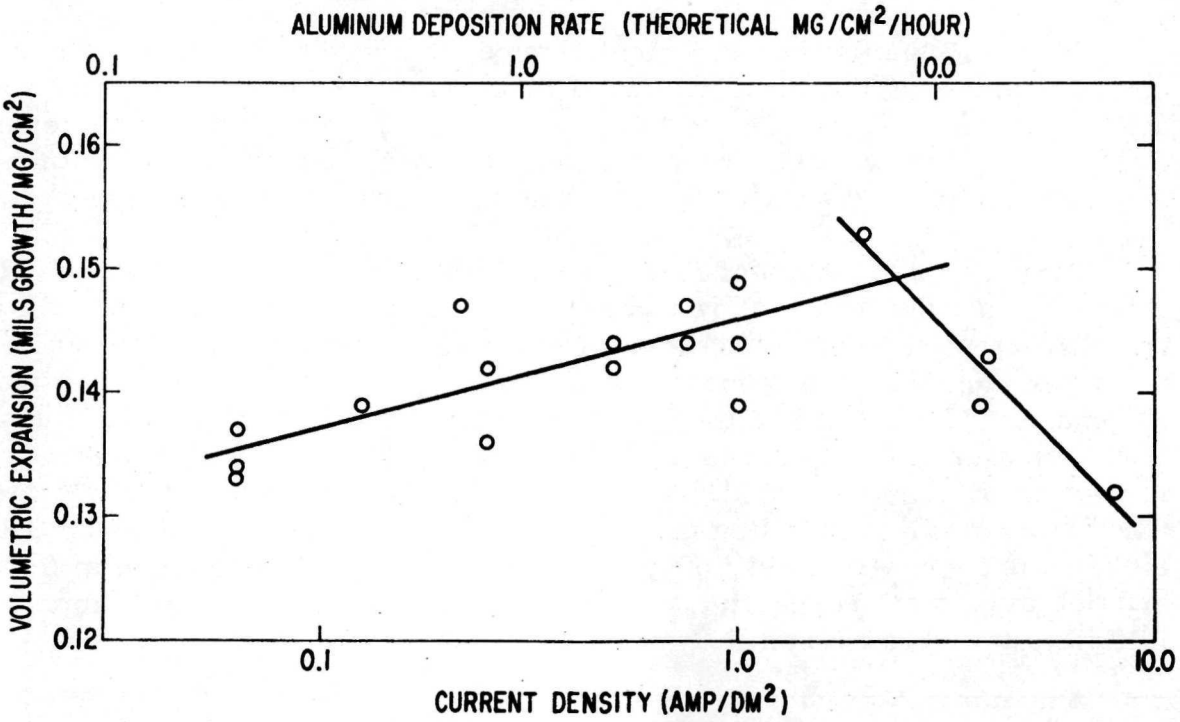

Fig. 12 Specific volumetric expansion vs aluminum deposition rate on IN-100.

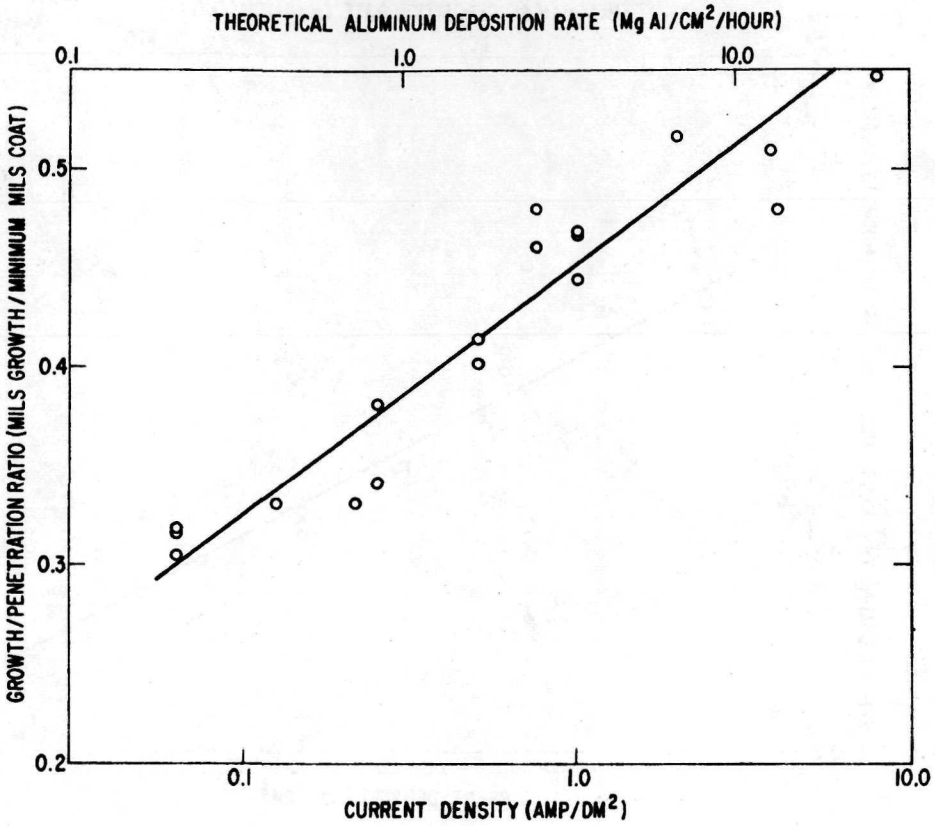

Fig. 13 Growth/coating thickness ratio vs aluminum deposition rate on IN-100.

Figure 17 shows the net weight change, averaged for each pair at the completion of the oxidation test, as a function of the current density at which the coating was made. The low activity and the high activity types separate into groups, with values for weight gain becoming erratic at current densities around 0.75 and 1.0 amp/dm^2, the transition range for the two types.

The microstructures of four samples after the 200-hour cyclic oxidation test in air at 2000°F are shown in Fig. 18. Unlike when observed in the as-metallided condition, the coatings are now very similar, consisting primarily of nickel-rich NiAl (the striated phase) and gamma phase, and differ mainly in thickness. The coating of the lowest current density sample, which was initially lowest in aluminum, decreased in thickness by 16% as a consequence of the formation of aluminum oxide on the surface. The net result of oxide formation, the further diffusion of aluminum into the substrate and the diffusion outward of nickel was a growth of 39%, 59%, and 72% for the coatings formed at 0.75, 1.0, and 3.8 amp/dm^2, respectively. The richer was the coating in aluminum initially, the greater was the growth.

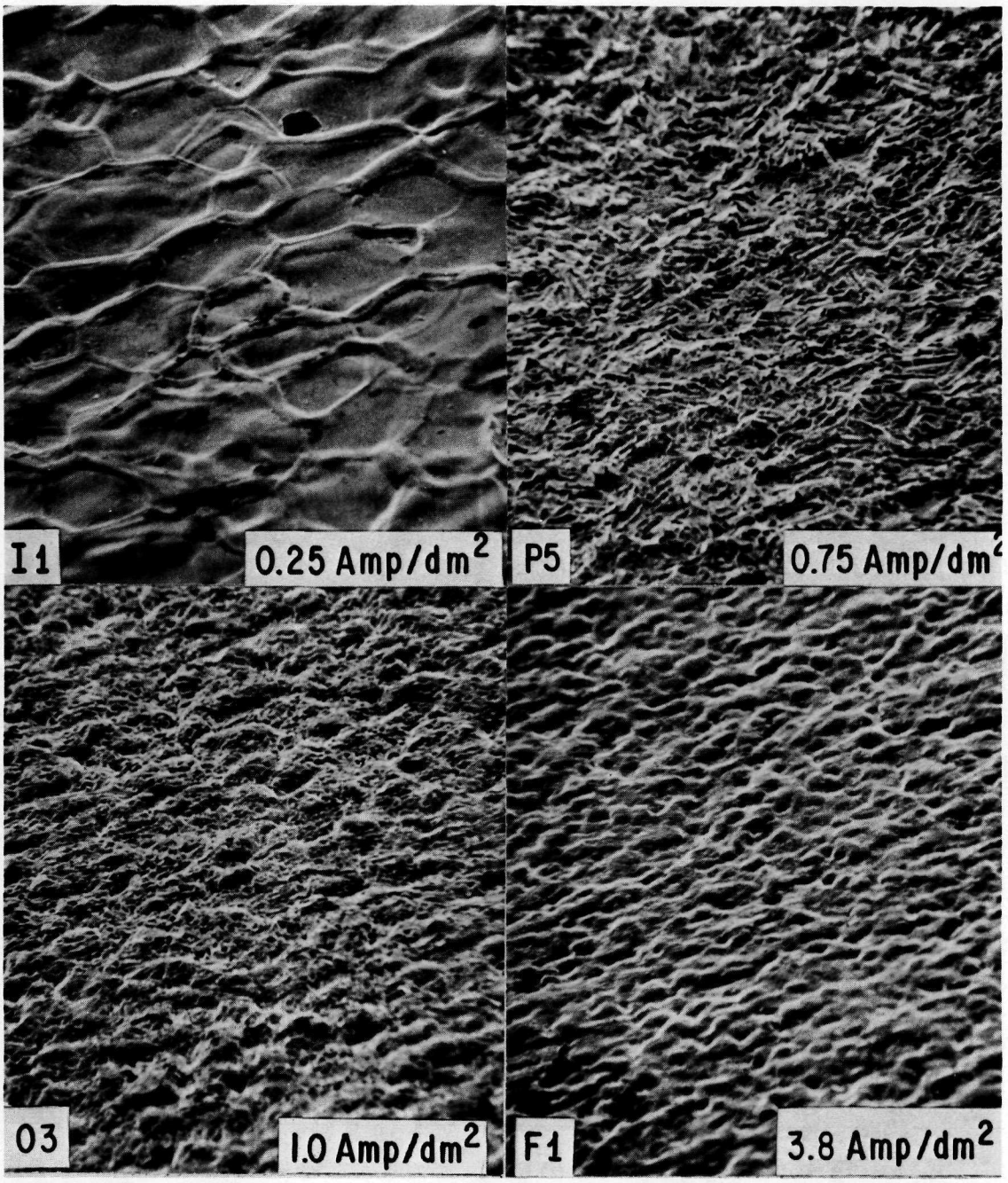

Fig. 14 Scanning electron micrographs of the surface of IN-100 discs aluminided at the current densities indicated. 250X

Due to the lack of contrast with the mounting material, the oxide scale is barely visible in the photomicrographs shown in Fig. 18. It is between 5 and 10 microns thick and is comprised of alpha Al_2O_3, TiO_2 (rutile) and a lesser amount of an oxide with a spinel structure (M_3O_4) and a lattice parameter of 8.13Å.

The microstructures show two different layers of carbide particles, the microprobe indicating that the smaller particles, which are nearer the surface,

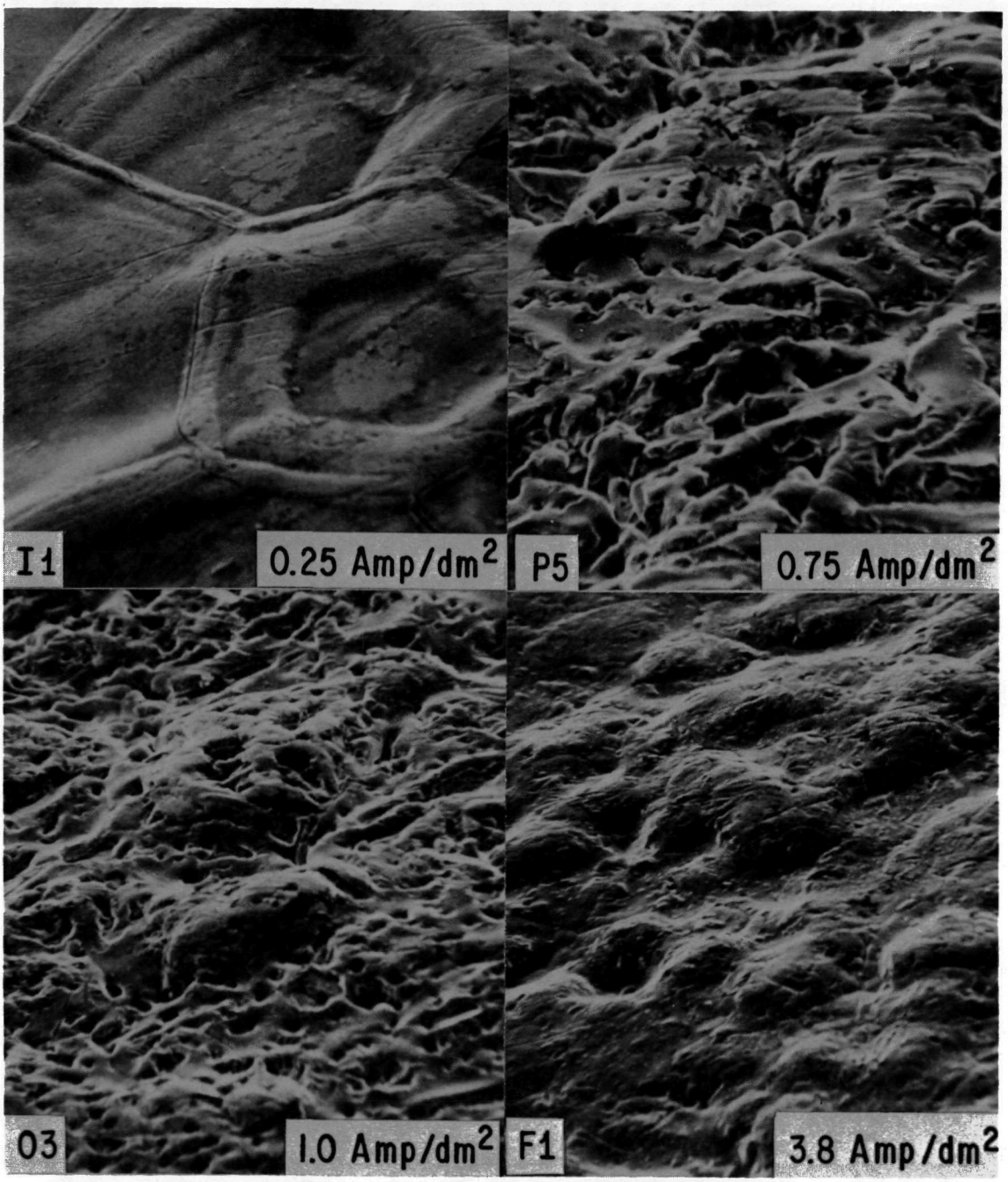

Fig. 15 Scanning electron micrographs of the surface of IN-100 discs aluminided at the current densities indicated. 1250X

are primarily TiC. The coarser particles near the base alloy have about a 2 to 1 ratio between Ti and Mo, and also contain about 4% V.

The grain boundary provides a preferential diffusion path for aluminum outward during oxidation as is apparent in the phtomicrographs. The narrow regions of gamma separating the darker nickel-rich NiAl phase frequently contain a grain boundary.

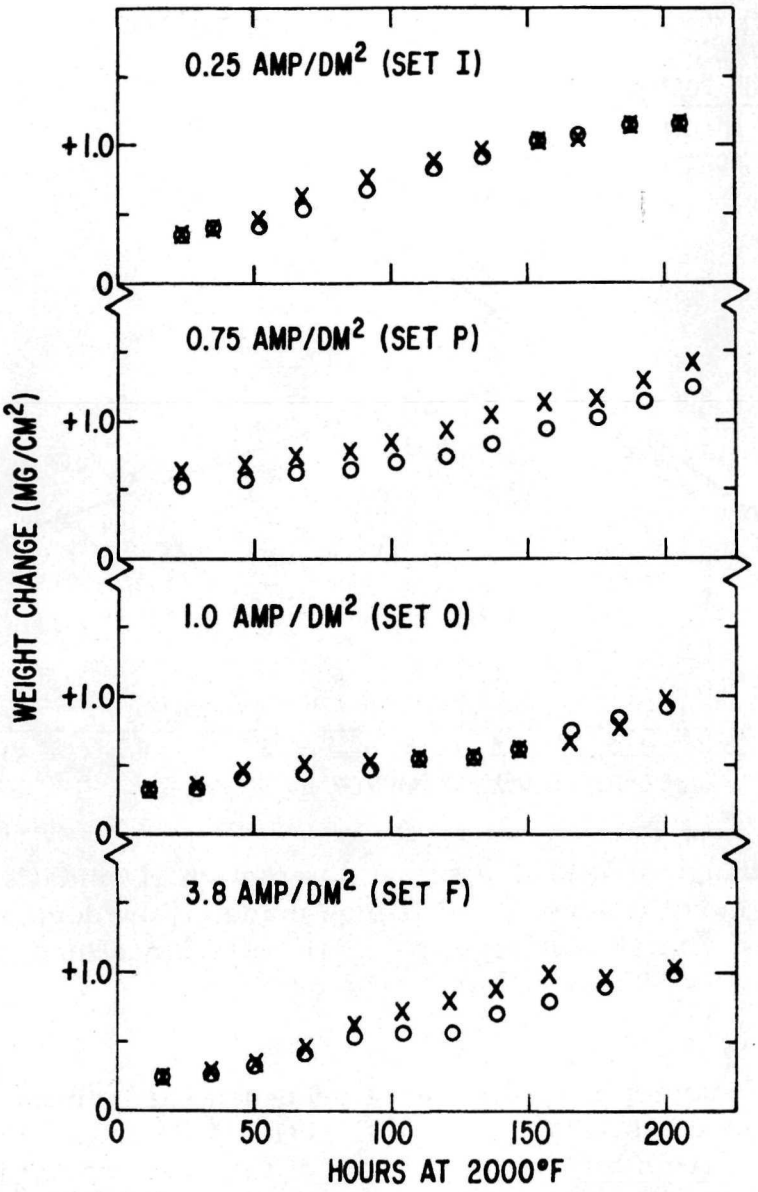

Fig. 16 Weight change of aluminided IN-100 discs during oxidation test.

Microprobe traces across the coating of the four samples in Fig. 18 are given in Figs. 19 and 20. The compositions of the striated, nickel-rich NiAl phase and the gamma phase are summarized in Table IV (page 27).

In the samples aluminided at 1.0 and 3.8 amp/dm^2 (Fig. 18) are small white particles in the same region as the coarse carbide particles. The microprobe traversed one of these particles in the F2 sample (Fig. 20) at a distance of about 90 microns below the surface. It is seen to be rich in chromium, and the etching characteristics[5] (dark brown in 100 ml H_2O, 100 ml 5% NaOH solution, and 5g $KMnO_4$) suggest that these particles are primarily Cr_6C.

Many of the samples showed one or more small areas of localized failure of the coating in the form of a surface eruption at the conclusion of the oxidation test. Examples of such areas are shown in Fig. 21. Many of these are too small to be seen with the unaided eye, whereas those on the I3 disc, (a), are readily

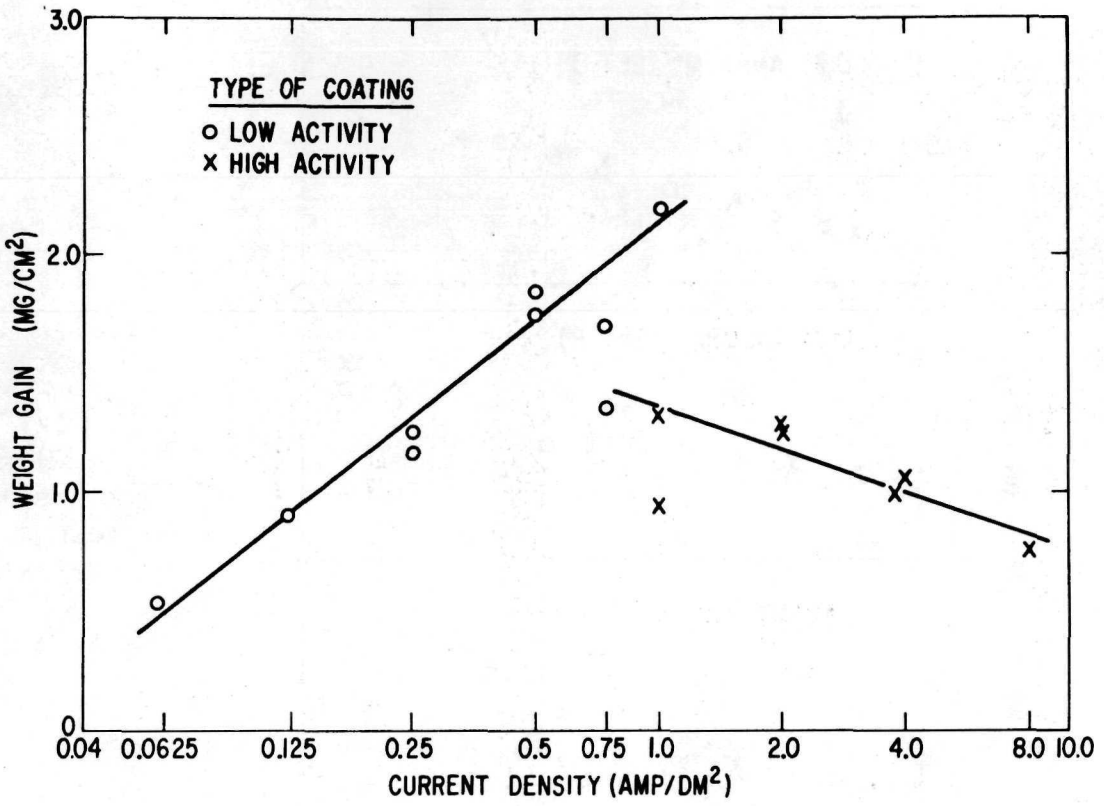

Fig. 17 Net weight change of IN-100 discs at completion of oxidation test vs aluminiding current density. Coatings made at low deposition rates are "low activity" type or Type I, whereas those made at high deposition rates are "high activity" type or Type II.

visible. Frequently, these surface eruptions were preceded early in the test by the appearance of small blue areas. The x-ray diffraction pattern of scrapings taken from a blue area indicated a high concentration of the same spinel that was previously found dispersed throughout the surface scale. Subsequent efforts to identify the metallic ions in the spinel with the electron microprobe were unsuccessful.

Hot Corrosion Behavior

Uncoated IN-100 showed some deterioration after the first few hours and was severely corroded when removed after 14 hours of testing. All of the coated samples survived longer than the uncoated samples, but failed well before the end of the 400- hour test, as shown in Table V. The coatings made at the higher current densities (0.75 to 4.0 amp/dm^2) are superior to those made at the four lower current densities (0.06 to 0.75 amp/dm^2) the exception being the coating made at 8.0 amp/dm^2. Metallographic examination of this sample after hot corrosion testing indicated that the corrosion was accompanied by cracking and spalling of the coating, which was exceedingly brittle.

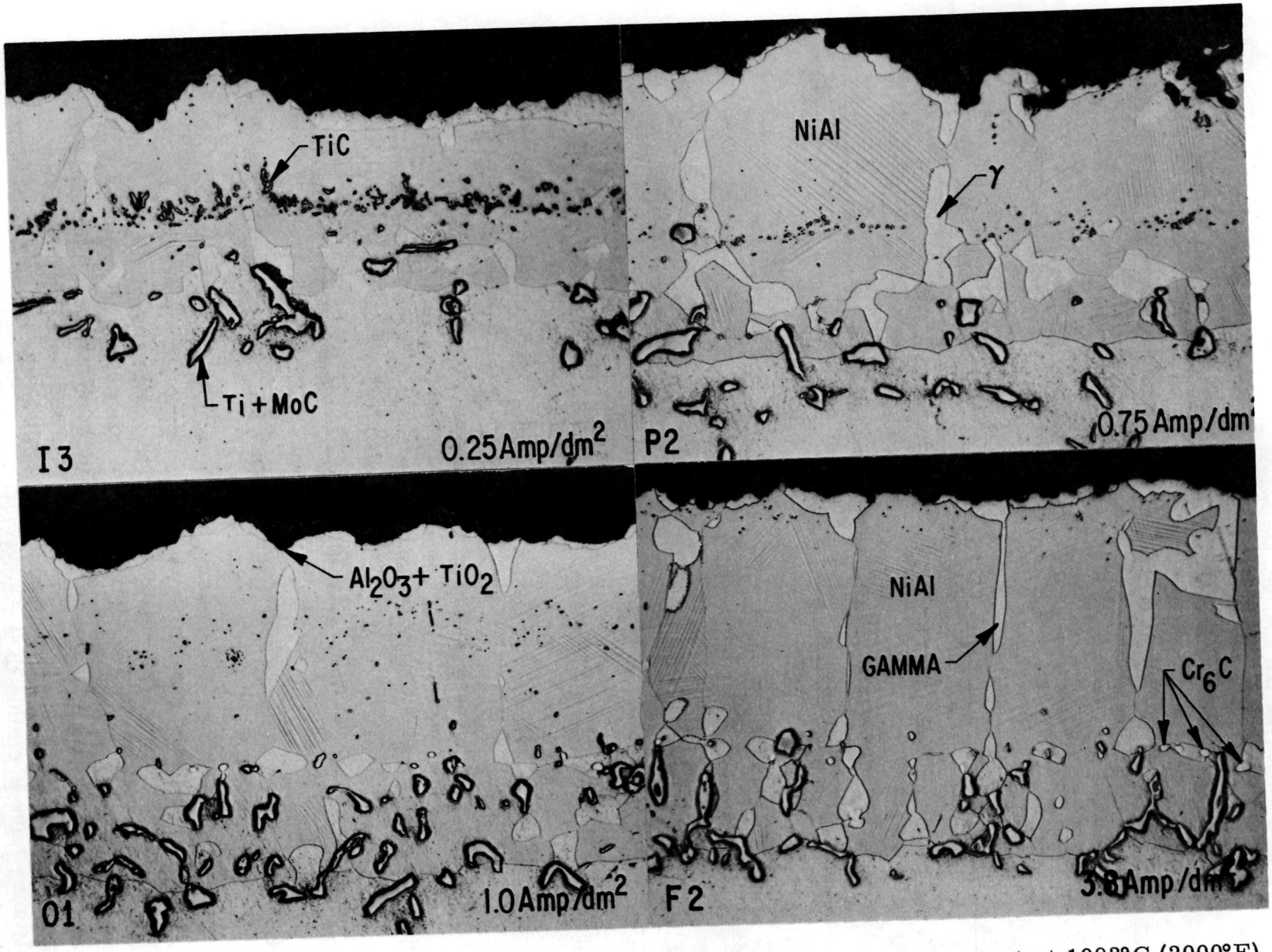

Fig. 18 Photomicrographs of IN-100 discs after 200 hour cyclic oxidation test at 1093°C (2000°F). 500X
Discs were aluminided at the current densities indicated.

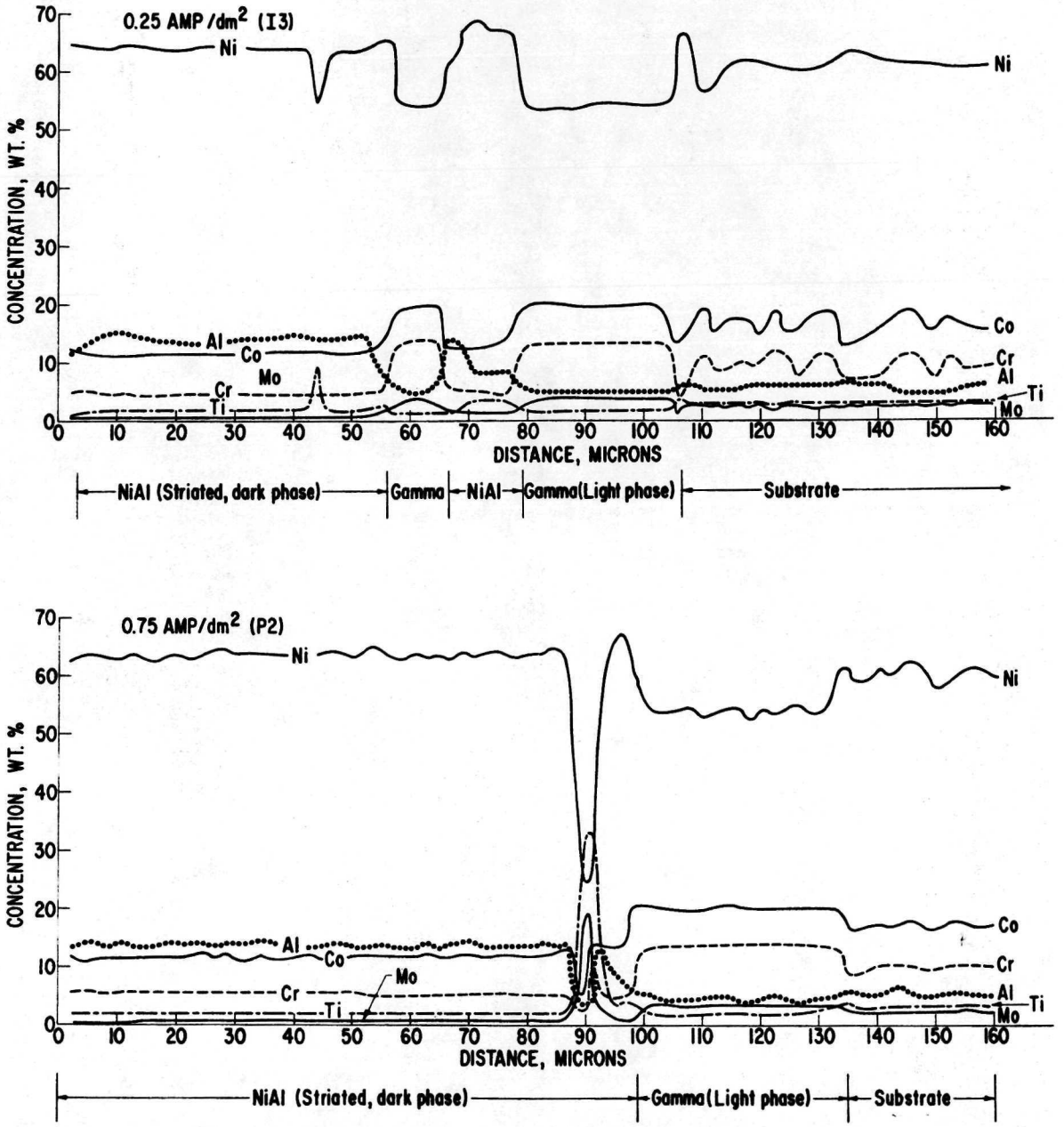

Fig. 19 Electron microprobe traces across the coating and into the substrate of IN-100 discs after oxidation test.

Photographs of four discs after corrosion testing are shown in Fig. 22. Frequently, the corrosion was observed to begin near the center hole. Once started, the attack spread rapidly through the hole to both sides of the disc. However, a disc was usually not removed from test until it was being attacked in more than one area. This apparent weakness of the coating in the vicinity of the hole may have been due to the necessity of supporting the disc on a hook in the hole during coating, or to casting defects, such as porosity.

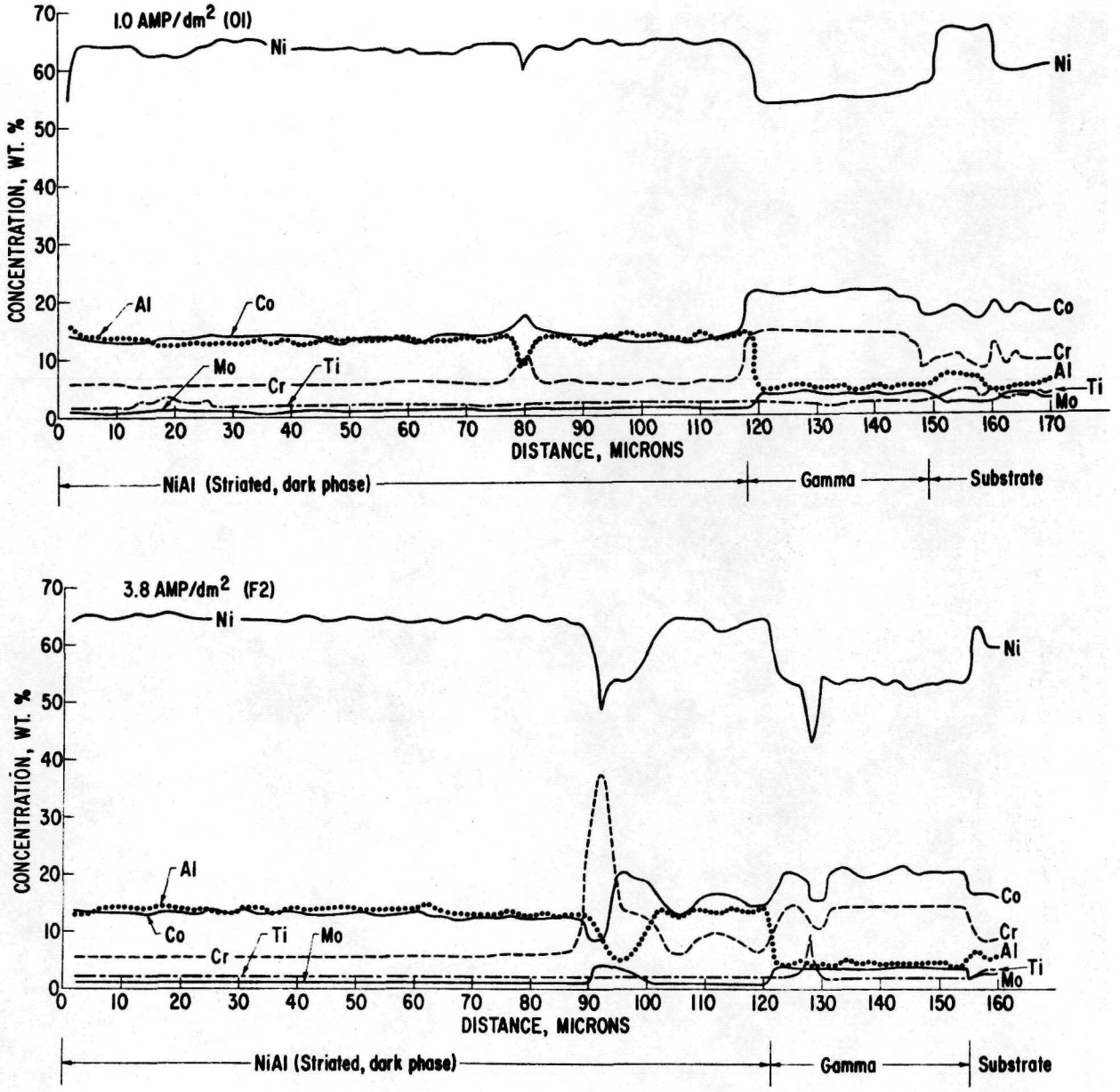

Fig. 20 Electron microprobe traces across the coating and into the substrate of IN-100 discs after oxidation test.

TABLE IV

Coating Composition after Oxidation Testing

	%Ni	%Al	%Cr	%Co	%Mo	%Ti	%V
Striated NiAl	64	14	5.5	12	1	3	0.5
Gamma	54	5	14	20	3.5	3	1.0

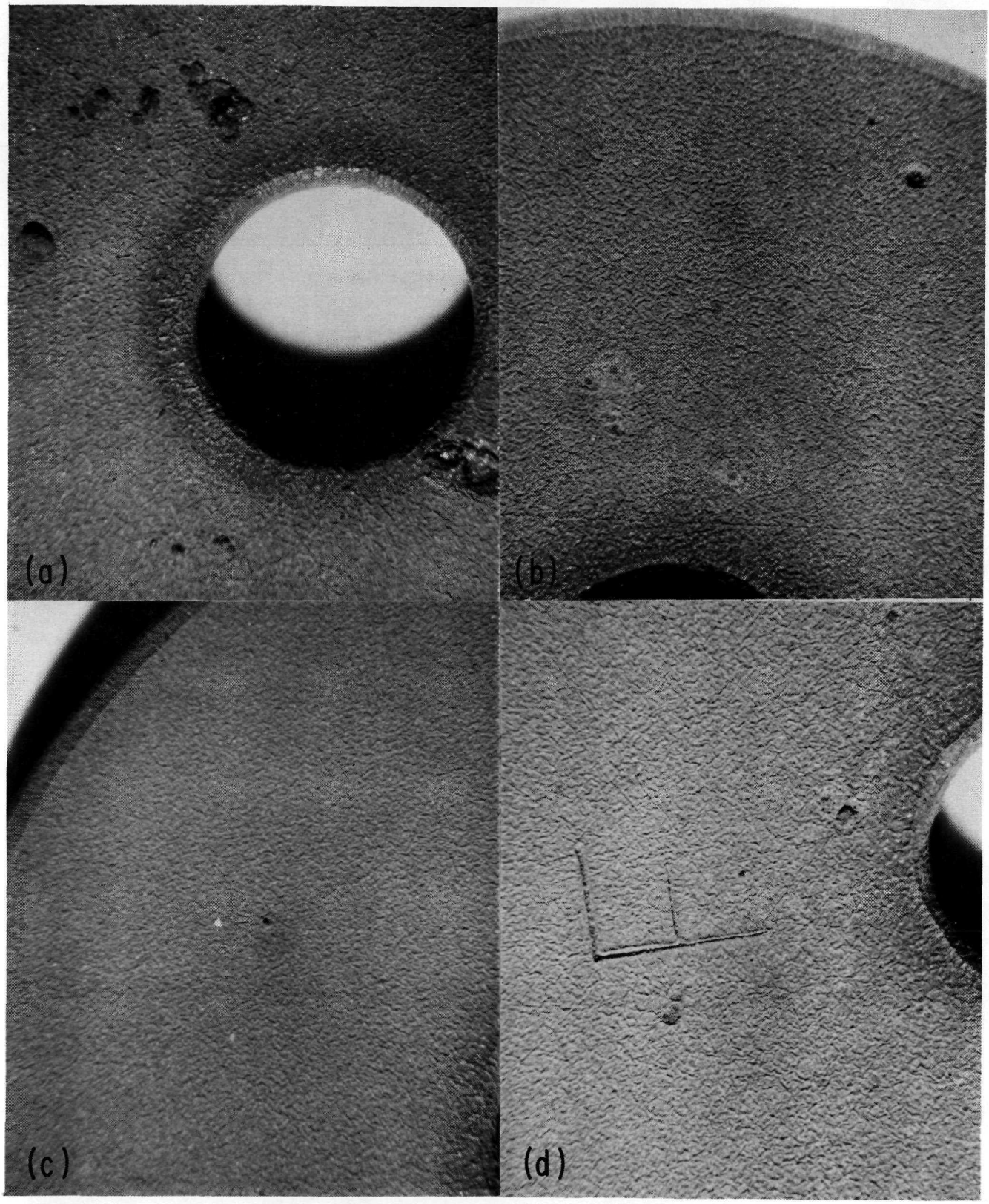

Fig. 21 Surface of discs after oxidation test: (a) Disc I3 (0.25 amp/dm^2); (b) Disc P2 (0.75 amp/dm^2); (c) Disc 05 (1.0 amp/dm^2); (d) Disc F2 (3.8 amp/dm^2). 10X

TABLE V

Hot Corrosion Tests of Coated and Uncoated IN-100

Set	Amp/dm^2	Disc No.	Time (hrs)	Avg. Time (hrs)
L	0.0625	2	22	
		3	38	30
U	.125	4	61	
		5	38	50
I	.250	4	38	
		5	38	38
Z	.50	4	98	
		5	29	63
P	.75	3	83	
		4	171	127
O	1.0	2	141	
		4	163	152
K	2.0	4	132	
		5	83	108
F	4.0	4	126	
		5	209	168
V	8.0	1	83	
		2	38	60
T	0.5 + 4.0	1	83	
		4	141	112
Uncoated		1	14	
		2	14	14

Higher magnification photographs (10X) of corrosion at the outer edges of the companion discs of those in Fig. 22 are shown in Fig. 23. A cross-section through one of the protrusions on I4 is seen in Fig. 24. While the coating itself has been severely attacked, only slight attack of the alloy substrate has occurred. A higher magnification view of the coating-corrosion product interface is shown in Fig. 25. Numerous examples of such apparent preferential attack of the coating having been observed.

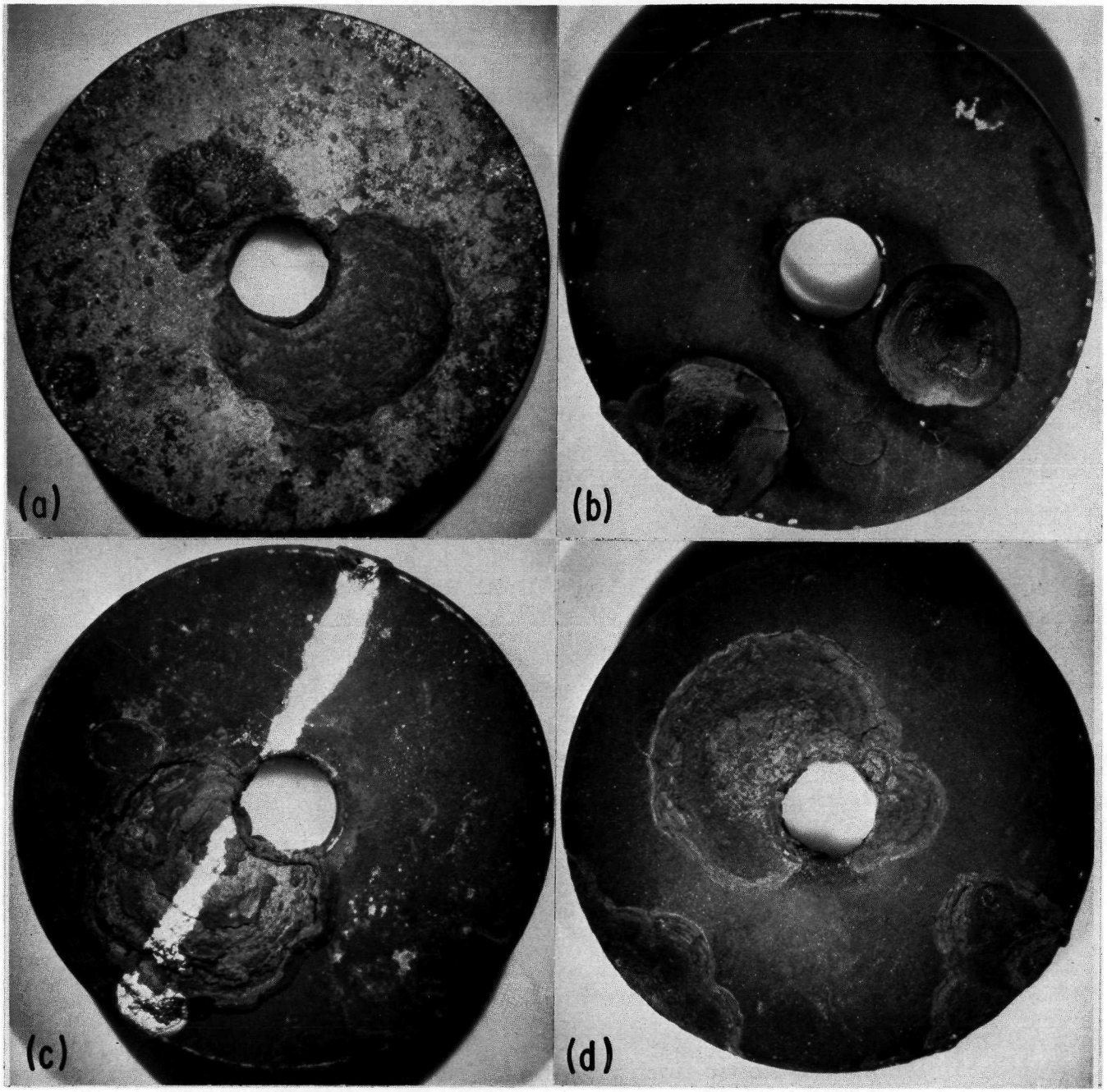

Fig. 22 Discs after hot corrosion testing: (a) Disc I5 - 38 hours; (b) Disc P3 - 83 hours; (c) Disc 02 - 141 hours; (d) Disc F5 - 209 hours. ~3.5X

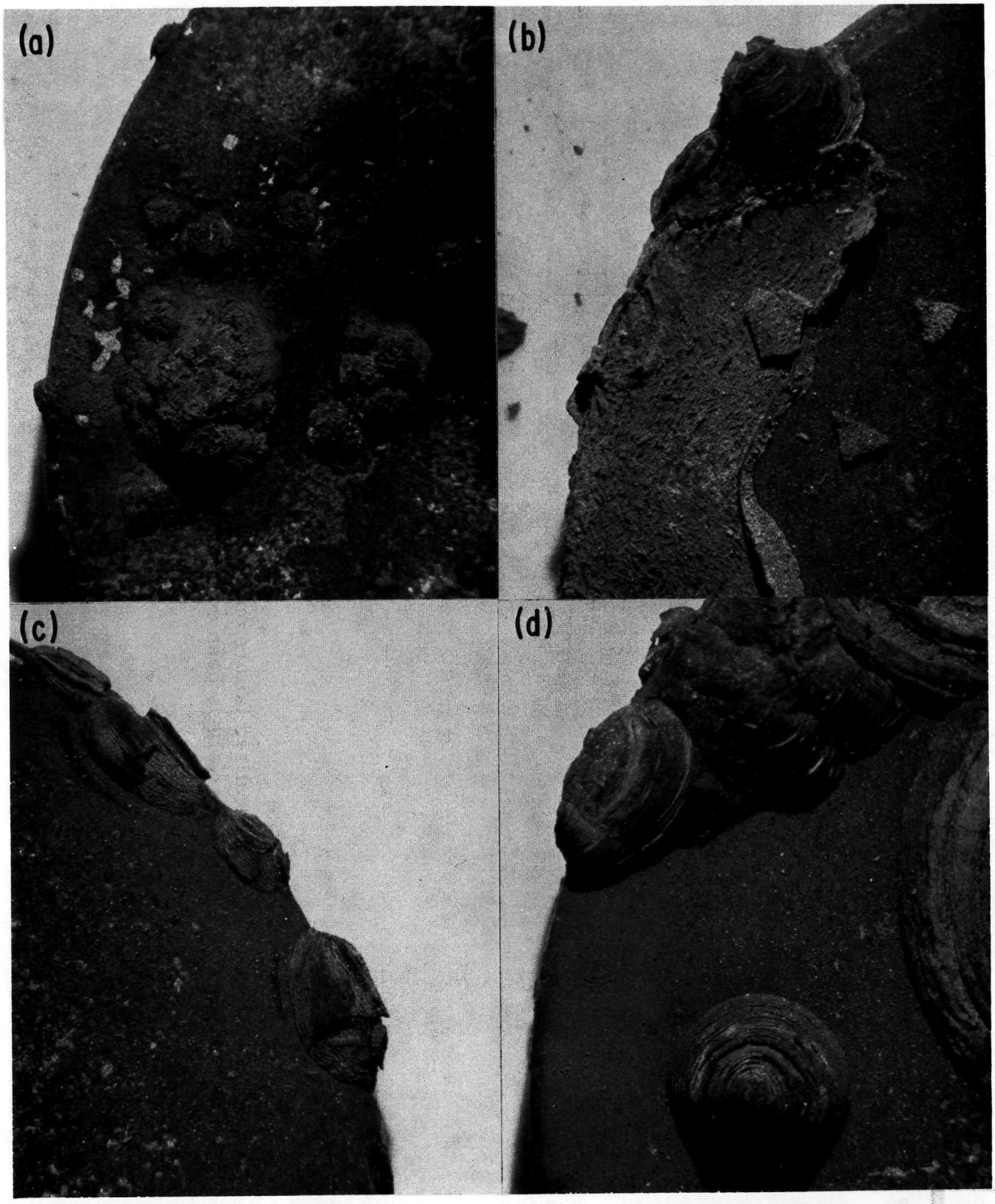

Fig. 23 Higher magnification view of edges of companion discs of those shown in Fig. 22: (a) I4; (b) P4; (c) O4; and (d) F4. 10X

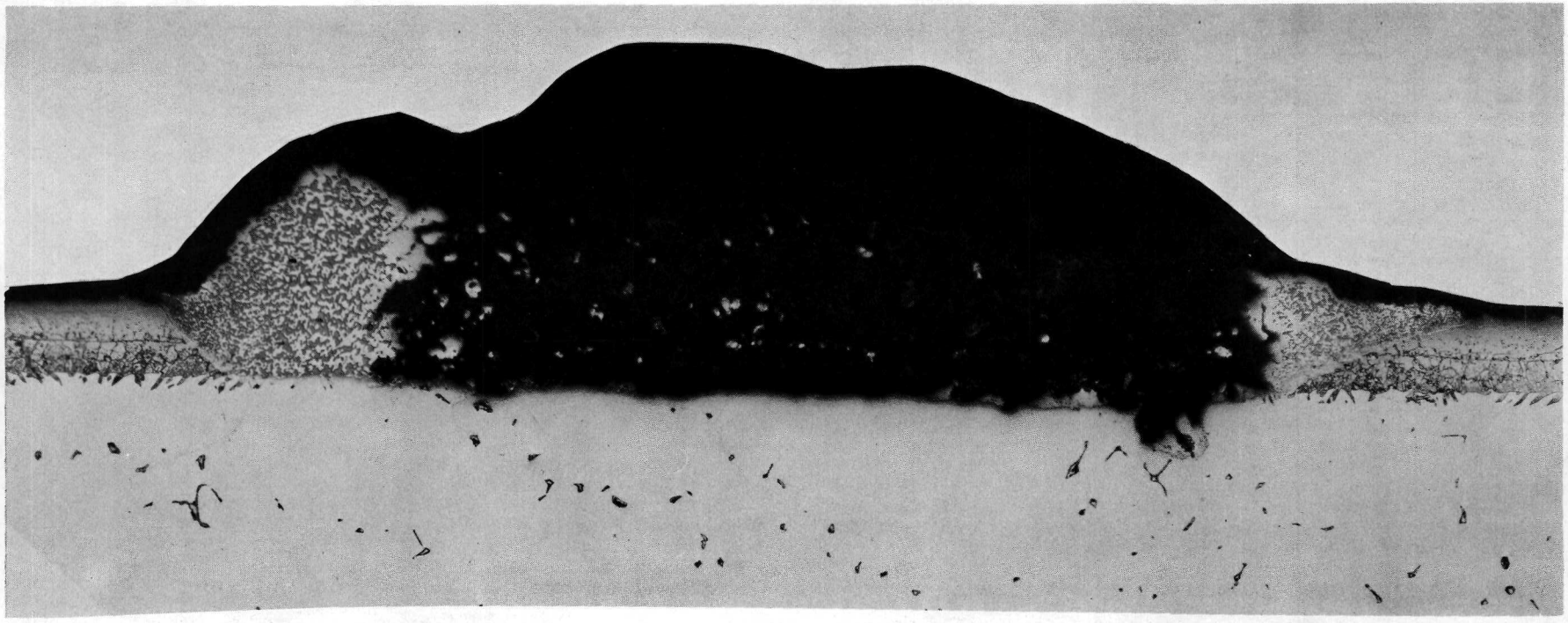

Fig. 24 Cross-section through area of localized failure on Disc I4 (Fig. 23a). The portion of the photomicrograph containing the mounting material has been cut away so as to show the oxide. 150X

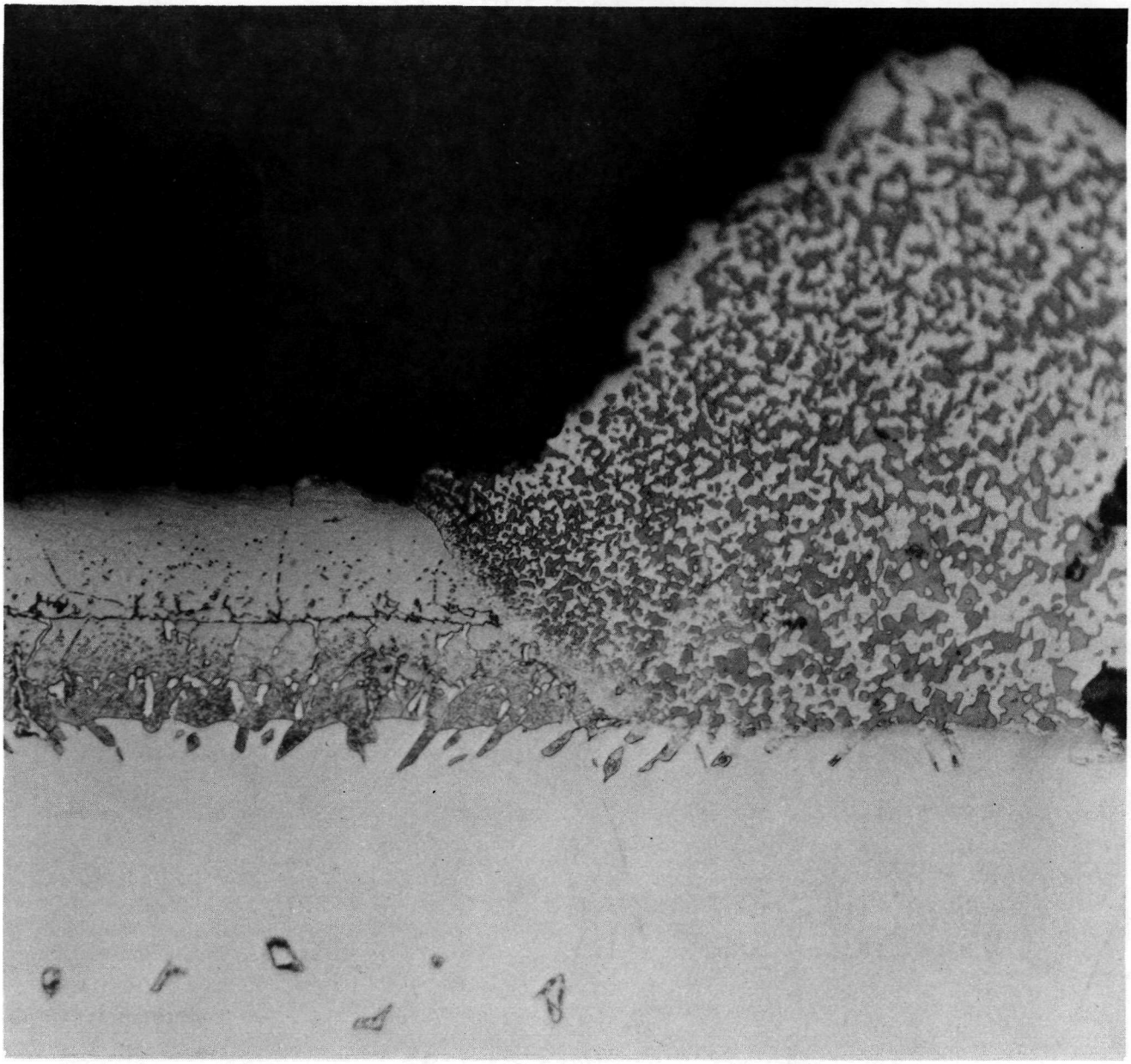

Fig. 25 Higher magnification view of interface between coating and corrosion product in same area shown in Fig. 24. 500X

Task II: Al-Si Simultaneous Deposition

Coating Characteristics

The metalliding parameters and characteristics of the coatings are listed in Table VI. The coatings made at a current density of 0.2 amp/dm^2 were done overnight and the discs were not rotated. The silicon content, as determined by x-ray fluorescence, represents an average value for the surface layers of the coating, whereas the values given for the electron microprobe are the maximum concentrations found in the outer layer.

TABLE VI

Simultaneous Deposition of Al and Si:
Metalliding Parameters and Coating Characteristics

Set	C. D. (amp/dm^2)	Hours	COATING mg/cm^2	COATING mils	COATING %Si-XRF	COATING %Si-EMP	Remarks
Z	0.50	7.0	7.03	2.5	0	0	Ni_2Al_3 anode
AA	.50	7.0	7.96	2.9	< 0.5	0	Added about 2.4 g SiF_4
AB	.19	14.8	6.74	3.1	< 0.5	-	Added about 2.4 g SiF_4
AC	.50	7.0	7.59	2.9	0	-	Added about 2.4 g SiF_4
AD	.20	14.9	4.03	2.1	1	0.5	Added about 2.4 g SiF_4
AE	.50	7.0	-17.6	1.7	4	-	Added about 12 g of SiF_4; dendritic crystals on surface.
AF	.20	15.6	7.49	3.4	< 0.5	-	
AG	.20	16.1	8.02	3.7	1	-	
AH	.20	16.0	7.28	3.5	2	1.5	
AI	.50	7.0	6.15	2.6	2	2.7	
AJ	.20	16.6	-36.2	1.5	6	21.0	Added about 5 g of SiF_4; dendritic crystals on surface.
AK	.50	7.0	4.68	2.9	5	15.2	

Initial Bath: LiF + 0.003 AlF_3 at 1100°C

Anode: Pyrolytic Graphite

It is evident in Fig. 26 that the graphite anode and the addition of SiF_4 made a marked change in the microstructure of the coatings as compared to the microstructure of disc Z3 (aluminided only). Additional micro-constituents appear in the outer layer and white phase in the inner layer has a different shape and is more profuse.

Electron microprobe traces for 6 discs are shown in Fig. 27 through 32. Many of the discs (but not the Z3 disc) show concentrations of Ti in the outer layer,

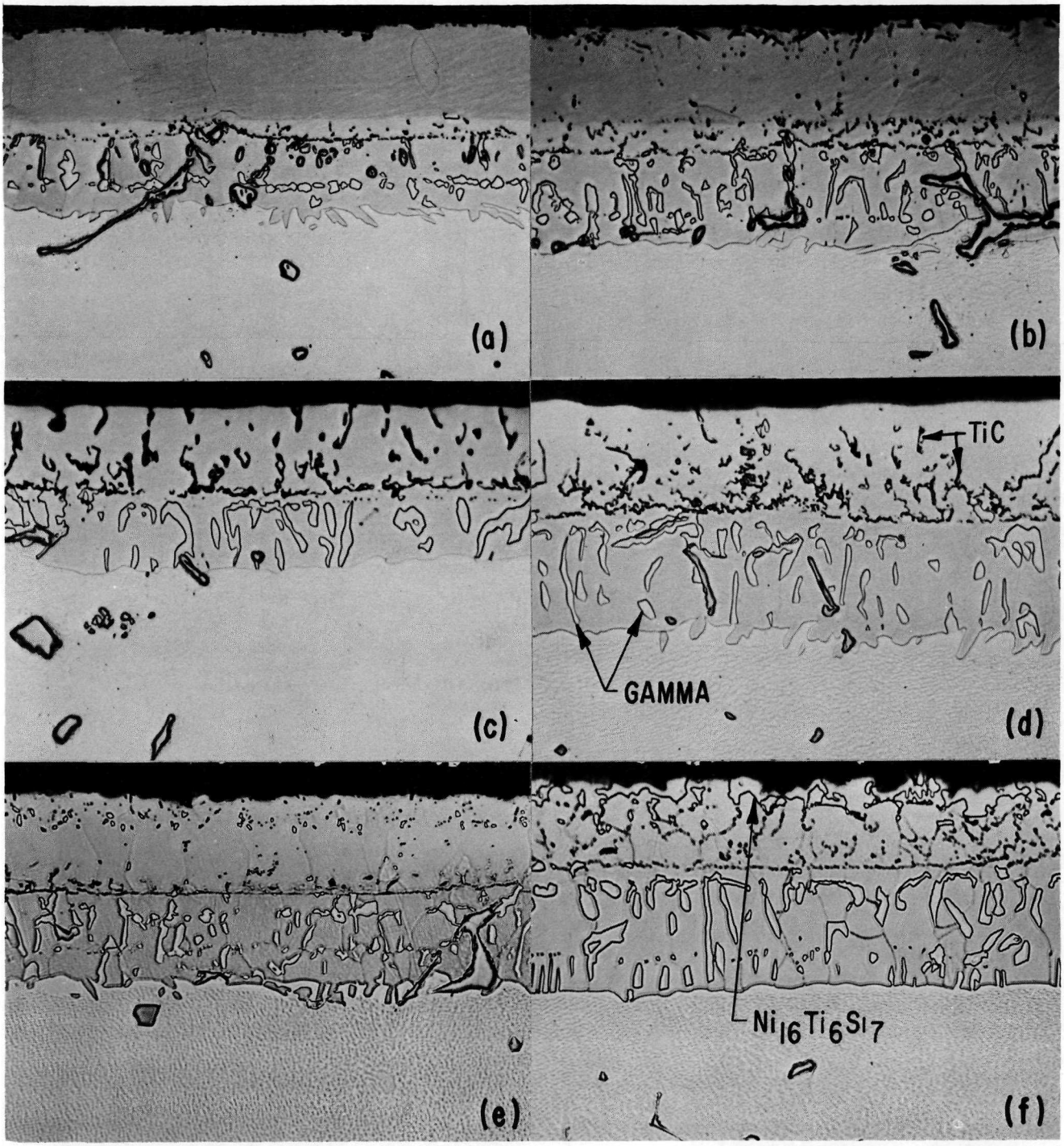

Fig. 26 Photomicrographs of coatings on IN-100. Disc Z3 was aluminided whereas aluminum and silicon were simultaneously deposited on the others: (a) Z3, 0.5 amp/dm^2; (b) AA4, 0.5 amp/dm^2; (c) AD3, 0.2 amp/dm^2; (d) AH4, 0.2 amp/dm^2; (e) AI4, 0.5 amp/dm^2; (f) AK1, 0.5 amp/dm^2. 500X

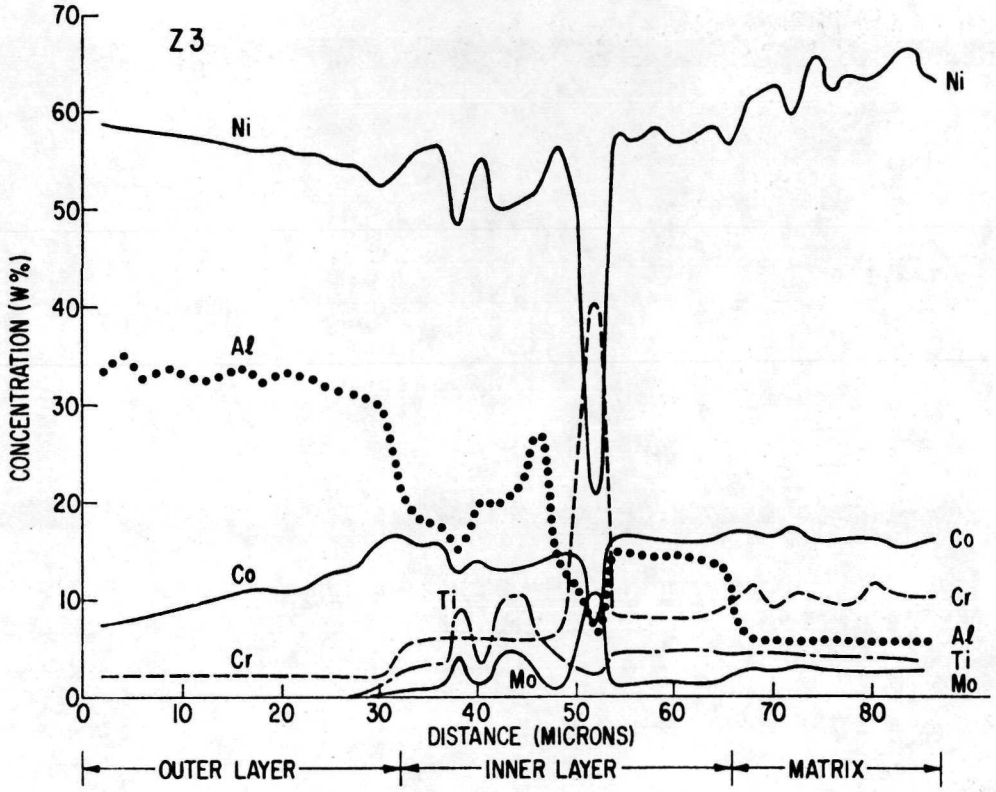

Fig. 27 Electron microprobe trace of coating on Disc Z3, aluminided at 0.5 amp/dm^2.

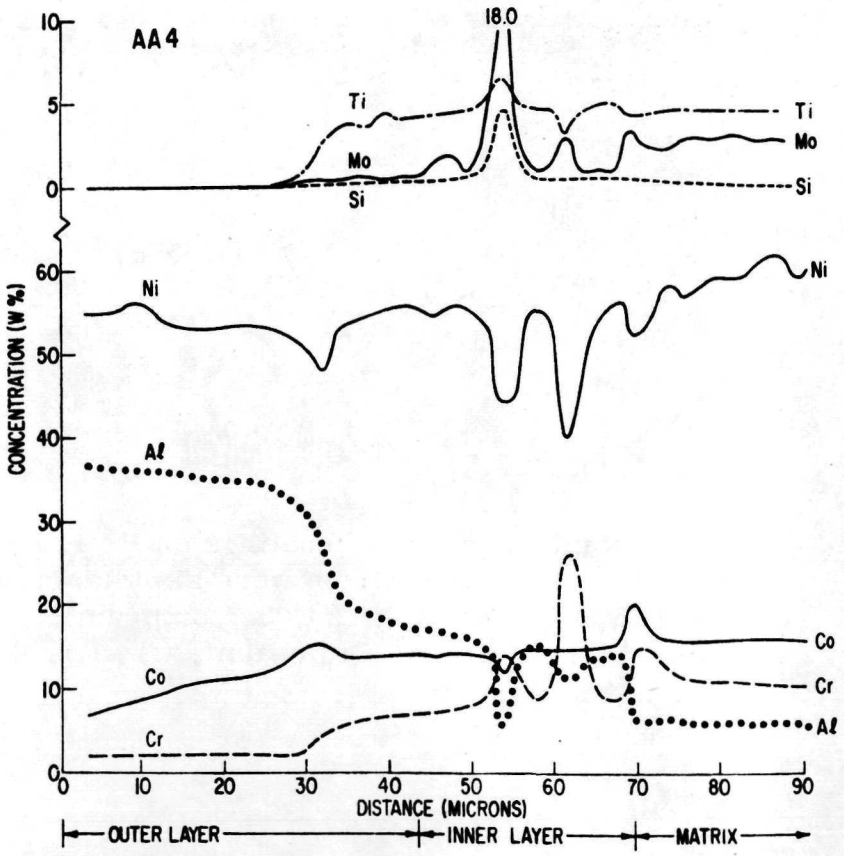

Fig. 28 Electron microprobe trace of coating on Disc AA4, aluminded-silicided at 0.5 amp/dm^2.

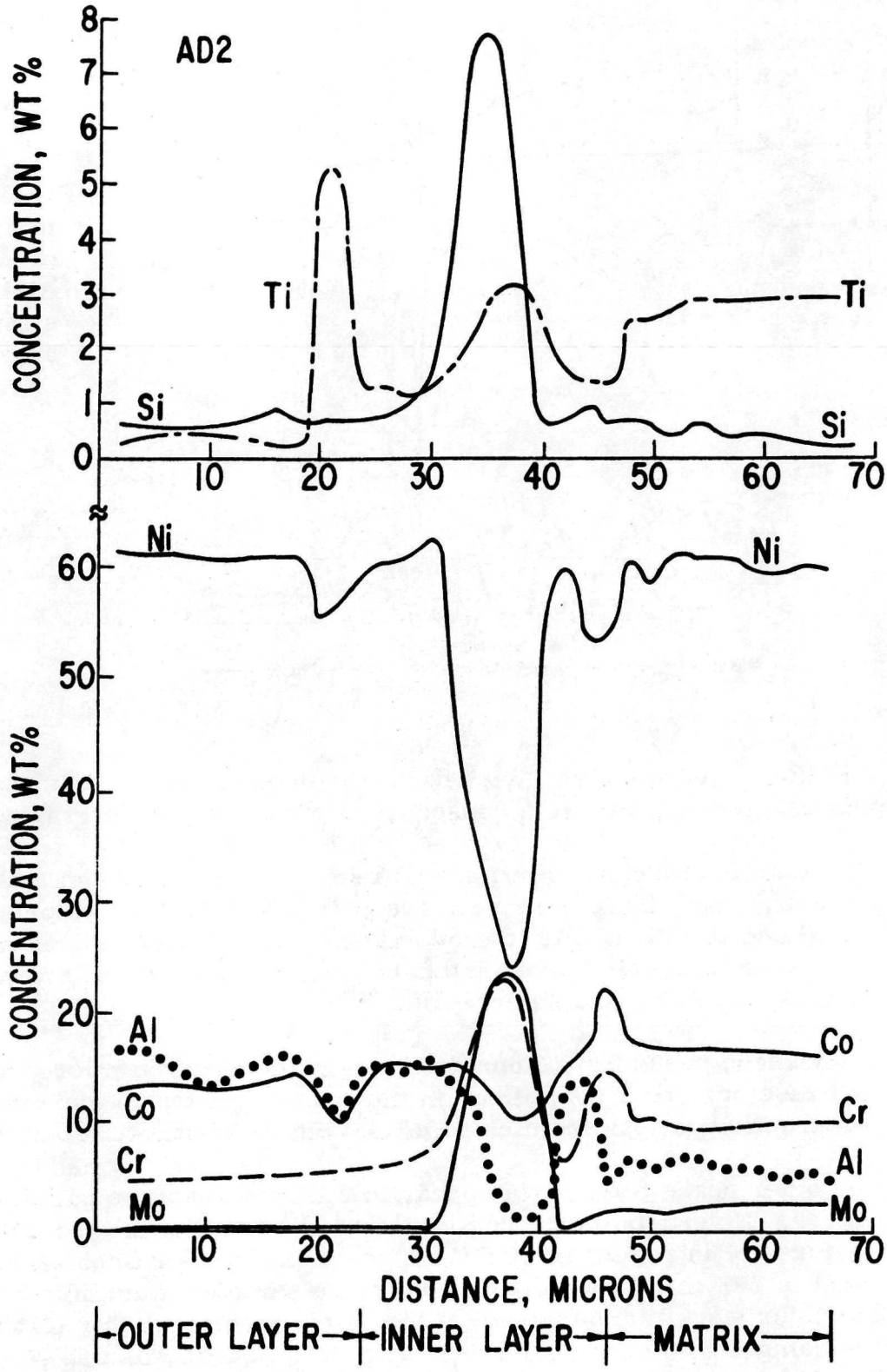

Fig. 29 Electron microprobe trace of coating on Disc AD2, aluminided-silicided at 0.2 amp/dm^2.

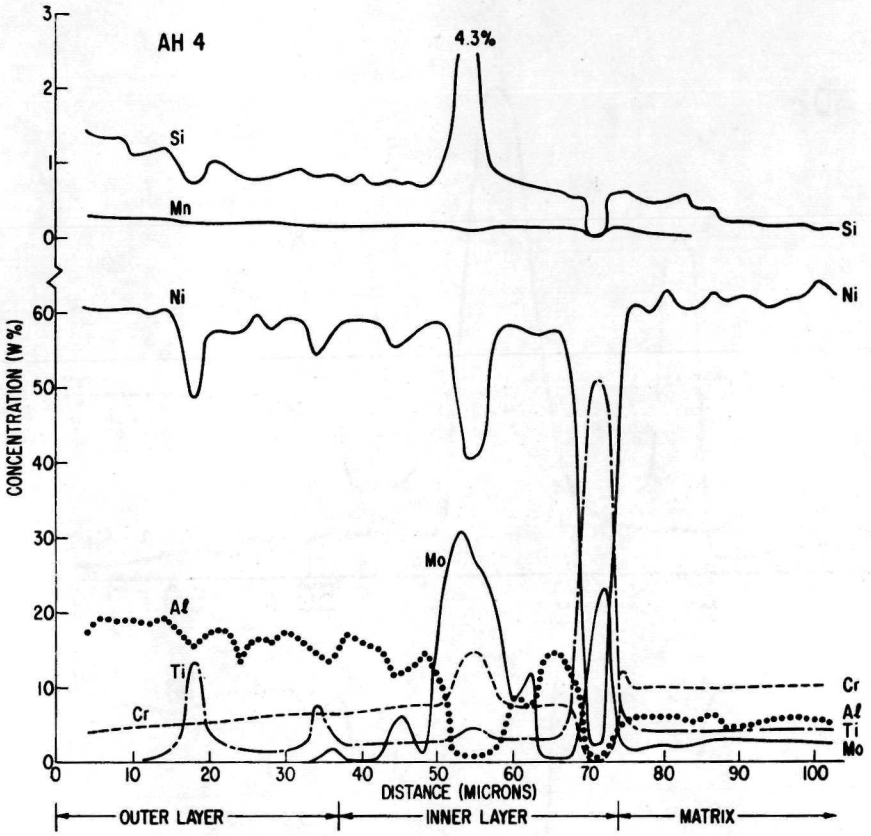

Fig. 30 Electron microprobe trace of coating on Disc AH4, aluminided-silicided at 0.2 amp/dm^2.

and it is likely that the small dark particles seen in the outer layers (Fig. 26) are titanium carbide, formed as a consequence of the use of the graphite anode.

The aluminum content of all of the discs other than Z3 and AA4 are low, being 20% or less. While the outer layer of Z3 and AA4 is comprised primarily of blue, aluminum-rich NiAl, the others show only brown, nickel-rich NiAl. The electron microprobe traces indicate that the solubility of silicon in nickel-rich NiAl is between 1 and 2 percent.

Pronounced peaks for silicon are seen in the electron microprobe traces. The AK1 disc has about 15% silicon in the phase adjacent to the surface, and the x-ray diffraction pattern from chips of this phase identified it as $Ni_{16}Ti_6Si_7$.

The other peaks for silicon appear to be from the white particles in the inner layer. No silicon was found in the white particles in disc Z3 which was made before the introduction of SiF_4. The presence of silicon in the white particles was found in 7 of the 8 traverses made on the samples aluminided with SiF_4 additions, the exception being one of the two traverses on the AI4 disc. The average composition of the particles containing silicon was 35% Ni, 18% Cr, 6% Ti, 21% Mo, 11% Co, 3% Al, and 5% Si. This phase is probably gamma, although because of the size of the beam and the smallness of the particles these compositions must be regarded as only approximate.

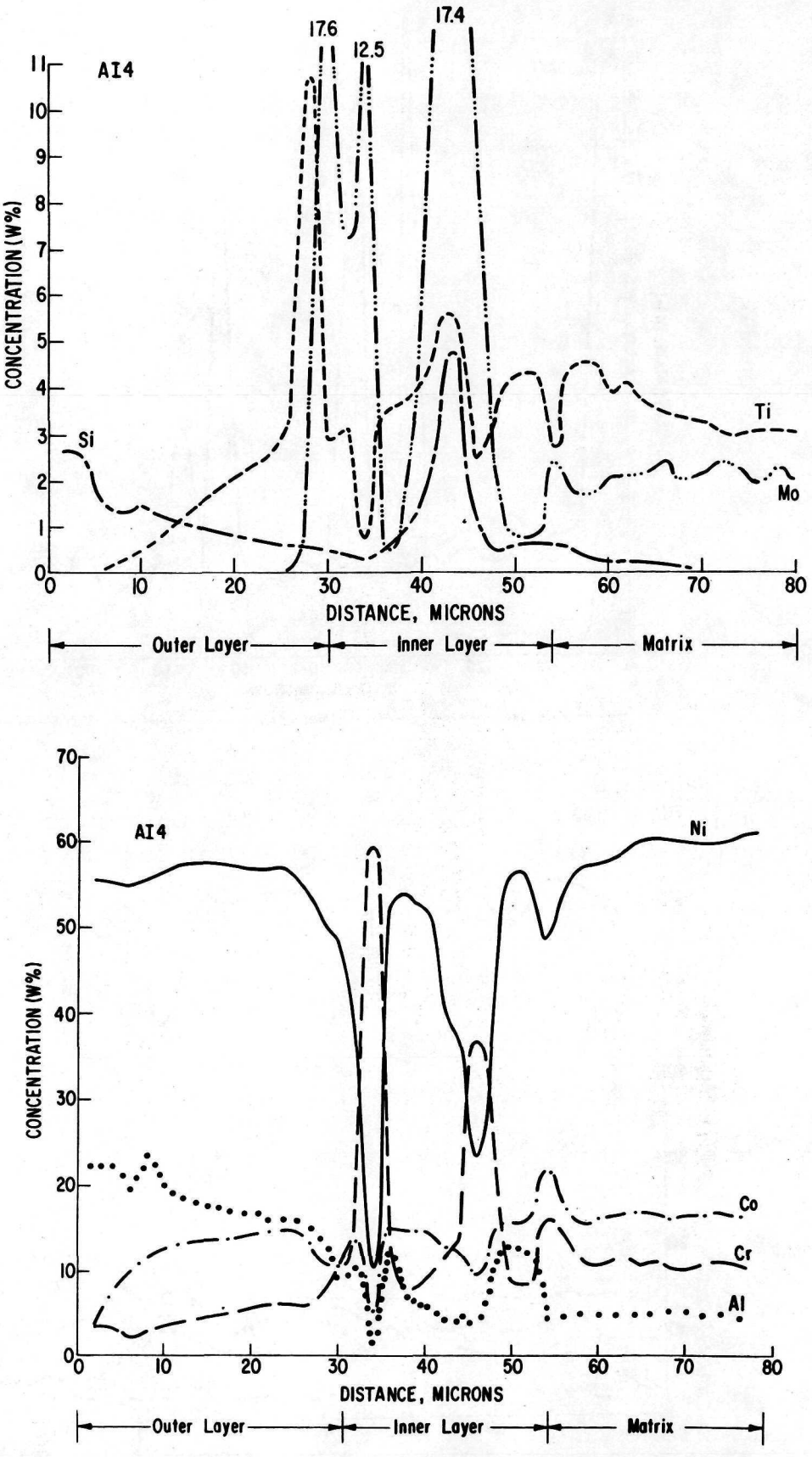

Fig. 31 Electron microprobe trace of coating on Disc AI4, aluminided-silicided at 0.5 amp/dm^2.

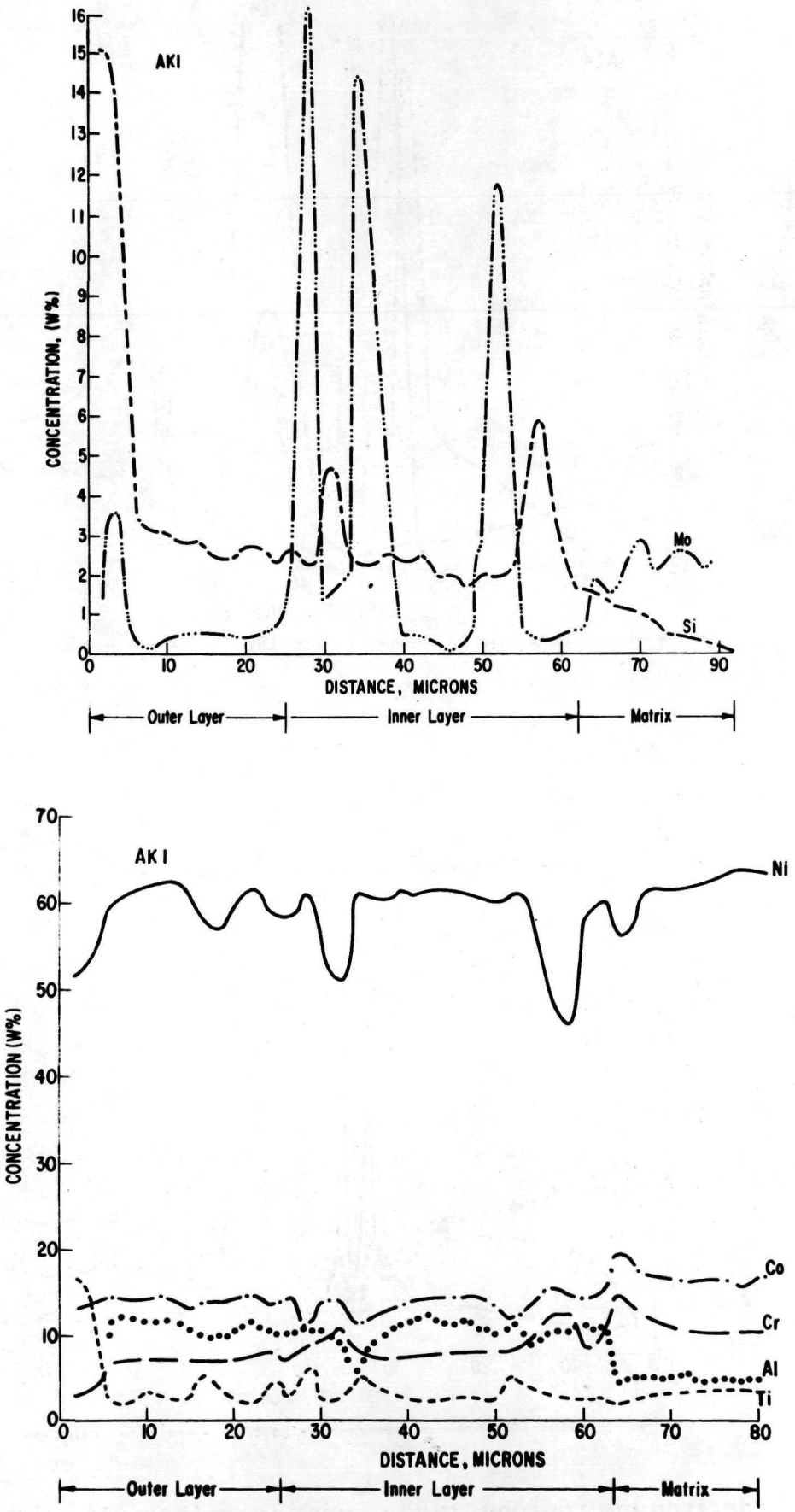

Fig. 32 Electron microprobe trace of coating on Disc AK1, aluminided-silicided at 0.5 amp/dm^2.

Oxidation and Hot Corrosion Behavior

The results of oxidation and hot corrosion testing are summarized in Table VII. (Discs from sets AE and AU, which lost weight during metalliding and had exceedingly rough surfaces, were not tested.)

With the exception of those from sets AD and AK, all of the discs showed good oxidation resistance, the weight change being typical of straight aluminided discs made at the same current density. Discs from sets AD and AK are shown in Fig. 33. The poor oxidation behavior of these sets is believed to be due to the thinness and low aluminum content of the coating on the AD set, and the presence of the $Ni_{16}Ti_6Si_7$ compound on the surface of the AK set.

Cross-sections of discs from four sets after oxidation testing are shown in Fig. 34. With the exception of disc AK2, all show a dark striated phase which is nickel-rich NiAl, surrounded by gamma. Disc AI1 has less NiAl remaining than has discs Z2 or AH1, and disc AK2 shows none. As when in the as-coated condition, the samples made using a graphite anode show a greater abundance of titanium carbide particles in and near what had been the outer layer. These samples also show a gray second phase in the gamma adjacent to the matrix. This phase, particularly prominent in the AK2 disc, was found by x-ray scan to be rich in chromium and molybdenum.

As seen in Table VII, none of the samples including those aluminided only survived the 400 hour hot corrosion test, although one disc, AD4, was judged to be still satisfactory after 274 hours in test. The companion disc, AD3, survived only 22 hours. Photographs of the two AD discs are shown in Fig. 35. The reason for the substantial difference between these two discs is unknown; examination of the microstructure of the coatings after hot corrosion testing was not informative.

TABLE VII

Results of Oxidation and Hot Corrosion Testing of Discs Made by Simultaneous Deposition of Al and Si

Set	CD (anp/dm^2)	XRF wt % Si	Oxidation Test		Hrs. to Failure in Hot Cor.	
			Hrs. to Failure	Wt Change, mg/cm^2		
Z	0.50	0	-	*(1) + 1.72	* (4)	98
			-	(2) + 1.80	(5)	29
AA	0.5	< 0.5	-	(3) + 1.79	(1)	143
			-	(5) + 1.75	(2)	203
AB	0.19	< 0.5	-	(1) + 0.86	(3)	56
			-	(2) + 0.83	(5)	39
AC	0.50	0	-	(2) + 1.80	(1)	116
			-	(4) + 1.50	(5)	94
AD	0.20	1	120	(1) - 5.80	(3)	22
			96	(5) - 1.65	(4)	274**
AF	0.20	< 0.5	-	(2) + 1.17	(1)	16
			-	(5) + 1.17	(4)	34
AG	0.20	1	-	(1) + 0.86	(2)	126
			-	(4) + 0.78	(5)	39
AH	0.20	2	-	(1) + 0.58	(2)	29
			-	(3) + 0.59	(5)	89
AI	0.50	2	-	(1) + 1.48	(3)	138
			-	(2) + 1.52	(5)	138
AK	0.50	5	159	(2) - 2.56	(3)	39
			159	(4) - 2.47	(5)	39

* Disc Number in ( ).

** Did not fail, removed for examination.

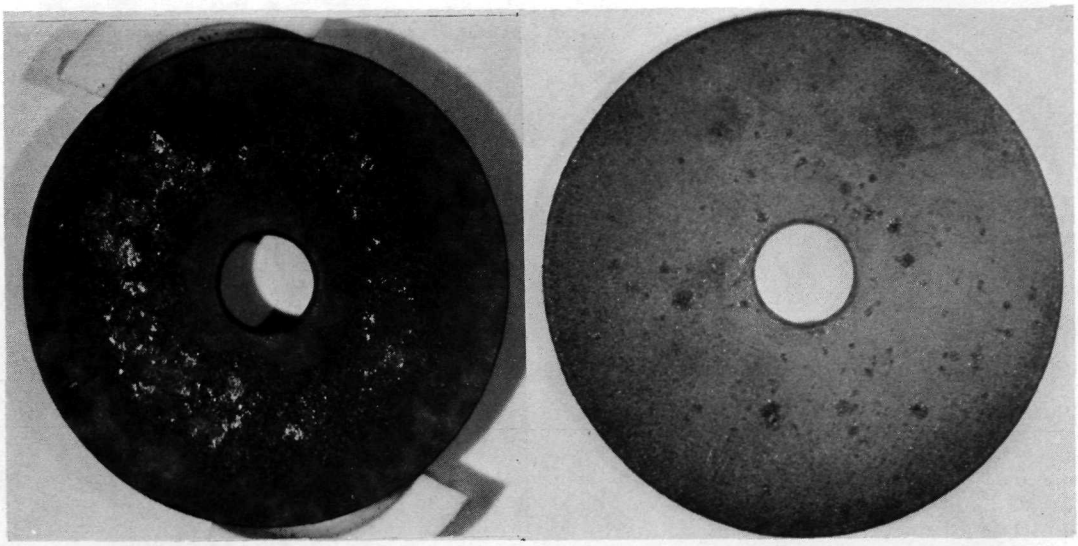

Fig. 33 Photographs of aluminided-silicided Discs AD1 (left) and AK2 (right) after oxidation testing. Disc AD1 was removed after 120 hours, Disc AK2 was removed after 159 hours.

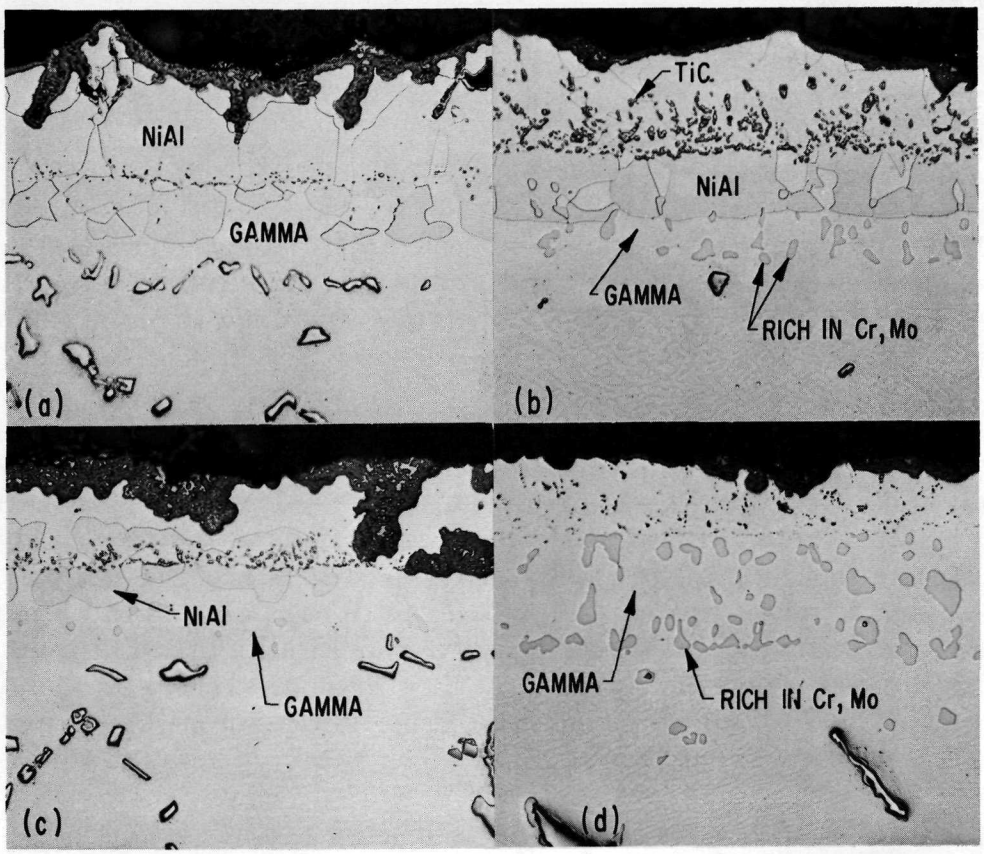

Fig. 34 Photomicrographs of IN-100 discs after oxidation testing at 1093°C (2000°F). The as-coated samples are seen in Fig. 26. (a) Disc Z2 after 200 hours; (b) Disc AH1 after 200 hours; (c) Disc AI1 after 200 hours; (d) Disc AK2 after 159 hours. 375X

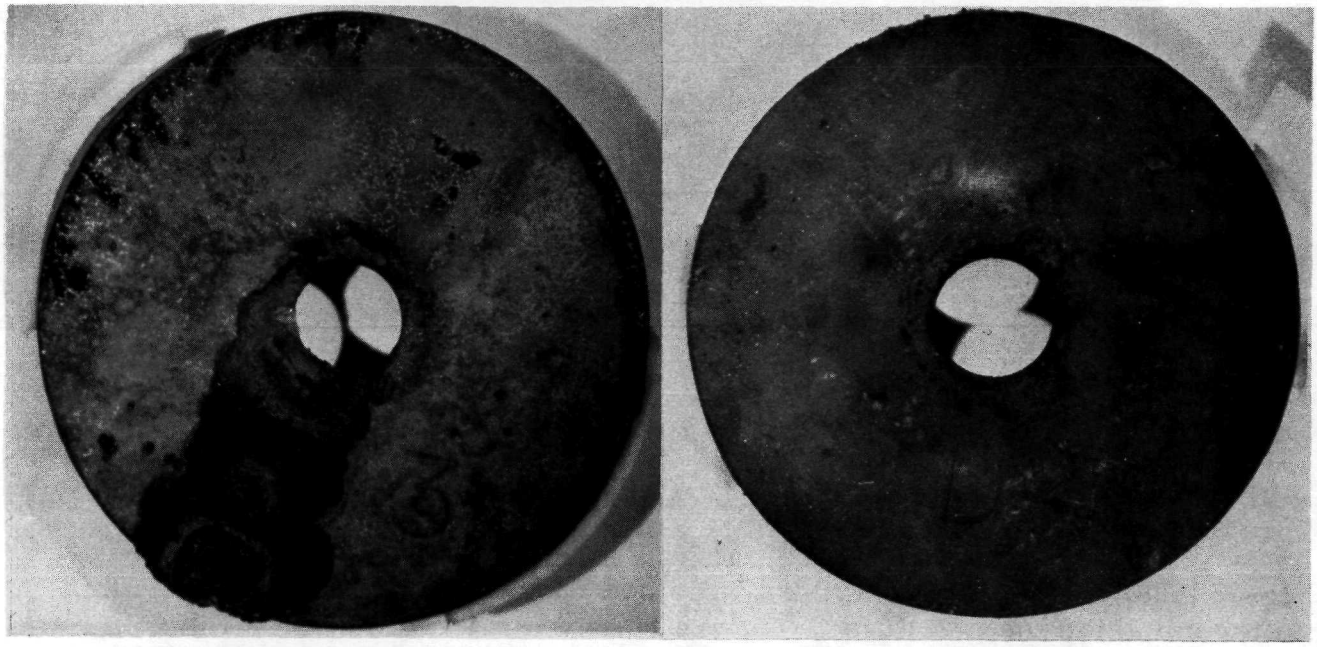

Fig. 35 Aluminided-silicided Discs AD3 (left) and AD4 (right) after hot corrosion testing. Disc AD3 was removed after 22 hours, whereas Disc AD4 was unattacked after 274 hours.

Task II: Al-Cr Simultaneous Deposition

Coating Characteristics

Table VIII summarizes the metalliding parameters and characteristics of the coatings. Discs were metallided while using a chromium anode either during the first half of the run or during the entire run. Included for comparison are data for the Z set, made while using a Ni_2Al_3 anode. A few of the sets have higher chromium content than does set Z.

Figure 36 shows the photomicrographs of 3 of the coatings, and in Figs. 37 and 38 are the corresponding microprobe traces. The coating on set AW is comprised of nickel-rich NiAl whereas the outer layer on the other two sets is comprised of aluminum-rich NiAl. All are Type I. There is no chromium rich phase in the outer layer of any sample. The white particles in the inner layer are chromium rich as were similar particles found in the straight aluminided samples. As discussed earlier in Task I, they are believed to be alpha and/or gamma phase. Both AX2 and AY3 show a chromium gradient with a maximum at the surface. It is apparent that at least 6% chromium is soluble in aluminum-rich NiAl.

Oxidation and Hot Corrosion Behavior

Table IX summarizes the results of oxidation and hot corrosion testing. In oxidation, only the samples from the AV set showed indications of localized

TABLE VIII

Simultaneous Deposition of Al and Cr:
Metalliding Parameters and Coating Characteristics

Set	C. D. (amp/dm^2)	Hrs.	Coating mg/cm^2	Coating mils	Coating % Cr-XRF	Coating % Cr-EMP	Remarks
Z	0.50	7	7.03	2.5	2	-	Ni_2Al_3 anode
AV	0.50	7	6.76	2.0	3	-	Cr anode
AW	0.10	30	8.37	3.2	4	3	Cr anode
AX	0.50 0.75	1.6 5.4	9.57	2.9	3	4	Cr anode
AY	0.75	7	9.48	2.8	8	6	Cr anode
AZ	0.10	15.2	7.76	3.0	3	-	Cr anode 1st half, Ni_2Al_3 anode 2nd half
BA	0.25	16	7.87	2.8	2	-	Cr anode 1st half, Ni_2Al_3 anode 2nd half
CA	0.40	30	11.69	-	2	-	Cr anode
CC	0.75	6.5	9.50	-	3	-	Cr anode
CE	0.062	61	10.62	-	4	-	Cr anode

Initial Bath: LiF_3 + 0.003 AlF_3 at 1100°C

failure of the coating. These samples had the least amount of aluminum added, and, after the 200-hour oxidation test, the thinnest layer of nickel-rich NiAl remaining. There were no unusual features in the photomicrographs after oxidation testing, and they are not shown.

All of the discs failed in hot corrosion well before the completion of the 400-hour test. Even the highest chromium discs, set AY, show no significant improvement over those with lower chromium content.

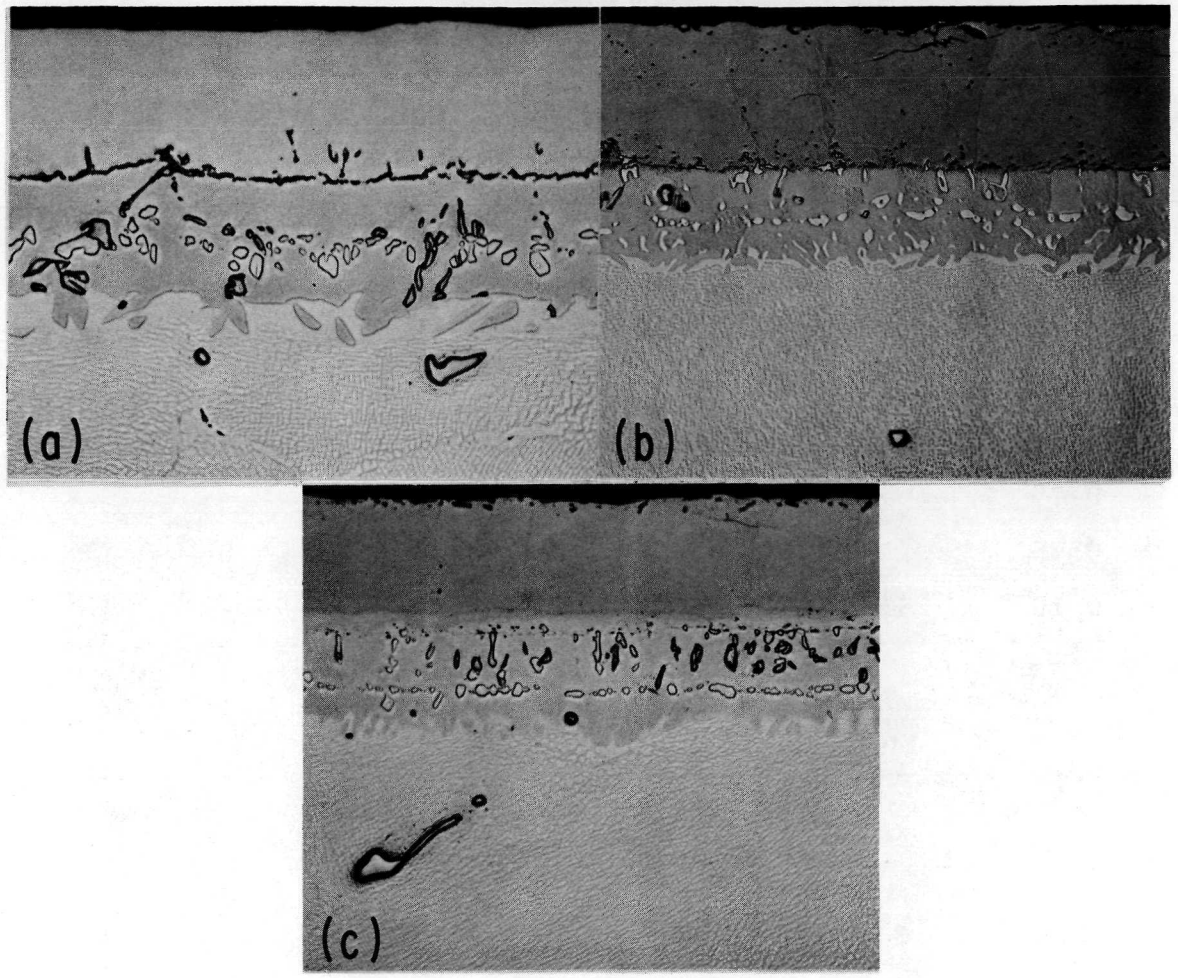

Fig. 36 Photomicrographs of discs of IN-100 on which aluminum and chromium were simultaneously deposited: (a) Disc AW4, 0.1 amp/dm^2; (b) Disc AX2, 0.5 and 0.75 amp/dm^2; (c) Disc AY3, 0.75 amp/dm^2. 430X

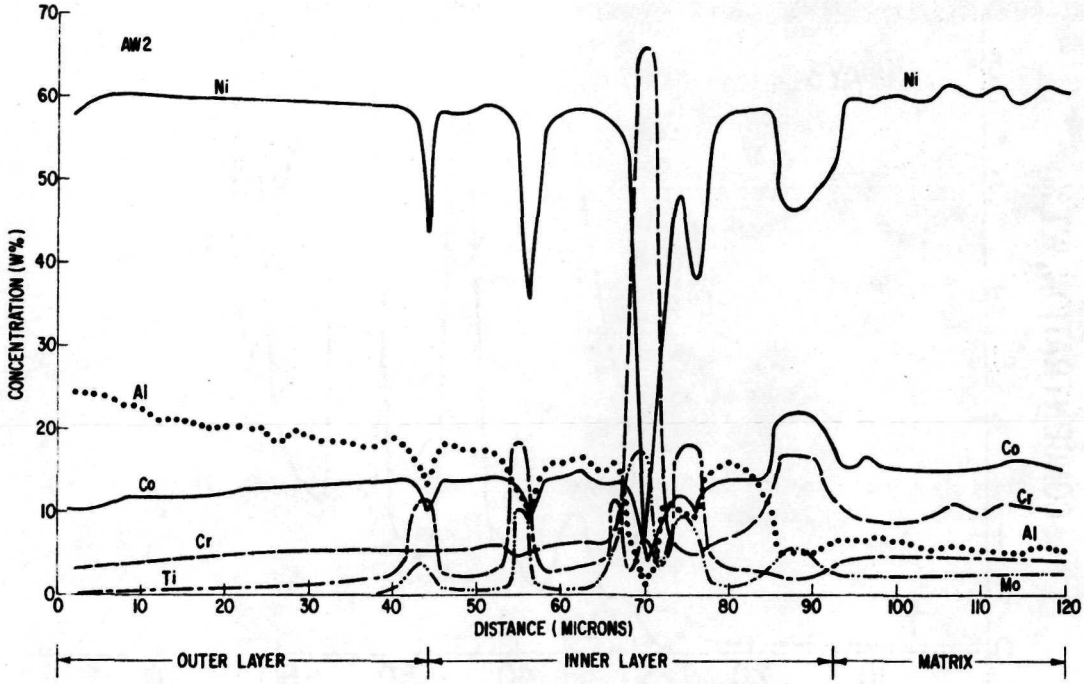

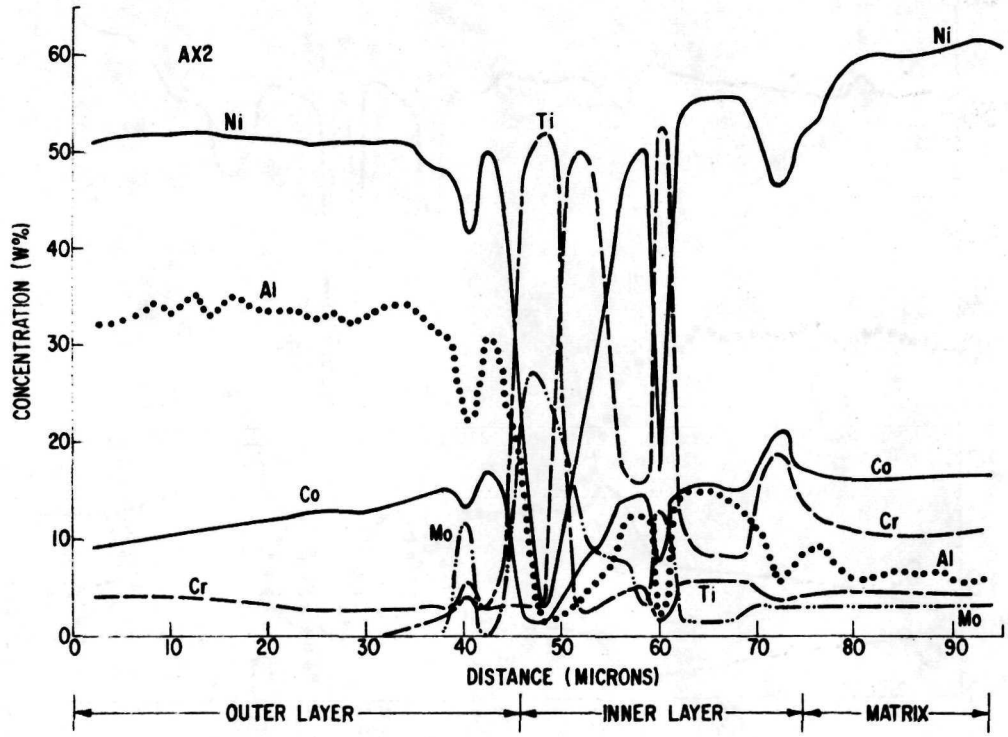

Fig. 37 Electron microprobe trace of coatings on aluminided-chromided Discs AW2 and AX2.

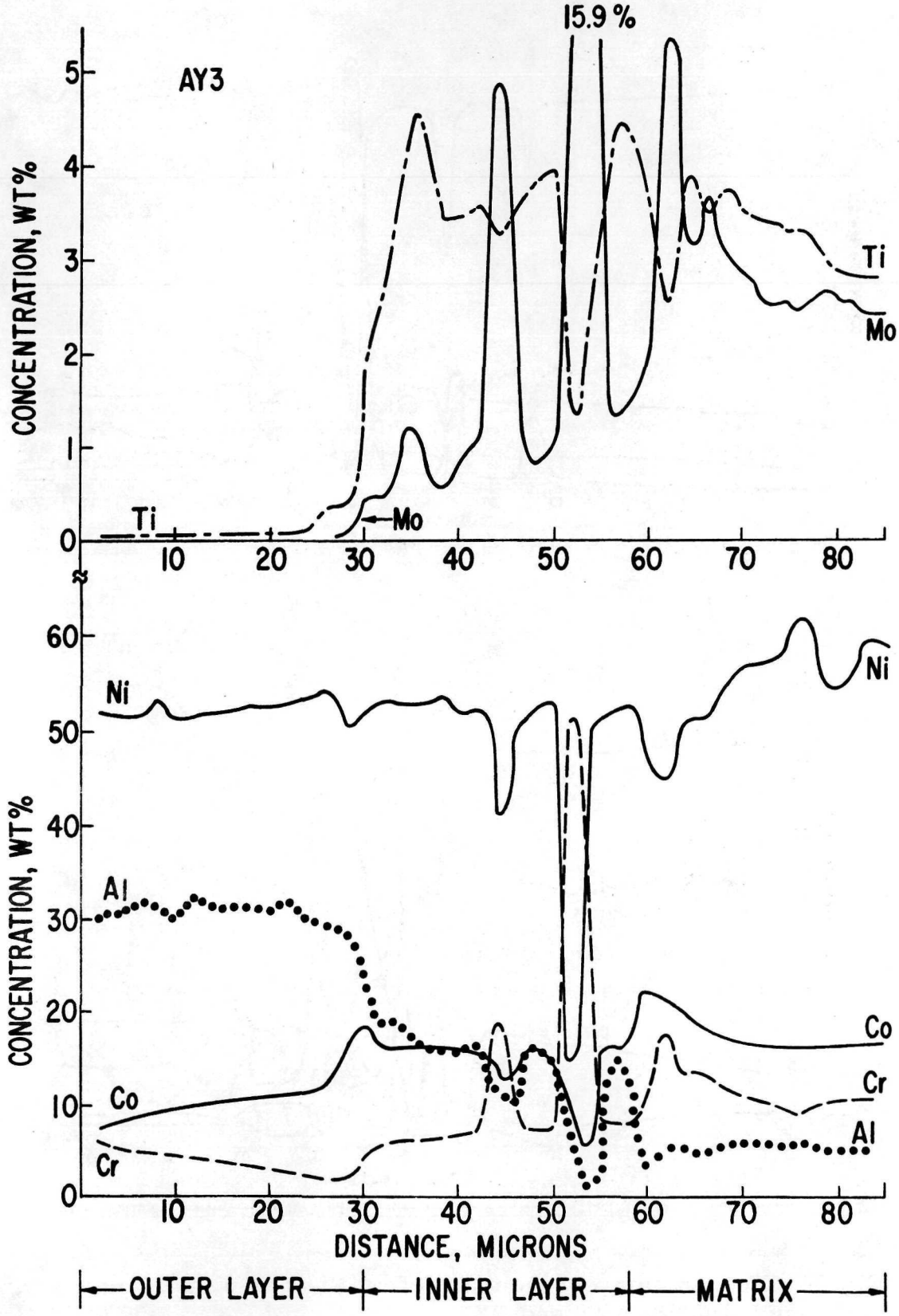

Fig. 38 Electron microprobe trace of coating on aluminided-chromided Disc AY3.

TABLE IX

Results of Oxidation and Hot Corrosion Testing
of Discs made by the Simultaneous Deposition of Al and Cr

Set	C. D. (amp/dm^2)	XRF wt % Cr	Wt Change in Ox., mg/cm^2	Hrs. to Failure in Hot Corr.
Z	0.50	2	(1)* + 1.72	(4)* 98
			(2) + 1.80	(5) 29
AV	0.50	3	(1) + 1.84	(3) 53
			(4) + 1.83	(5) 76
AW	0.10	4	(3) + 1.01	(1) 43
			(5) + 0.88	(2) 53
AX	0.50, 0.75	3	(1) + 1.55	(3) 29
			(4) + 1.98	(5) 91
AY	0.75	8	(1) + 1.60	(1) 98
			(5) + 1.59	(2) 116
AZ	0.10	3	(1) + 0.84	(4) 43
			(2) + 0.79	(5) 21
BA	0.25	2	(1) + 1.63	(3) 94
			(2) + 1.66	(4) 25
CA	0.40	2	(2) + 0.93	(1) 150
			(5) + 1.00	(4) 112
CC	0.75	3	(1) + 1.17	(3) 65
			(4) + 2.60	(5) 112
CE	0.062	4	(1) + 0.51	(2) 95
			(4) + 0.47	(5) 67

*Disc Number in ( ).

Task II: Al-Ti Simultaneous Deposition

Coating Characteristics

Table X lists disc sets with both low and very high titanium contents. Nine high titanium sets were made in a cell that had previously been used for titaniding. The solvent LiF initially contained about 0.2 mole % TiF_3, and despite repeated additions of AlF_3, the titanium content of the coatings remained consistently too high. The lower titanium sets, which are in the desired range, were made in an aluminiding cell to which was added small amounts of TiF_3 via a titanium anode.

TABLE X

Simultaneous Deposition of Al and Ti:
Metalliding Parameters and Coating Characteristics

Set	C. D. (amp/dm^2)	Hours	COATING mg/cm^2	COATING Mils	COATING % Ti-XRF	Remarks
BF	0.75	6.5	10.76	3.2	2.1	LiF + 0.003 AlF_3, Ni_2Al_3 anode.
BG	0.75	6.5	11.32	3.4	3.2	LiF + 0.003 AlF_3, 1100°C, Ti anode first half of run.
BH	0.19	20	7.44	--	0.2	LiF + 0.003 AlF_3, 1100°C, Ni_2Al_3 anode.
BI	0.19 0.40	1 15	10.84	--	0.8	LiF + 0.003 AlF_3, 1100°C, Ni_2Al_3 anode.
BJ	0.75	6.5	11.79	3.4	5.9	LiF + 0.003 AlF_3, 1100°C, Ti anode first half of run.
AO	0.50 0.20	3.5 15.5	11.29	2.2	36	LiF + 0.002 TiF_3, 1060°C, Ni_2Al_3 anode.
AR	0.04	15.3	15.3	3.0	41	LiF + 0.002 TiF_3, 1060°C, Ni_2Al_3 anode.
AT	0.10	31.5	10.51	2.8	23	LiF + 0.002 TiF_3, 1060°C, Ni_2Al_3 anode.

Set BF was aluminided only for comparison purposes. Set BJ with 5.9% Ti on the surface contains only 3.8% Ti above that found on the reference set, but as dendrite formation was noted on the surface both at the middle and the end of the run, it appeared that higher titanium contents were not possible at the current densities and concentrations used.

The microstructures of three coatings containing increasing amounts of titanium are shown in Fig. 39. As the average titanium content increases, as indicated by x-ray fluorescence measurements, there is an increase in the number of white particles, which are presumed to be rich in titanium, in the center portion of the outer layer. The sample with the highest titanium content, BJ1, also has what appears to be the same phase at the surface.

Microstructures of some of the higher titanium content samples are shown in Fig. 40. An electron microprobe trace across sample A05 is shown in Fig. 41. The phase immediately at the surface is seen to contain about 40% titanium and about 22% aluminum.

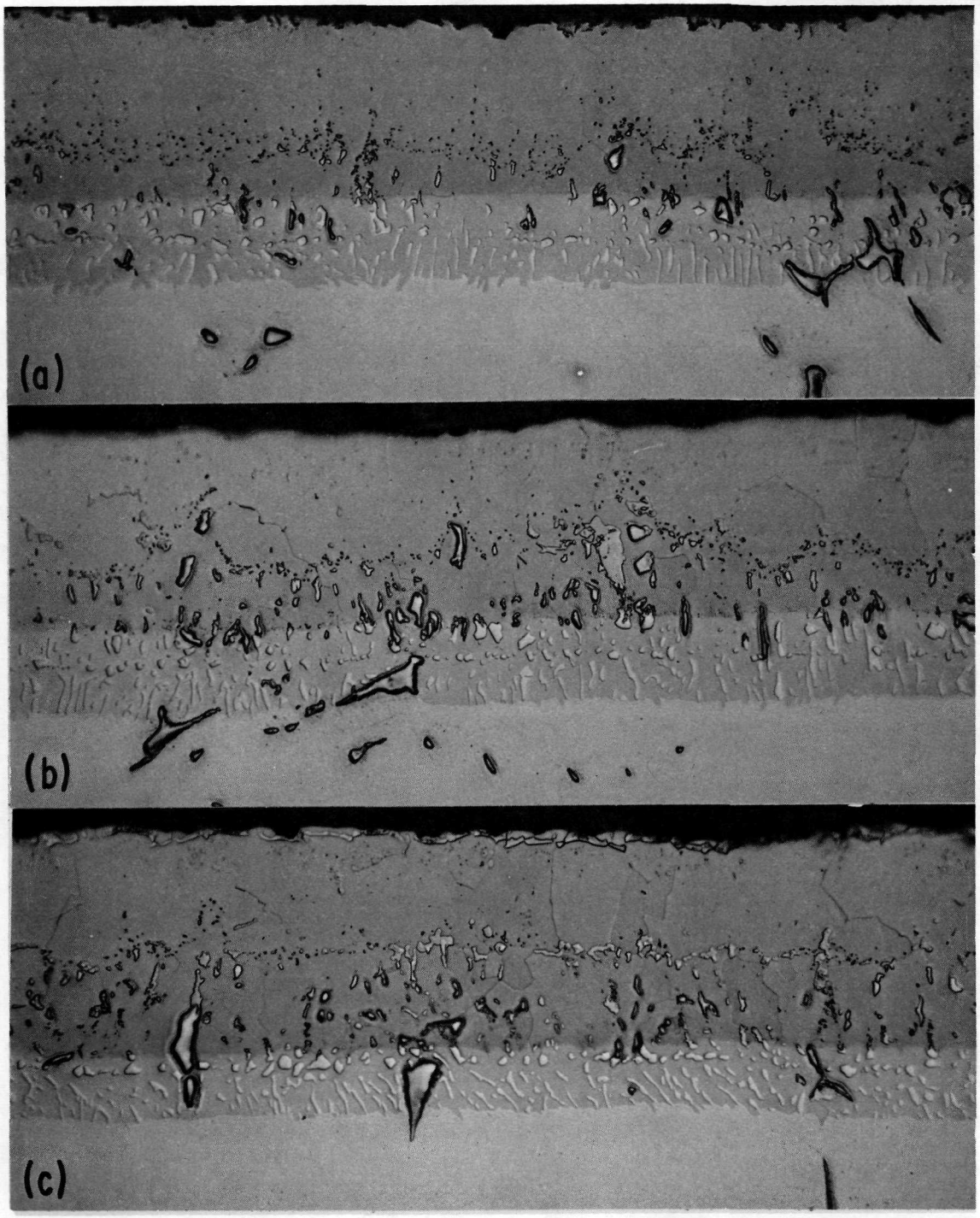

Fig. 39 Photomicrographs of coatings on IN-100 made by the simultaneous deposition of aluminum and titanium at a current density of 0.75 amp/dm^2:
(a) Disc BF1 - approximately 2% Ti; (b) Disc BG5 - approximately 3% Ti;
(c) Disc BJ1 - approximately 6% Ti. 500X

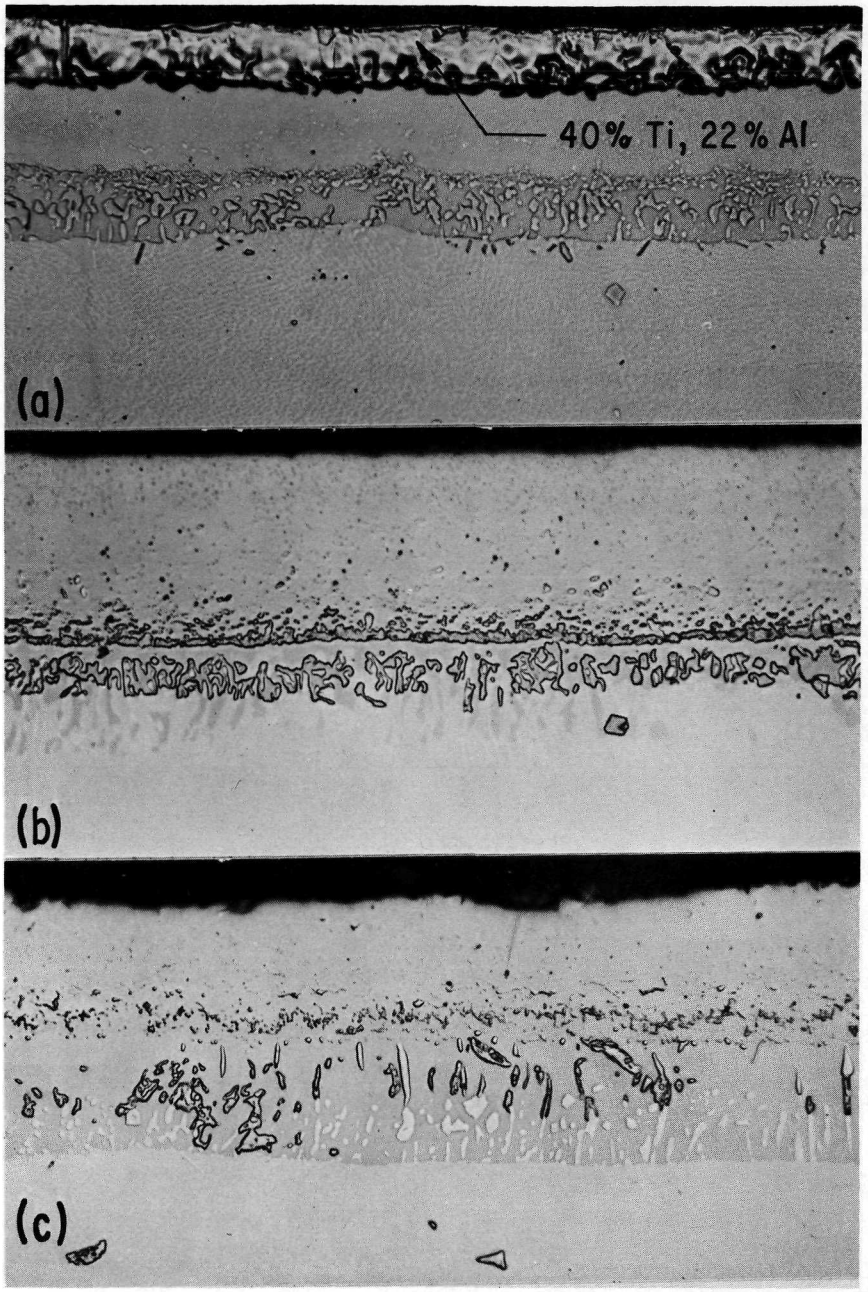

Fig. 40 Photomicrographs of high titanium content coatings on IN-100 made by simultaneous deposition of titanium and aluminum: (a) Disc AO5 - approximately 40%; (b) Disc AR2 - approximately 41% Ti; (c) Disc AT2 - approximately 23% Ti.
500X

One set (AL) was titanided at 0.5 amp/dm^2. The microstructure, which is not shown, resembled that of an aluminide coating made at the same current density.

Oxidation and Hot Corrosion Behavior

The results of oxidation and hot corrosion testing are summarized in Table XI. A titanium content of up to 3.2% (set BG) is not harmful to oxidation resistance, but with 5.9% titanium in the coating, the samples (set BJ) failed in less than 200 hours. Photographs of discs from these two sets are shown in Fig. 42. With greater amounts of titanium, the oxidation resistance is further lowered.

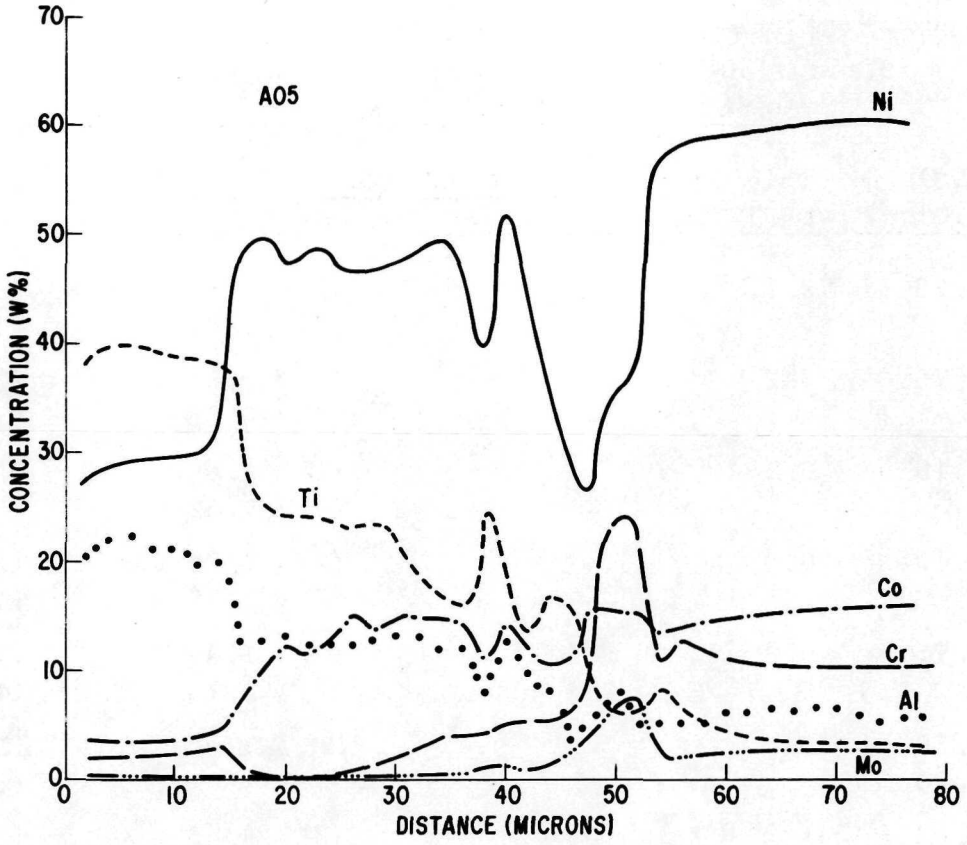

Fig. 41 Electron microprobe trace of coating on titanided-aluminided Disc AO5.

Titanium contents of up to 5.9% do not appear to reduce hot corrosion resistance, but much greater amounts drastically reduce the hours to failure in hot corrosion.

Task II: Al-Y Simultaneous Deposition

Coating Characteristics

Table XII summarizes the metalliding parameters and coating characteristics of discs aluminided in a bath containing equal amounts of BaF_2 and CaF_2 along with 1.6 mole % AlF_3. Aluminiding with current densities of 0.4 and 0.75 amp/dm^2 was done at 1150°C (2102°F), whereas the temperature was reduced to 1120°-1130°C (2048°-2066°F) for aluminiding at higher current densities.

Despite the increasing amounts of YF_3 added to the bath, only insignificant amounts of yttrium were deposited. For example, the x-ray fluorescence counts on 0.5 and 1.0% Y, balance NiAl, standards were 950 and 1950 CPS/2cm^2, respectively. The highest number of counts obtained with any of the samples in Table XII was only 90 CPS/2cm^2, found with discs from sets BP and BR.

TABLE XI

Results of Oxidation and Hot Corrosion Testing Discs Made by Simultaneous Deposition of Al and Ti

Set	C. D. (amp/dm^2)	XRF wt % Ti	Oxidation Test Hrs. to Failure	Oxidation Test Wt Change, mg/cm^2	Hrs. to Failure in Hot Corr.
BF	0.75	2.1	-	*(2) + 1.44	(3) 177
			-	(5) + 1.41	(4) 122
BG	0.75	3.2	-	(2) + 0.91	(1) 112
			-	(4) + 0.96	(3) 112
BH	0.19	0.2	-	(1) + 1.46	Not Tested
			-	(4) + 1.52	
BI	0.19	0.8	-	(2) + 1.20	(1) 112
	0.40		-	(5) + 1.38	(4) 217
BJ	0.75	5.9	184	(2) - 1.43	(3) 64
			184	(5) - 1.75	(4) 262
AO	0.50	36	-	Not Tested	(1) 17
	0.20				(3) 19
AR	0.04	41	3	(3) - 4.45	(1) 5
			3	(4) - 8.40	(5) 14
AT	0.1	23	26	(1) - 2.84	(4) 17
			26	(3) - 3.72	(5) 19

*Disc Number in ( ).

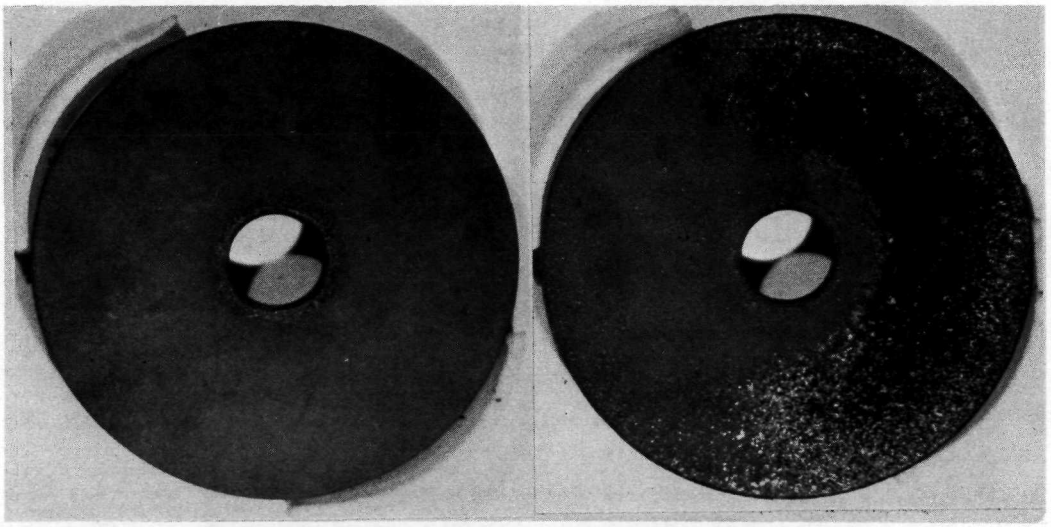

Fig. 42 Disc BG4 (3.2% Ti) after completion of 200 hour oxidation test (left) and Disc BJ5 (5.9% Ti) after 184 hours in oxidation test (right).

TABLE XII

Attempted Simultaneous Deposition of Al and Y:
Metalliding Parameters and Coating Characteristics

Set	C. D. (amp/dm^2)	Hrs.	Coating mg/cm^2	Coating Mils	Grams YF_3 Added	Grams YF_3 Total in Salt
BK	0.75	6.5	10.81	-	0	0
BL	0.4	15.4	10.40	-	2	2
BM	0.75	6.5	7.97	-	0	2
BN	0.4	15.5	10.11	-	2	4
BO	0.75	7.5	9.25	-	0	4
BP	0.4	14.8	9.91	-	20	24
BQ	0.75	7.5	8.63	-	0	24
BR	0.4	14.8	9.71	-	46	70
BT	2.0	3.0	13.69	3.6	0	70
BY	4.0	1.5	15.59	-	0	70
CB	2.0	3.0	14.08	3.6	461	531
CD	2.0	3.0	15.70	-	2155	2688

Initial Bath: (BaF_2-CaF_2) + 0.016 AlF_3

Anode: Ni_2Al_3

Oxidation and Hot Corrosion Behavior

The oxidation life of the discs made in the BaF_2-CaF_2 bath were substantially poorer than aluminide coatings made in the LiF bath. As seen in Table XIII, most of the discs failed well before 200 hours. Their life in hot corrosion was similar to that found with discs aluminided in LiF.

Task III: Aluminiding of TD NiCr

Background

It is well known that nickel aluminide coatings on TD NiCr and TD Ni are extremely porous.[7] An example of such a porous coating is seen in Fig. 43. (The metalliding conditions for this sample, A7, are included in Table XIV.) Porosity has been attributed to the unequal diffusivities of nickel and aluminum in NiAl, with nickel leaving the substrate and diffusing out faster than aluminum diffuses in from the surface. This unequal diffusion flux results in vacancies. While the creation of vacancies is a common result of interdiffusion, the vacancies

TABLE XIII

Results of Oxidation and Hot Corrosion Testing Discs
Made by Attempted Simultaneous Deposition of Al and Y

Set	C. D. (amp/dm^2)	Oxidation Test		Hrs. to Failure in Hot Corr.	
		Hrs. to Failure	Wt Chg., mg/cm^2		
BL	0.4	--	*(1) + 1.07	Not Tested	
		65	(3) + 0.49		
BM	0.75	59	(1) + 0.95	*(2)	37
		64	(4) + 0.62	(5)	140
BO	0.75	74	(1) + 0.84	(4)	36
		74	(3) + 0.72	(5)	116
BQ	0.75	59	(2) + 0.74	Not Tested	
		59	(4) + 0.62		
BR	0.40	36	(4) + 0.24	Not Tested	
		36	(5) + 0.46		
BT	2.0	87	(1) - 1.20	(4)	181
		87	(3) + 0.10	(5)	138
CB	2.0	--	(1) + 0.43	(2)	45
		--	(3) + 0.55	(5)	112
CD	2.0	--	(2) + 0.84	(1)	181
		--	(5) + 0.24	(4)	134

*Disc Number in ( ).

in these materials appear to coalesce, probably on the few larger thoria particles, forming voids rather than producing a volumetric decrease in the original substrate as seen in aluminided IN-100. Monson and Pollock[7] have discussed this phenomenon in detail.

Figure 44 shows the electron microprobe traces of the aluminided sample shown in Fig. 43. Assuming that the thoria particles do not move, it is seen that the visible coating, which is NiAl, formed mainly as a result of the diffusion of nickel and chromium outwards through the coating, meeting the aluminum at the steadily expanding surface. The gamma solid solution adjacent to the NiAl phase contains 8 wt % or 17 A/o % aluminum. [Taylor and Floyd[4] have shown that Ni_3Al is not a stable phase at 1150°C (2102°F) in a NiAl alloy containing 20 wt % Cr - a portion of this Al-Cr-Ni ternary diagram is seen in Fig. 9. Furthermore, their limit of the gamma solid solubility, shown in Fig. 45, is in excellent agreement with the electron microprobe value.]

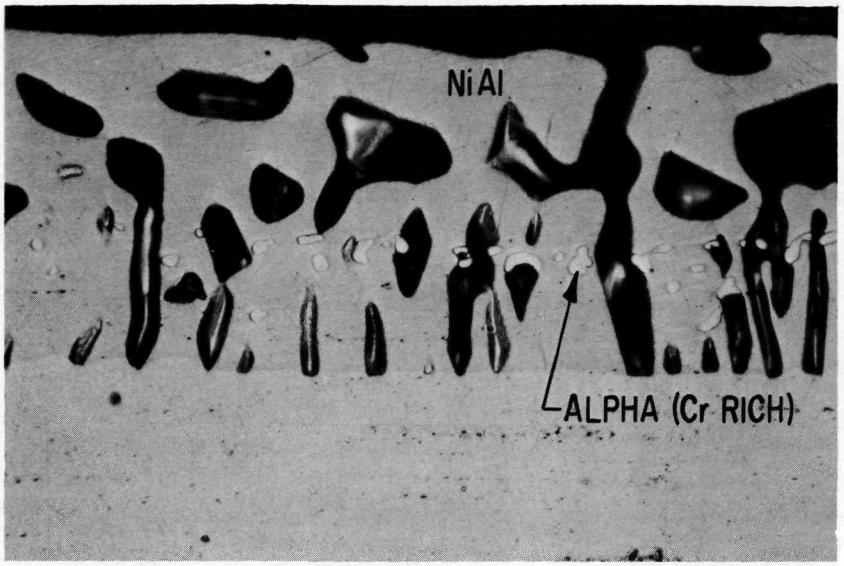

Fig. 43 Photomicrograph of aluminided TD NiCr sample A7. The porosity does not extend below the NiAl phase. 500X

TABLE XIV

TD NiCr: Metalliding Parameters and Coating Characteristics

Samples	Temp., °C	C. D. (amp/dm^2)	Hours	mg/cm^2	% Al XRF	% Al EMP
A5, B9, B10	1140	0.0065	62.9	1.47	5.6	5.5
A10, A11, A12	1200	0.0067	16.1	2.22	6.4	5.0
A7	1150	0.0096	64.3	10.74	14.5	20

Interestingly, there is no porosity below the NiAl phase. Apparently, voids do not develop until the aluminum concentration exceeds the solubility limit of the gamma phase and NiAl begins to form at the surface. Since the gamma phase is formed by the inward diffusion of aluminum, the NiAl phase appears first at the original surface, which is marked in Fig. 44 by the thoria concentration going to zero. Since NiAl forms primarily by the diffusion of nickel outwards through the NiAl, voids form virtually simultaneously with the appearance of NiAl at the NiAl-gamma interface. As the NiAl phase thickens, the voids continue to grow by vacancy accretion, hence their predominantly finger morphology in coatings formed slowly at high temperatures.

It is seen in the photomicrograph and the microprobe trace that a chromium-rich phase (α phase in Fig. 9) is concentrated near the original surface. The

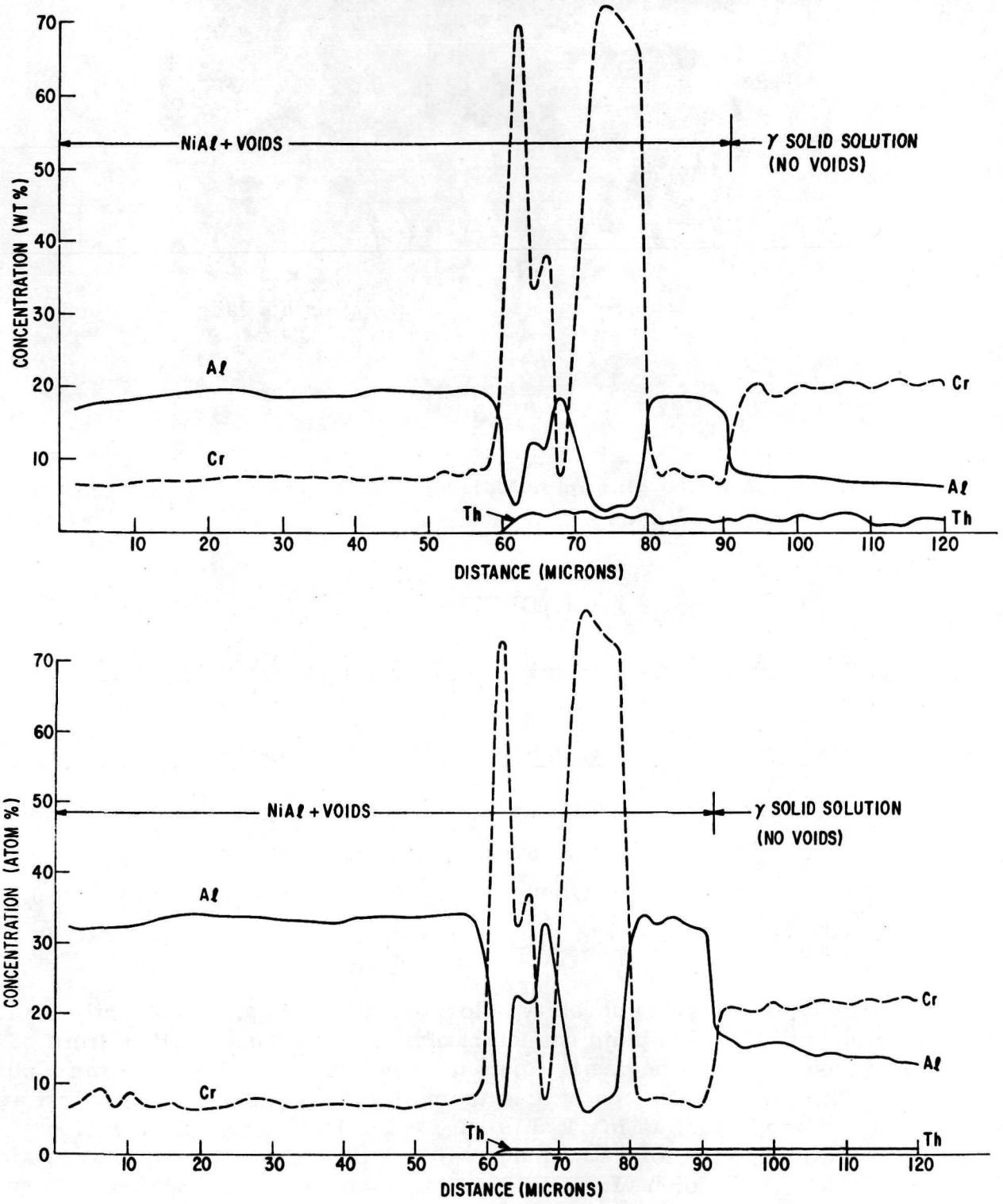

Fig. 44 Electron microprobe trace of TD NiCr sample A7, the photomicrograph of which is shown in Fig. 43.

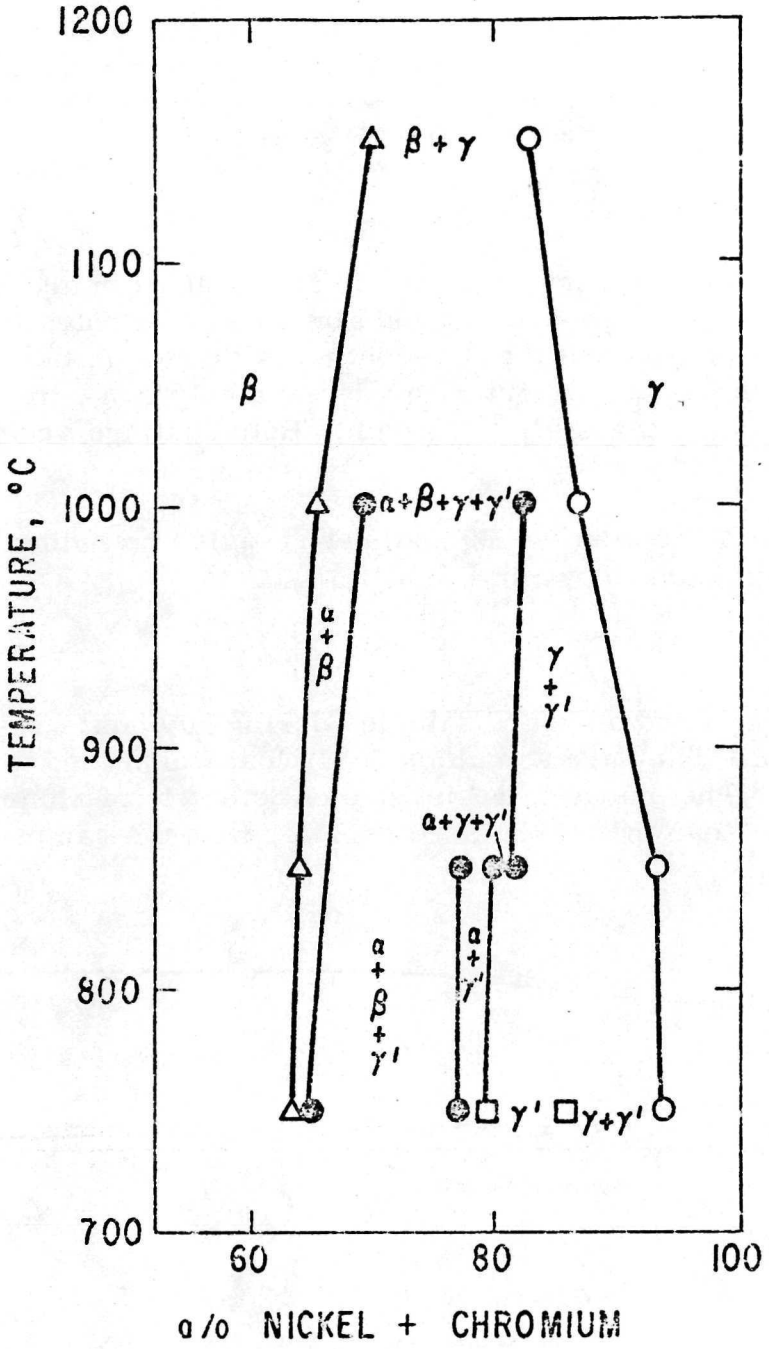

Fig. 45 Partial phase diagram of Al-Ni-Cr system constructed from Al-Cr-Ni isothermal sections[4] for alloys with Ni-Cr ratio of 78/22.

concentration of chromium in NiAl is only about 8 wt % so that along with the voids a chromium-rich phase begins to form when the solubility limit of aluminum in gamma is exceeded.

Coating Characteristics

The objective of this task was to form a 3-mil-thick coating containing 5% aluminum. A coating of this composition would consist of gamma solid solution, and it is apparent from the above discussion that as long as the aluminum concentration does not exceed 8%, the limit of solubility in the gamma phase, such a coating should be free of porosity.

Table XIV gives the metalliding parameters and characteristics of the coatings formed on two sets of TD NiCr samples, each sample being 0.5 in. wide and 2.0 in. long. The 1140°C (2084°F) run was done in a LiF-0.003 AlF_3 bath and the 1200°C (2190°F) run in a CaF_2-BaF_2-0.016 AlF_3 bath. The low aluminum deposition rate was used to avoid having the aluminum concentration on the surface exceed the gamma solubility limit.

Microprobe traces across the coating on a sample from each run are shown in Fig. 46. While both samples have about the same aluminum concentration at the surface (5.0% to 5.5%), it is apparent that the coating is thinner in the second run than in the first despite the higher weight gain. Presumably more impurities were deposited in the run made in the CaF_2-BaF_2 bath. Both coatings are substantially thinner than the desired 3 mils.

Metallographic examination of samples B9 and A11 revealed no indication of porosity. Photomicrographs are shown in Fig. 47.

Oxidation Behavior

The changes in weight of coated and bare samples during 300 hours at 1205° (2200°F) are shown in Fig. 48. The bare sample steadily lost weight due to spalling throughout the test. The oxidation resistance of both sets of aluminided samples was markedly better than that of the bare sample, with the samples

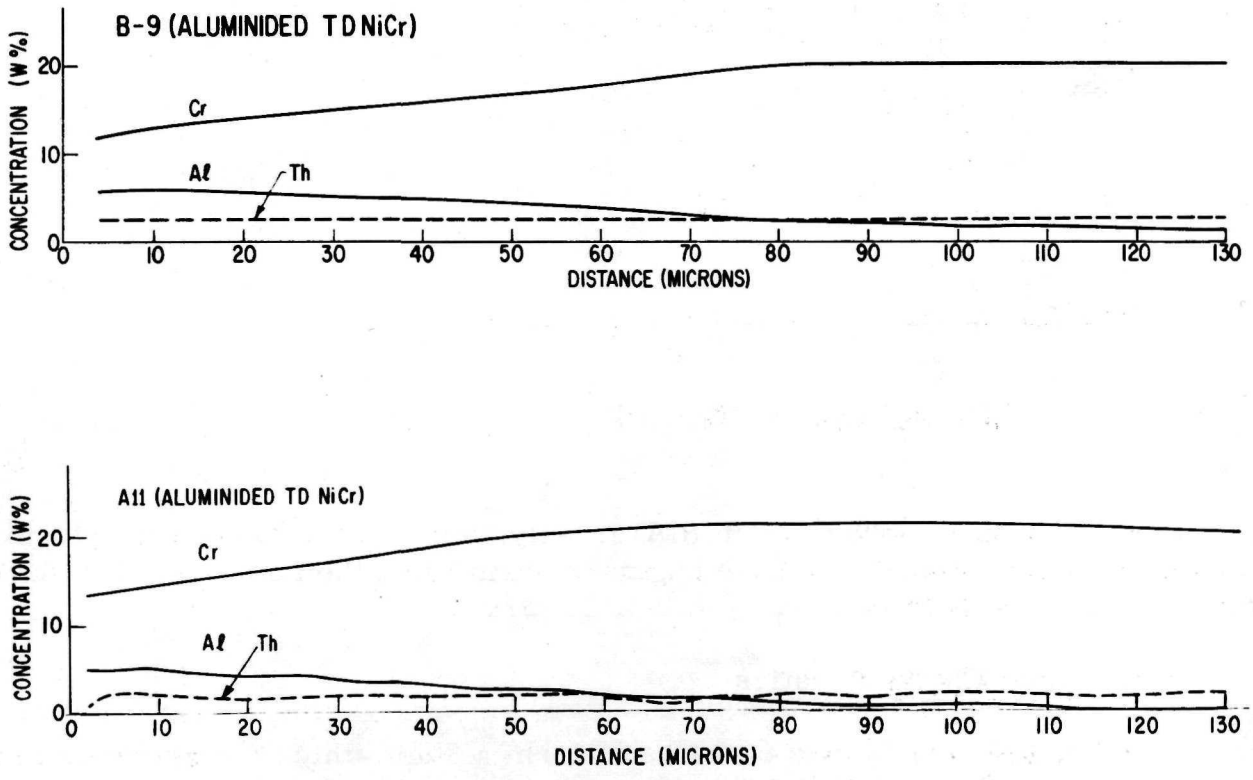

Fig. 46 Electron microprobe trace of coatings on aluminided TD NiCr samples B9 and A11.

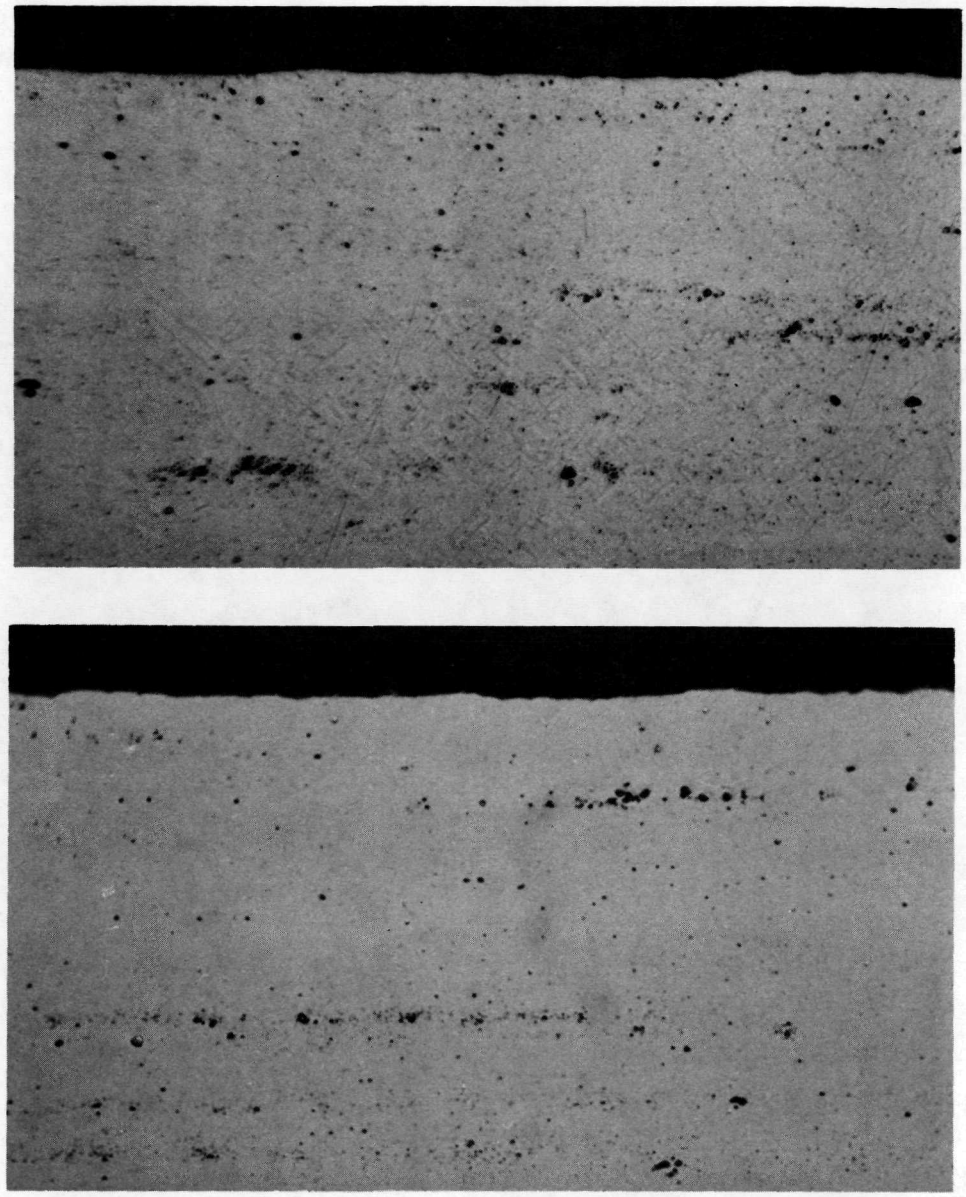

Fig. 47 TD NiCr samples B9 (top) and A11 (bottom) as-aluminided. There is no indication of porosity. 1000X

having the slightly thicker coating (A5, B10) showing less weight loss than the pair (A10, A12) with the thinner coating.

The samples after oxidation testing are shown in Figs. 49 and 50. The uncoated sample has on the surface a yellowish green substance identificed by x-ray diffraction as being principally NiO plus a small amount of spinel ($a_0 \approx 8.2 +$ Å) plus lesser amounts of Cr_2O_3 and NiO. The coated samples are gray with brown blotches, the gray areas being principally Al_2O_3 and the brown area spinel with a_0 from 8.1 to 8.2 + Å. The edges of the two samples with the

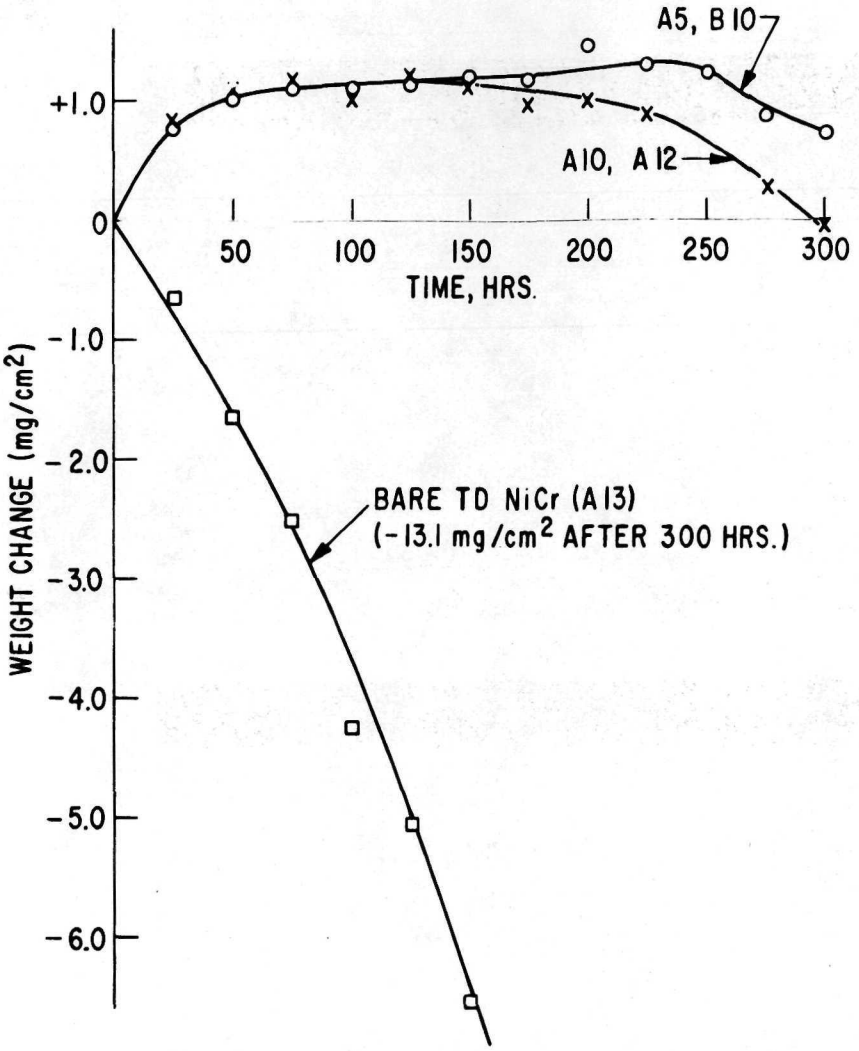

Fig. 48 Weight change of coated and bare TD NiCr samples during cyclic oxidation test at 1205°C (2200°F).

thinner coatings (A10 and A12) show green areas, presumably the NiO found on the uncoated samples. Of the 5 samples tested, the uncoated sample and A5 had square edges; the edges of the others had a slight radius.

The microstructures of the bare sample and one from each of the coated pairs are shown in Fig. 51. Unfortunately, there is insufficient contrast between the mount and the oxide to distinguish them in the figure, but the oxide on the uncoated sample is up to 2 mils thick whereas the oxide layer on the coated samples, except where penetration has occurred, is 0.2 mil in thickness.

TD NiCr contains large particles of Cr_2O_3 strung out in the rolling direction. In the uncoated sample, there has been an appreciable growth of these particles as a consequence of internal oxidation. In the coated samples, the original oxide particles are missing for a distance of about 14 mils extending into the samples. The loss of chromium oxide particles from this region is a consequence of the greater affinity of aluminum than chromium for oxygen.[8] It is postulated that the chromium oxide dissolves, with the oxygen ions diffusing toward the surface

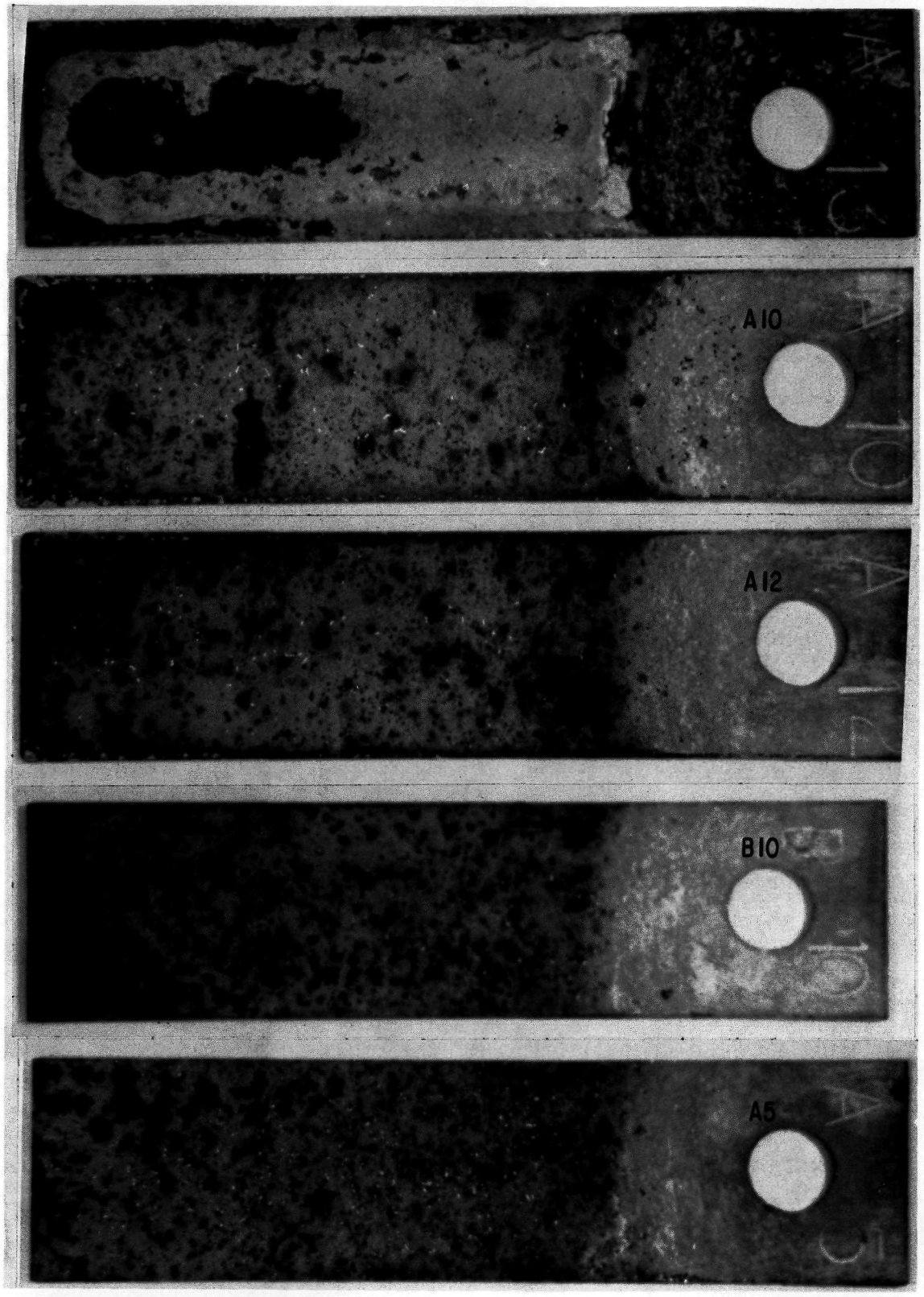

Fig. 49 Appearance of bare (A13) and coated TD NiCr samples after 300 hour cyclic oxidation test at 1205°C (2200°F). ~3X

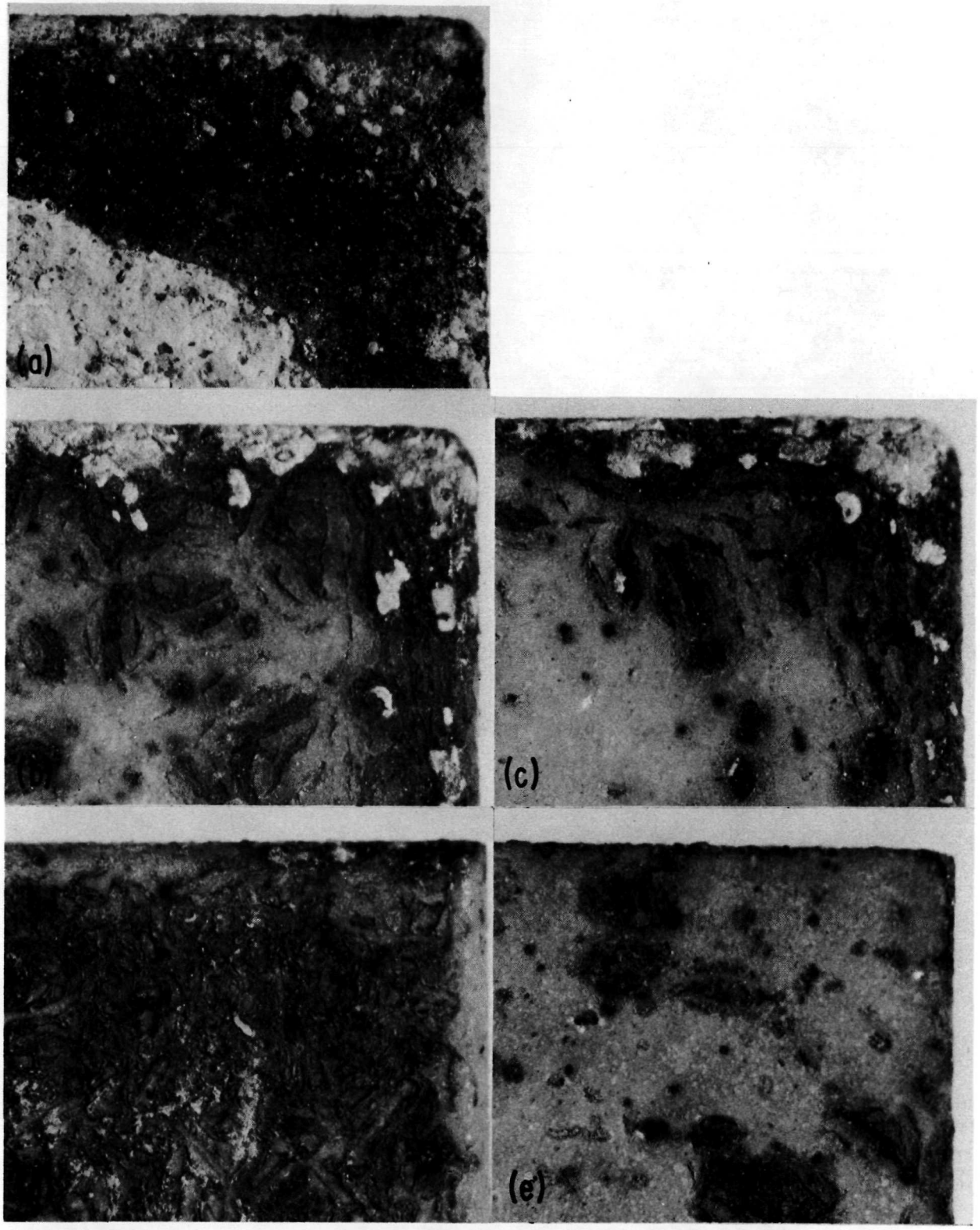

Fig. 50 Higher magnification view of surface of bare and coated TD NiCr samples after oxidation test: (a) A13 (bare); (b) A10; (c) A12; (d) B10; (e) A5. 18X

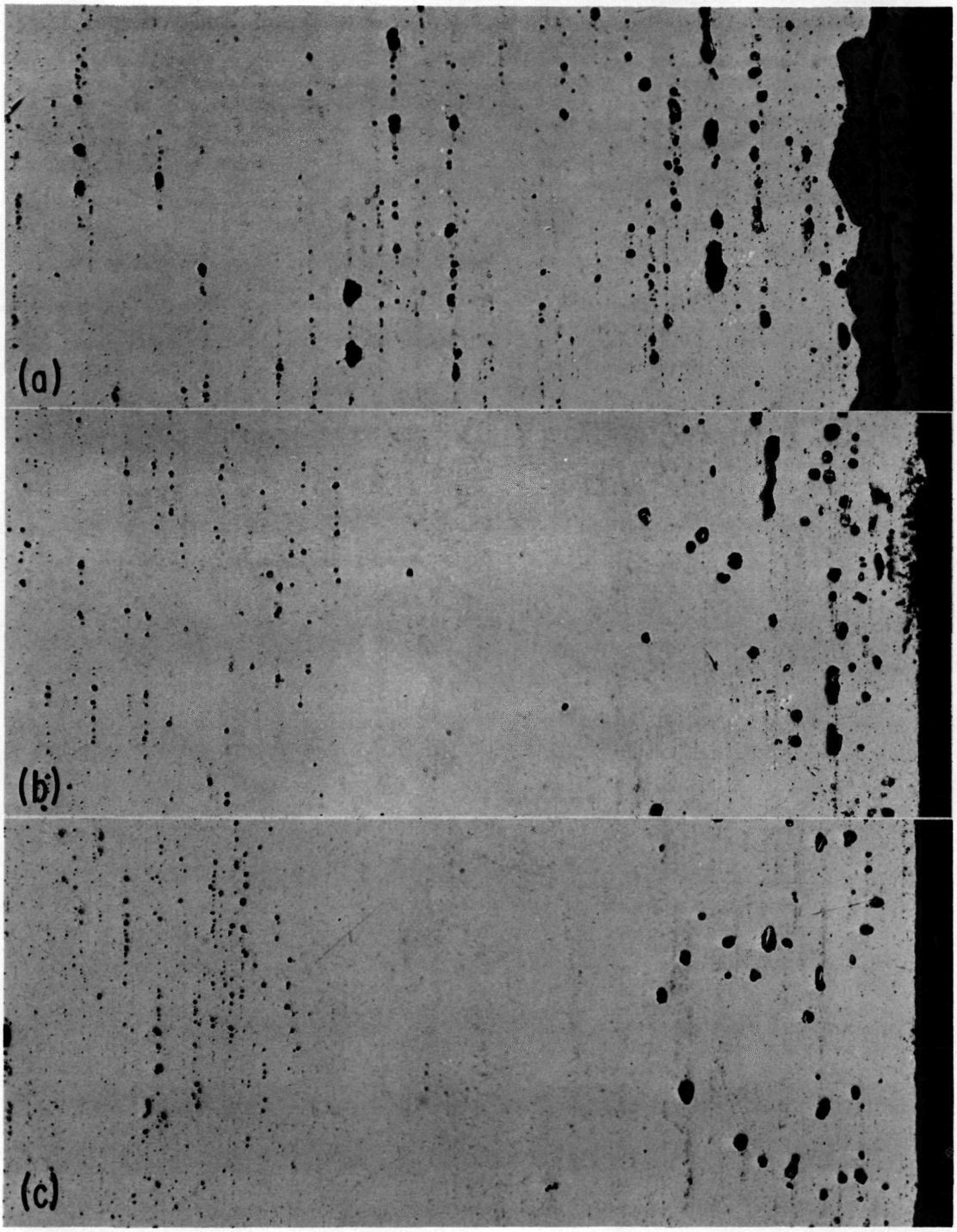

Fig. 51 Cross-section of TD NiCr samples after oxidation test. The exposed surface is at right: (a) A13 (bare); (b) A10; (c) A5. 250X

region which is low in dissolved oxygen as a result of the formation of Al_2O_3 and complex chromium-aluminum oxides. Although the total oxide content is high at and near the surface, there may be an oxygen activity gradient from the interior to the surface because of the stability of oxides containing aluminum. There may also be submicroscopic particles of Al_2O_3 in the region that appears to be devoid of particles.

Task V: Coating of Erosion Test Bars for NASA

IN-100

A Type II or "high activity" coating that would not be excessively brittle was selected for the Erosion Test Bars. The bars were aluminided in LiF - 0.003 AlF_3 at 1.0 amp/dm^2 and 1100°C for 4 hours. Table XV lists the aluminiding parameters. The faint darkening of the upper portion of the bars noted under Color in the table is the result of trace nitrogen contamination in the salt.

From the correlation in Fig. 11 and the average weight gain of 10.79 mg/cm^2, the predicted coating thickness is 3.5 mils. If the correlation in Fig. 13 and the average growth of 1.21 mils are used, the predicted coating thickness is 2.9 mils. Both methods indicate that the desired 3-mil-thick coating was obtained.

TD NiCr

The intent was to coat the bars at a sufficiently low current density so that the desired coating thickness of 3 mils would be approached while not exceeding the solubility of aluminum in gamma phase, which is about 8%. The aluminiding was done at 1100°C under the conditions given in Table XVI. As noted in the table, a variety of problems, including electrical shorting at the cell doors, impurities in the salt and welding of the Nickel 270 electrode to the cell wall, prevented obtaining the desired concentration of aluminum in the coating on six of the ten bars. The coatings with more than 7% aluminum are expected to be porous.

TABLE XV

Aluminiding Parameters for IN-100 Erosion Bars: Task V

Bar	mg/cm^2	% Eff.	Growth Mils	Color	Comments
3	11.01	82.0	1.0	Lt. Gray	
4	10.43	77.9	0.75	Lt. Gray	Edges Chipped
Average	10.72	80.0	0.87		
5	10.79	80.4	1.46	Lt. Gray	
6	10.77	80.3	0.64	Lt. Gray	
Average	10.78	80.4	1.05		
13	10.67	79.5	1.54	Lt. Gray	Emery Paper
14	10.86	80.9	0.85	Lt. Gray	Surface Treat-
Average	10.77	80.2	1.20	Both slightly dark at top	ment
9	10.57	78.7	1.27	Lt. Gray	Emery Paper
10	10.68	79.5	1.56	Darker at	Surface Treat-
Average	10.63	79.1	1.42	top than above run	ment
11	10.77	80.2	1.55	Lt. Gray	Emery Paper
12	11.20	83.3	1.48	Possibly	Surface Treat-
Average	10.98	81.7	1.51	Faint Dark- ening at top	ment
15	10.84	80.7	0.63	Same	Emery Paper
16	10.94	81.7	1.78		Surface Treat-
Average	10.89	81.2	1.45		ment
Average Overall	10.79	80.4	1.21		

TABLE XVI

Aluminiding Parameters for TD-NiCr Erosion Bars

Run	(amp/dm^2)**	Hours	mg/cm^2		Mils Growth		w/o Al	Comments
			(1)*	(2)	(1)	(2)		
231A	0.0065	72.0	0.24	0.12	0.15	0.16		Shorted
233B	0.0065	1.2	-0.40	-0.38	-0.06	-0.03		Shorted
244C	0.0065	72.0	7.48	7.46	1.17	1.12	(15)	Impure Salt
	TOTAL	145.2	7.32	7.20	1.26	1.26		
			(3)	(4)	(3)	(4)		
232A	0.0065	72.0	-0.38	-0.26	0.05	0.10		Shorted
245B	0.0065	23.0	1.74	1.74	0.30	0.24	(12)	Impure Salt
	TOTAL	95.0	1.36	1.48	0.35	0.34		
			(5)	(6)	(5)	(6)		
250A	0.0043	23.6	0.87	0.84	0.08	0.05		
252B	0.0043	23.5	0.91	0.86	0.10	0.17	(6)	
	TOTAL	47.1	1.78	1.70	0.19	0.17		
			(7)	(8)	(7)	(8)		
251A	0.0043	23.2	6.72	7.30	1.02	0.65	12-17	Ni welded to wall
			(9)	(10)	(9)	(10)		
253A	0.0043	22.4	0.43	0.37	0.05	0.09		
255B	0.0043	23.5	0.80	0.81	0.08	0.02		
256C	0.0043	7.2	0.22	0.24	0.02	0.04		
258D	0.0043	7.0	0.27	0.27	0.09	0.05	(7)	
	TOTAL	60.1	1.72	1.69	0.24	0.19		

*BAR number in ( ).

**Current held constant at 0.016 amp.
TD NiCr Area = 1.24 dm^2

Nickel 270 Area = 1.24 dm^2 or 2.48 dm^2

Total Cathode Area = 2.48 dm^2 or 3.72 dm^2

CONCLUSIONS

1. Two types of aluminide coatings are formed on IN-100, with Type I characteristic of low deposition rates and Type II of high deposition rates. The transition between the two types occurred at theoretical rates of 2.5 - 3.4 mg $Al/cm^2/hr$ (current densities of 0.75 - 1.0 amp/dm^2).

2. Growth and coating thickness measurements revealed the outward diffusion of nickel to form NiAl away from the surface of IN-100 in Type I coatings without incurring porosity.

3. Electron microprobe analysis of coatings made by simultaneous deposition show that the solubility of chromium in the aluminide coating on IN-100 is at least 6%, while that of silicon is between 1% and 2%.

4. The 200-hour, 1090°C (2000°F) cyclic oxidation test in air showed that all of the coatings on IN-100 except those with 6% or more titanium had good oxidation resistance.

5. Hot corrosion resistance is a more difficult requirement to satisfy than is oxidation resistance, with none of the IN-100 samples surviving the 400-hour screening test. The best resistance was obtained with Type II simple aluminide coatings, which are made at high deposition rates.

6. Porosity-free coatings with good oxidation resistance are formed on TD NiCr by depositing aluminum at such a rate that the gamma phase solubility limit (approximately 8%) is never exceeded.

REFERENCES

1. Goward, G. W., "Current Research on the Surface Protection of Superalloys for Gas Turbine Engines," Journal of Metals, Oct. 1970, pp. 31-39.

2. Cook, N. C., "Metalliding," Scientific Am., Vol. 221, No. 2, Aug. 1969, pp. 38-46.

3. Sanders, W. A., Barrett, C. A., and Probst, H. B., "Evaluation of High-Gas-Velocity and Static Oxidation Behavior of Fused-Salt-Aluminided IN-100 Between 1038° and 1149°C," NASA TN D-6400, July 1971.

4. Taylor, A. and Floyd, R. W., "The Constitution of Nickel-Rich Alloys of the Nickel-Chromium-Aluminum System," J. Inst. Metals, Vol. 81, May 1953, pp. 451-464.

5. Redden, T. K., "Ni-Al Coating-Base Metal Interactions in Several Nickel-Base Alloys," Trans. AIME, Vol. 242, No. 8, Aug. 1968, pp. 1695-1702.

6. Moore, V. S., Bretnall, W. D., and Stetson, A. R., "Evaluation of Coatings for Cobalt- and Nickel-Base Superalloys," Vol. 1, Rep. RDR-1474-2, Solar Div. International Harvester Co. (NASA CR-72359), Jan. 31, 1969.

7. Monson, L. A. and Pollock, W. I., "Development of Coatings for Protection of Dispersion Strengthened Nickel from Oxidation," Technical Report AFML-TR-66-47, Part 1, March 1966.

8. Handbook of Chemistry and Physics, Forty-Sixth Edition, Chemical Rubber Co.

Contract NAS3-14300

DISTRIBUTION LIST

Addressee	Copies
NASA Headquarters 600 Independence Avenue, S. W. Washington, DC 20546	
Attn: Mr. G. Deutsch (RW)	1
Mr. N. Rekos (RLC)	1
Mr. J. Gangler (RWM)	1
Mr. J. Maltz (RWM)	1
National Technical Information Service Springfield, VA 22151	40
NASA-Lewis Research Center 21000 Brookpark Road Cleveland, OH 44135	
Attn: Aeronautics Procurement Section (M. S. 77-3)	1
Technology Utilization Office (M. S. 3-19)	1
Library (M. S. 60-3)	2
Patent Counsel (M. S. 500-311)	1
Report Control Office (M. S. 5-5)	1
Technological Util. Off. (M. S. 3-19)	1
Mr. G. M. Ault (M. S. 3-13)	1
Mr. S. S. Manson (M. S. 49-1)	1
Mr. R. W. Hall (M. S. 105-1)	1
Mr. N. T. Saunders (M. S. 105-1)	1
Mr. J. C. Freche (M. S. 49-1)	1
Mr. S. J. Grisaffe (M. S. 49-1)	1
Mr. J. P. Merutka (M. S. 49-1)	41
Mr. R. L. Ashbrook (M. S. 49-1)	1
Mr. B. Stein, M. S. 188-A NASA-Langley Research Center Hampton, VA 23365	1
Dr. J. Buckley, M. S. 206 NASA-Langley Research Center Hampton, VA 23365	1
Library NASA-Ames Research Center Moffett Field, CA 94035	1
Library NASA-Goddard Space Flight Ctr. Greenbelt, MD 20771	1

Library 1
NASA Flight Research Ctr.
P.O. Box 273
Edwards, CA 93523

Library 1
Jet Propulsion Laboratory
4800 Oak Grove Drive
Pasadena, CA 91102

Library 1
NASA-Langley Research Center
Langley Field, VA 23365

Library 1
NASA-Manned Space Flight Center
Houston, TX 77058

Library 1
NASA-Marshall Space Flight Center
Huntsville, AL 35812

Mr. H. Geyer 1
AFML/LLP
Headquarters
Wright-Patterson AFB, OH 45433

Capt. J.R. Williamson 1
AFML/LTF
Headquarters
Wright-Patterson AFB, OH 45433

Mr. A.E. Wright, SANEPJ 1
USAF
San Antonio Air Mtl. Area
Kelly AFB, TX 78241

Mr. M. Levy 1
Army Matls. Res. Agency
Watertown Arsenal
Watertown, MA 02172

Mr. I. Machlin, Code AIR-52031B 1
Department of the Navy
Naval Air Systems Command
Washington, DC 20360

Mr. H. Rosenthal, MRL 1
Metallurgy Research Lab.
Frankfort Arsenal
Philadelphia, PA 19137

Mr. P. Goodwin, AIR-5203 1
Naval Air Systems Command
Navy Department
Washington, DC 20360

Mr. Y. Telang 1
Ford Motor Company
2000 Rotunda Drive
P.O. Box 2053
Dearborn, MI 48123

Mr. L.P. Jahnke, Manager 1
Materials Dev. Lab. Oper.
General Electric Company
Cincinnati, OH 45215

Mr. M. Levinstein 1
General Electric Company
Materials Dev. Lab. Oper.
Adv. Engine & Tech. Dept.
Cincinnati, OH 45215

Mr. D. Hanink, Manager 1
Materials Laboratory
Allison Division
General Motors Corp.
Indianapolis, IN 46206

Mr. V. Hill 1
I.I.T. Research Inst.
Technology Center
Chicago, IL 60616

Mr. J. Wurst 1
University of Dayton Res. Inst.
Dayton, OH 45409

Mr. J.V. Long 1
Director of Research
Solar, Int. Harvester
2200 Pacific Highway
San Diego, CA 92112

Mr. A. Stetson 1
Solar Division
Int. Harvester Corp.
2200 Pacific Highway
San Diego, CA 92112

Dr. J. Berkowitz 1
Arthur D. Little, Inc.
20 Acorn Park
Cambridge, MA 02140

Mr. R. Perkins 1
Lockheed Palo Alto R. Labs
Mat. and Science Lab.
3251 Hanover Street
Palo Alto, CA 94304

Reports Acquisition 1
Aerospace Corporation
P.O. Box 95085
Los Angeles, CA 90045

Supervisor, Materials Engineering 1
Airesearch Company
402 East 36th Street
Phoenix, AZ 85034

Mr. G. Cook 1
Alloy Surfaces, Inc.
100 S. Justison St.
Wilmington, DE 19899

Mr. W.H. Freeman 1
Lycoming Division
AVCO Manufacturing Co.
505 South Main Street
Stratford, CT 06497

Mr. E. Bartlett 1
Battelle Memorial Inst.
505 King Street
Columbus, OH 43201

Dr. R.I. Jaffee 1
Battelle Memorial Inst.
505 King Street
Columbus, OH 43201

Mr. M. Negrin 1
Chromalloy Corp.
160 Western Highway
West Nyack, NY 10994

DMIC 1
Battelle Memorial Institute
Columbus Laboratories
505 King Avenue
Columbus, OH 43201

Mr. H.E. Marsh, Manager 1
Information Services
Stellite Division
Cabot Corporation
1020 West Park Avenue
Kokomo, IN 46901

Mr. G.J. Wile 1
Polymet Corporation
11 West Sharon Road
Cincinnati, OH 45246

Mr. W.D. Lang 1
Kaman Sciences Corporation
Garden of the Gods Road
Colorado Springs, CO 80907

Mr. L. Sama 1
Sylvania Electric Prod., Inc.
Chem. and Met. Division
Cantiague Road
Hicksville, NY 11802

Mr. Gene Wakefield 1
Texas Instruments, Inc.
M. & C. Division
Post Office Box 5474
Dallas, TX 75222

Dr. J. Gadd 1
TRW, Inc.
1400 N. Cameron St.
Harrisburg, PA 17105

Dr. E. Steigerwald T/M 3296 1
TRW Equipment
TRW, Inc.
23555 Euclid Avenue
Cleveland, OH 44117

Dr. W. Goward 1
Adv. Mat. R. & D. Labs.
Pratt & Whitney Aircraft
Middletown Plant
Middletown, CT 06158

Mr. E. F. Bradley 1
Pratt & Whitney Aircraft
United Aircraft Corp.
400 Main Street
East Hartford, CT 06108

Mr. D. Maxwell 1
Pratt & Whitney Aircraft
United Aircraft Corp.
West Palm Beach, FL 33402

Mr. D. Goldberg 1
Westinghouse Electric
Astronuclear Lab.
Pittsburgh, PA 15236

Mr. R. Grekila 1
Westinghouse Electric
Research Labs.
Beulah Rd., Churchill Bur.
Pittsburgh, PA 15235

Mr. G. R. Sippel, Supervisor 1
Applied Materials Research
Materials Science Laboratory, W5
Allison Division of General Motors
Indianapolis, IN 46206

Library 1
University of Dayton
Research Institute
300 College Park Ave.
Dayton, OH 45409

Prof. R. A. Rapp 1
Dept. of Metall. Engrg.
Ohio State University
Columbus, OH 43210

Dr. J. Wert 1
Matls. Engr. Dept.
Box 1621
Vanderbilt University
Nashville, TN 37203

Dr. J. Mueller 1
University of Washington
Ceramics Department
Seattle, WA 98101

GENERAL ELECTRIC

CORPORATE RESEARCH AND DEVELOPMENT

GENERAL ELECTRIC COMPANY, RESEARCH AND DEVELOPMENT CENTER, P. O. BOX 43
Building 37, Rm. 207, SCHENECTADY, NEW YORK 12301, Phone (518) 374-2211
Ext. 5-5467

February 15, 1972

National Aeronautics & Space Administration
Lewis Research Center
21000 Brookpark Road
Cleveland, Ohio 44135

Attention: Mr. John P. Merutka (Mail Stop 49-1)

Subject: Contract NAS 3-14300, Final Technical Report CR-120871

Gentlemen:

Your letter #5553 dated 01 February gave approval of the revised draft of our Final Report for the subject contract. Using the instructions and distribution list you provided, we have reproduced the required quantity in finished form. Enclosed herewith is one (1) bound copy for your immediate use. The balance of forty (40) additional bound copies is being forwarded to your attention in a carton, under separate cover. When added to the total of 109 additional copies sent to the other names and addresses shown on the official distribution list, this aggregates the required total of 150 copies.

Also enclosed in the package with this letter is one complete unbound copy (using only one side of each sheet), plus a complete set of glossy photos of all 51 figures in the report. We assume that you may wish to preserve these items for possible future use in the event of a reprinting.

This is the final deliverable item. As required in Article XVII of our contract, a Material Inspection and Receiving Report (DD Form 250) is enclosed with this delivery. We believe this submission discharges our final reporting obligation under the subject expiring contract.

Very truly yours,

S.C. Conrad
Contract Administrator

Enc. - 4, including 1 copy of DD-250

cc: Aeronautics Proc. Sect. (Mail Stop 77-3), NASA-Lewis (enc.-4)
NASA-STIF, PO Box 33, College Park, Md. 20740 (w.enc.-2)
RJ Harrington, ACO, DCASD, Hartford
DCRB-DHPE-Mr. E.A. Galica, DCASD Hartford
MC Toth, APRD-GE, 5100 West 164th St., Cleveland (w.enc.-2)